LABORATORI NAZIONALI DI FRASCATI
SIS – Pubblicazioni

LNF-96/033 (P)
29 Luglio 1996

DAΦNE Machine Project

Contributions to the
Fifth European Particle Accelerator Conference (EPAC 96)
Sitges, Barcelona, 10-14 June 1996

CONTENTS

Invited Papers

Contributed Papers

DAΦNE, THE FIRST Φ-FACTORY

G. Vignola and DAΦNE Project Team*, INFN-LNF, C.P. 13, 00044 Frascati, Italy

Abstract

DAΦNE, a high luminosity e^+/e^- Φ-factory, is presently under construction in Frascati.

The beginning of the collider commissioning is scheduled by winter 1997, with a short term luminosity goal $L=1.3\ 10^{32}\ cm^{-2}\ sec^{-1}$.

DAΦNE shall be the first of the new generation of very high luminosity colliders, called factories, to come in operation.

Other factories under construction are PEP-II [1] and KEK-B [2]: first collision, for both machines, is planned for 1998.

1 INTRODUCTION

The construction of the Φ-factory DAΦNE (including a completely new injector) was approved by the INFN Board of Directors in June 1990, while the engineering design started in spring 1991. This new facility is housed in the existing building of the ADONE accelerator, which has been shut down in April 1993.

An artist's view of DAΦNE is shown in Fig. 1.

The collider design is optimized at the Φ energy (1.02 GeV c.m.). It consists of two high current separate rings, crossing at a total horizontal angle of 25 mrad in two interaction regions, equipped with superconducting solenoids for the experimental detectors. The components of the Main Rings are being installed into the DAΦNE hall. Start of commissioning is expected by winter 1997.

In the following we will present briefly the main features and the status of the injector complex, the collider and its principal subsystems: more detailed information can be found in a series of papers presented at this Conference [3].

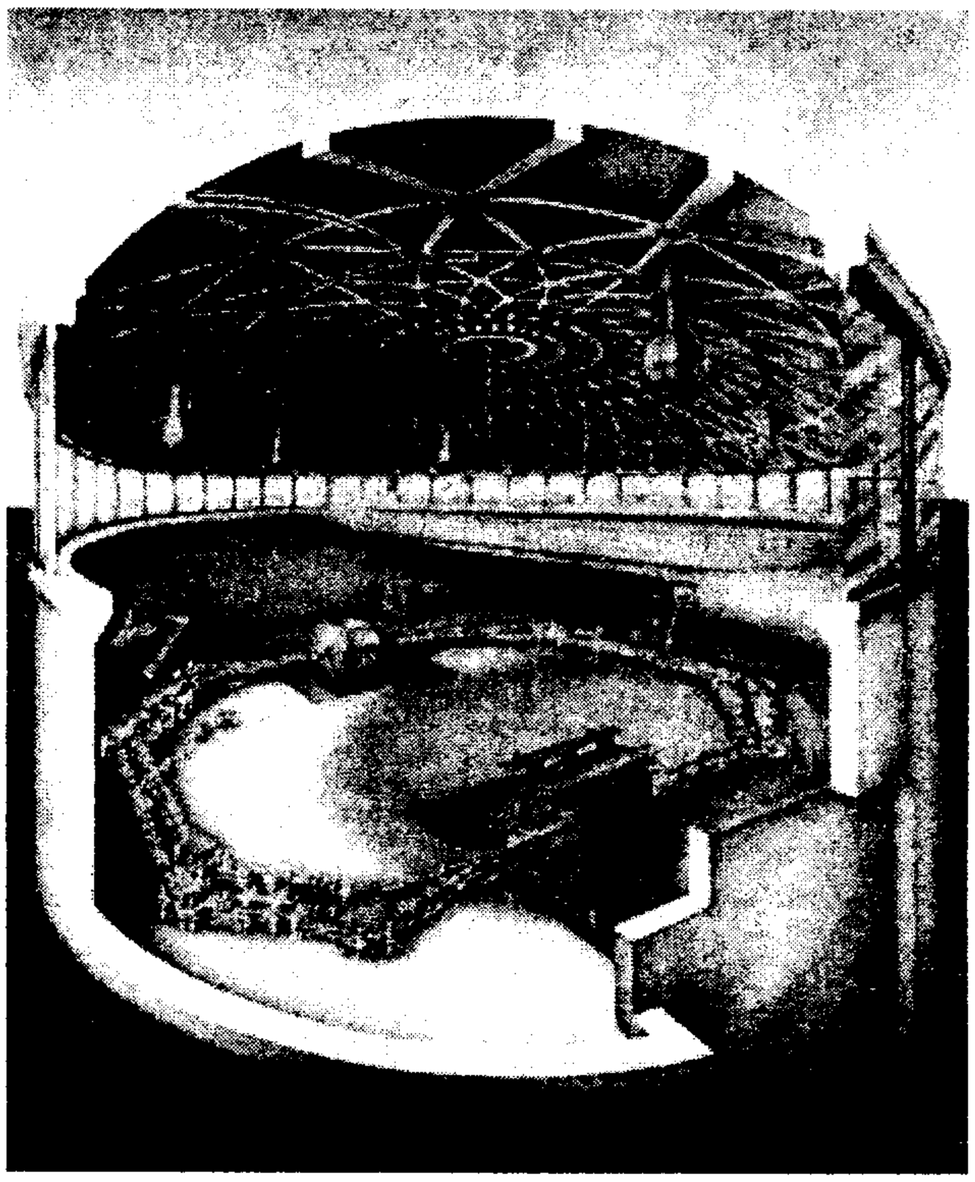

Figure 1 : An artist's view of DAΦNE showing the magnets layout and the two detectors, KLOE on the right and FINUDA on the left.

2 INJECTOR

The injector consists of an e^-/e^+ Linac and an Accumulator/damping ring, connected to DAΦNE through ~160 m long Transfer-lines.

The Linac, built by Titan Beta, has been already installed and commissioned with electrons. Positron commissioning is under way. The main design parameters for electrons and positrons are listed in Table I.

Table I - DAΦNE LINAC parameter list

	e^-	e^+
Max Energy (MeV)	800	550
Emittance (mm-mrad)	1.0	10.0
Relative energy spread	±.005	±.01
Pulse width(ns)	10.0	10.0
Peak current (mA)	150.0	40.0
Max repetition rate (Hz)	50.0	50.0

* M. Bassetti, M.E. Biagini, C. Biscari, R. Boni, S. Chen, V. Chimenti, A. Clozza, G. Delle Monache, S. De Simone, G. Di Pirro, H. Dong, A. Drago, S. Faini, A. Gallo, N. Ganlin, A. Ghigo, S. Guiducci, Y. He, F. Marcellini, C. Marchetti, M.R. Masullo, M. Migliorati, C. Milardi, M. Modena, L. Palumbo, L. Pellegrino, M. Preger, G. Raffone, C. Sanelli, F. Sannibale, M. Serio, F. Sgamma, B. Spataro, A. Stecchi, C. Vaccarezza, M. Vescovi, S. Vescovi, G. Vignola, D. Yao, M. Zobov.

The Accumulator is used to damp the transverse and longitudinal emittances of the Linac beam (e^- or e^+), thus relaxing the injection requirements in the design of DAΦNE.

The injection chain works as follows: LINAC beam is first injected at ~ 50 pps in one RF Accumulator bucket, damped, extracted at ≈1 Hz, and injected into a single DAΦNE bucket.

The Accumulator (whose main parameters are listed in Table II) has been built by Oxford Instruments and completely installed (see Fig. 2) together with the transfer lines.

Accumulator commissioning is under way and first beam has already circulated.

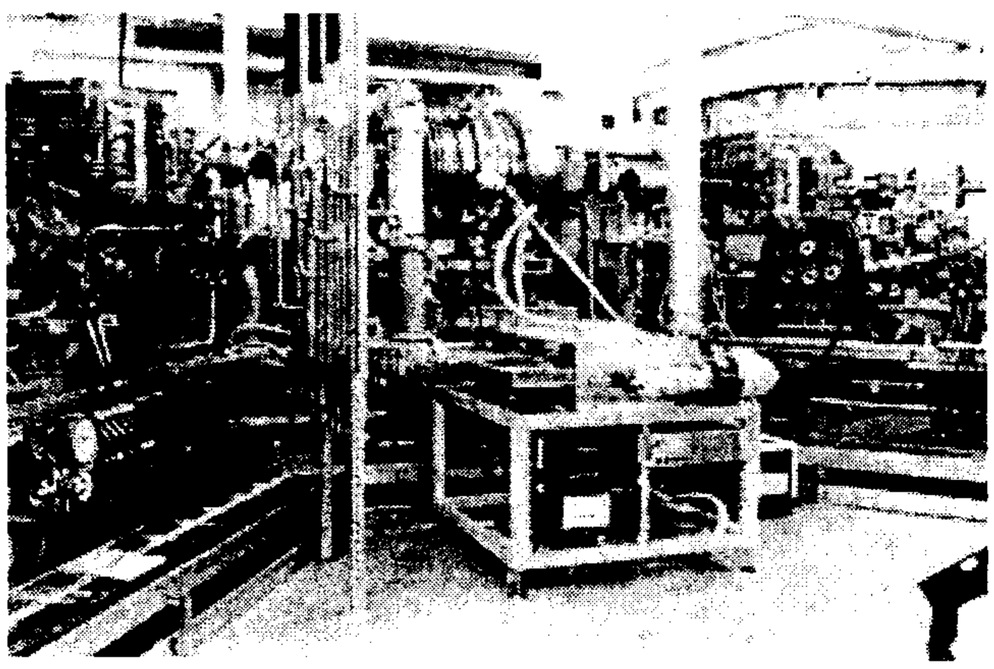

Figure 2 : View of the Accumulator with the RF cavity.

Table II - Accumulator Main parameters

Max Energy (MeV)	550
Circumference (m)	32.56
Emittance (mm-mrad)	0.26
RF frequency (MHz)	73.65
RF peak voltage (kV)	200
Single bunch av. current (mA)	150
Bunch length (cm)	3.0
Synchrotron loss (keV/turn)	5.2
Damping time, τ_ε/τ_x (ms)	10.7/21.4

3 DAΦNE

The major physics motivation for the construction of DAΦNE is the observation of direct CP-violation in K_L decays, i.e. the measurement of ε'/ε with accuracy in 10^{-4} range by the KLOE detector [4].

A second detector FINUDA [5] for nuclear physics is also approved and under construction.

In order to achieve a very high luminosity, mandatory target for any factory, the DAΦNE design is based on the high current, double ring approach, adopted also by PEP-II and KEK-B. This high current approach allows to use single bunch parameters quite conservative from an accelerator physics point of view, but it moves the difficulties to engineering challenges (vacuum, RF, multibunches). The correctness of such a statement can be easily deduced by inspection of the DAΦNE design parameters listed in Table III together with the PEP-II and KEK-B ones.

Table III - DAΦNE, KEK-B and PEP-II design parameters

	DAΦNE	KEK-B		PEP-II	
		L.E.R.	H.E.R.	L.E.R.	H.E.R.
Energy (GeV)	0.51	3.5	8.0	3.1	9.0
Maximum luminosity [$cm^{-2}s^{-1}$]	5.3×10^{32}	1010^{34}		3×10^{33}	
Trajectory length [m]	97.69	3016.26		2199.32	
Emittance, $\varepsilon_x/\varepsilon_y$ [mm·mrad]	1/0.01	0.018/0.00036		0.064/0.0026	0.048/0.0019
Beta function, $\beta^{*,x}/\beta^{*,y}$ [cm]	450/4.5	33.0/1.0		37.5/1.5	50.0/2.0
Tranverse size, $\sigma^{*,x}/\sigma^{*,y}$ [mm]	2/0.02	0.077/0.0019		0.16/.006	
Beam-beam tune shift, ξ_x/ξ_y	0.04/0.04	0.039/0.052		0.03/0.03	
Crossing angle, θ_x [mrad]	± 12.5	± 11		0	
Betatron tune, ν_x/ν_y	5.09/6.07	45.52/45.08	47.52/43.08	36.57/34.64	24.57/23.64
RF frequency, f_{RF} [MHz]	368.25	508.9		476	
Number of bunches	120	5120		1658	
Minimum bunch separation [cm]	81.4	58.9		126	
Particles/bunch [10^{10}]	8.9	3.3	1.4	5.9	2.7
RF voltage [MV]	0.250	5 ÷ 10	10 ÷ 20	5.5	14.0
Bunch length σ_z [cm]	3.0	0.4		1.0	1.1
Synchr. radiation loss [keV/turn]	9.3	1500*	3500	700*	3570
Damping time, τ_ε/τ_x [ms]	17.8/36.0	23/46		26.4/52.8	19.8/39.6
Single bunch lum. [$cm^{-2}s^{-1}$]	4.4×10^{30}	1.95×10^{30}		1.8×10^{30}	

* Wiggler on.

3.1 Main features and optics.

In DAΦNE electrons and positrons circulate in two separated storage rings (see Fig. 3) laying in the same horizontal plane with horizontal crossing in 2x10 m long interaction regions (IR1 and IR2), at an angle of ± 12.5 mrad.

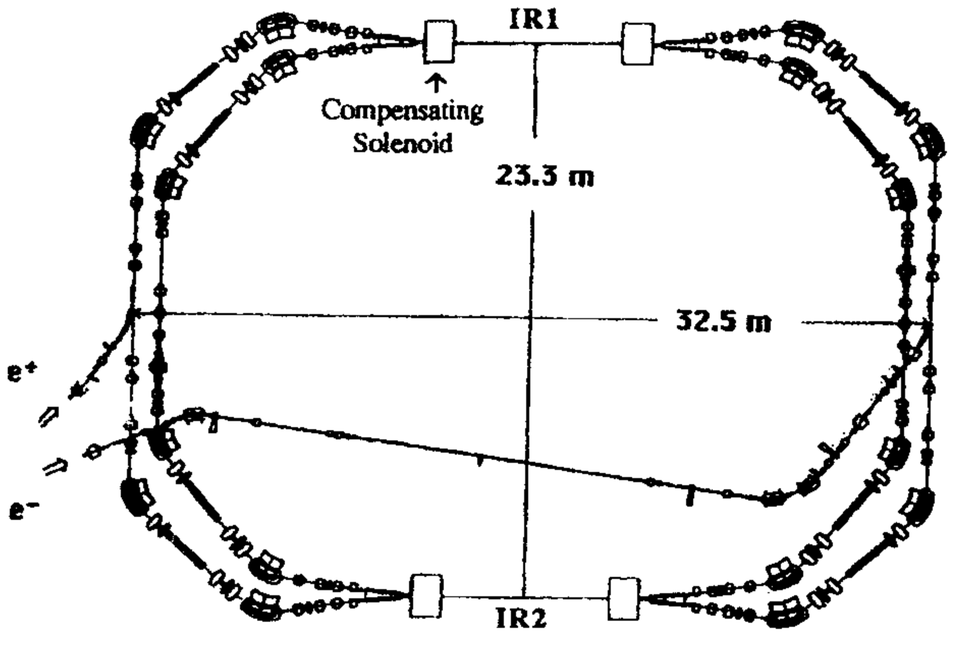

Figure 3 : DAΦNE magnetic layout.

The regular lattice is a modified Chasman-Green type: it consists of 4 achromats, each housing a 2 m long, 1.8 T normal conducting wiggler to increase beam emittance and radiation damping.

The straight sections orthogonal to the IR are used for injection, RF and feedback systems.

Such a magnetic structure, with all the quadrupoles and sextupoles powered independently, has built in enough flexibility to cover a wide range of betatron tunes keeping good dynamic aperture for single beam.

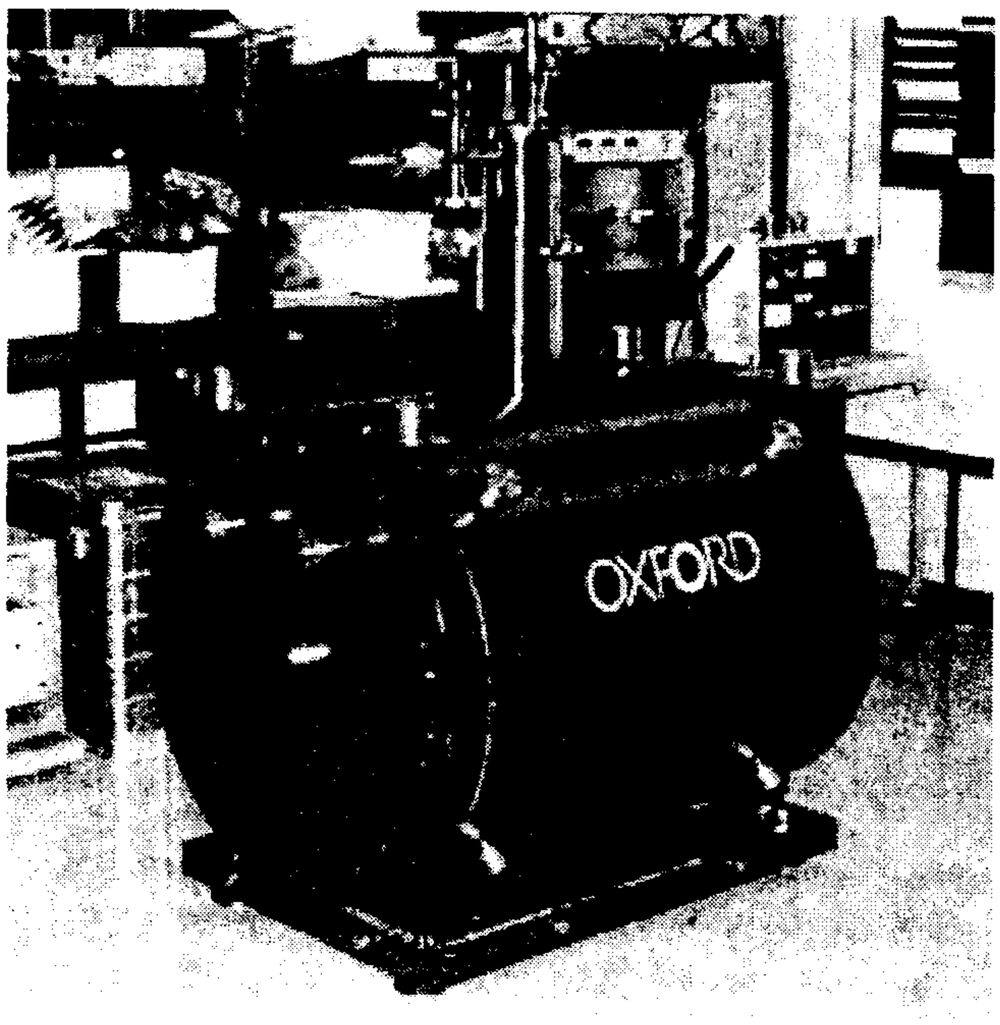

Figure 4 : Compensating s.c. solenoid.

The IRs are equipped with a compensating s.c. solenoid (see Fig. 4) at each end.

Three different low-β optics designs have been developed [6], one without longitudinal field for commissioning purposes, the other two with permanent magnet quadrupoles, for KLOE and FINUDA experiments. The three IR designs are completely equivalent and interchangeable from an optic point of view.

At the IR the experiments have a 500 μm thick Be vacuum pipe.

The KLOE's Be pipe (see Fig. 5) has a very complicate bulb-like shape, with a very thin (50 μm Be) inner shield to prevent RF losses. This shape is needed to avoid K_S regeneration effects. The chamber is now being built by K-TEK.

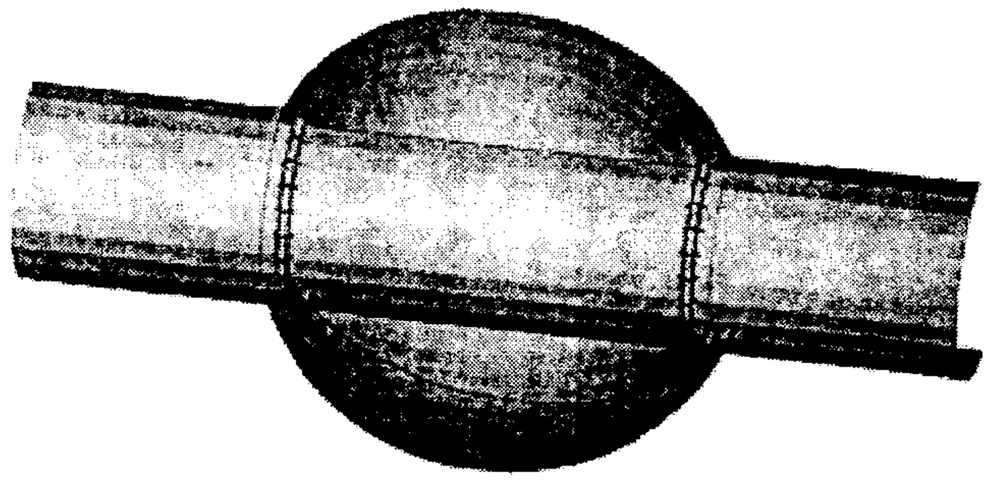

Figure 5 : View of KLOE vacuum chamber.

As far as the two beam operation is concerned (let us remind that DAΦNE can operate with one or two interactions points) a careful study of the betatron tune working point with a beam-beam simulation code (10^6 turns) is in progress.

At present there are two working point candidates with different β-tunes, depending if one assumes 1 or 2 crossing per turn.

The results are summarized in Table IV where L/L_o is the calculated single bunch luminosity reduction with respect to the nominal one.

Table IV : Beam-beam simulation results

Crossing	ν_x	ν_y	L/L_o (%)
1	4.53	6.06	98
2	5.09	6.07	86

3.2 Vacuum system

The DAΦNE vacuum system is dimensioned for an operating pressure of 1 nTorr with 5 A circulating current.

A design of the arc vacuum vessel, similar to ALS, has been adopted, consisting of 2 chambers connected through a narrow slot.

Figure 6 : The first 2 arc vacuum chambers during acceptance tests.

The beam circulates in the first chamber while the synchrotron radiation photons hit a system of water cooled copper absorbers located in the second one (antechamber). In this way more than 95% of the photon flux is collected in the antechamber. The achromat vessel (~10 m long) is made by two halves of Al alloy 5083-H321 plates which, after machining, are welded along the middle plane. The inner surface is mirror finished. The 8 arc chambers (see Fig. 7) are under construction and half of them have been completely tested. The main inconvenient with this long vacuum chamber is the large expansion during bakeout (~35 mm in the longitudinal direction and ~10 mm in the transverse one). To cope with these large displacements a special shielded bellow (see Fig. 7) with no sliding contacts has been designed and a prototype tested both from mechanical and the HOM induced modes points of view.

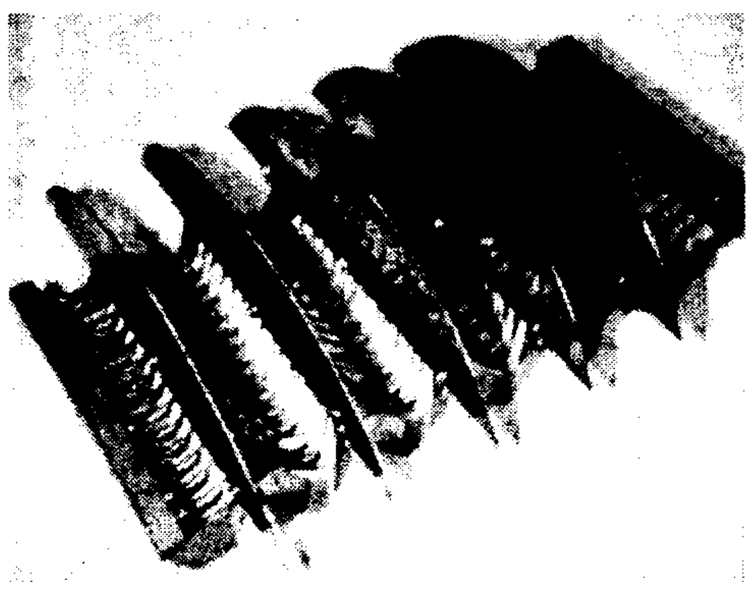

Figure 7 : DAΦNE bellow prototype (one half).

3.3 RF System

The RF System of each ring consists of a normal conducting single cell cavity fed by a 150 kW/cw klystron.

The RF cavity (see Fig. 8) is equipped with three waveguides to damp the parasitic modes that are dissipated into external 50 Ω loads.

The first cavity has been successfully power tested up to 30 kW, corresponding to ~350 kV, and the HOM behavior (see Fig. 9) found in agreement with expectation.

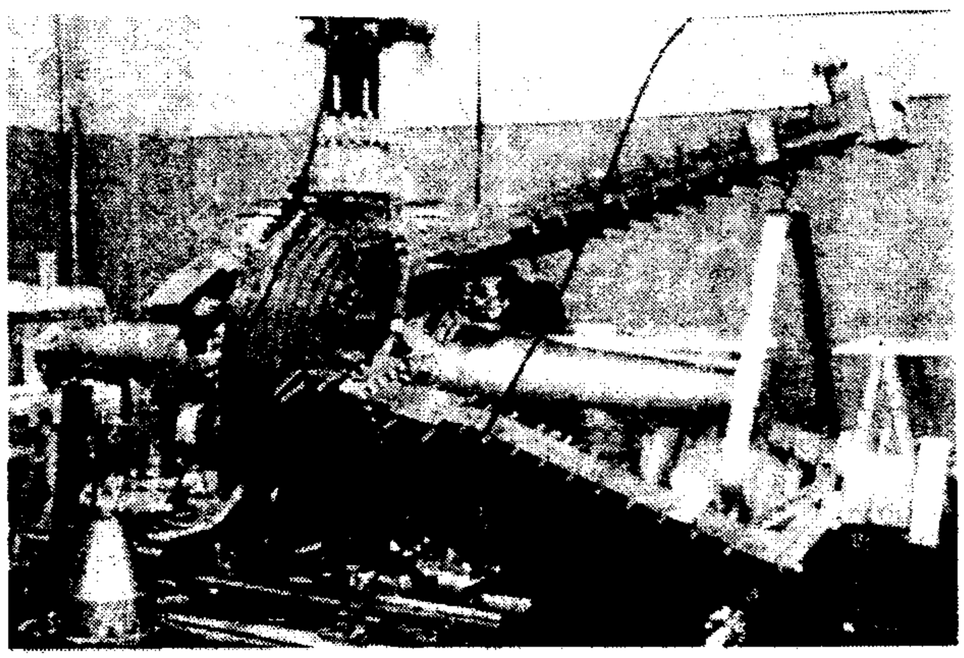

Figure 8 : The DAΦNE Cavity.

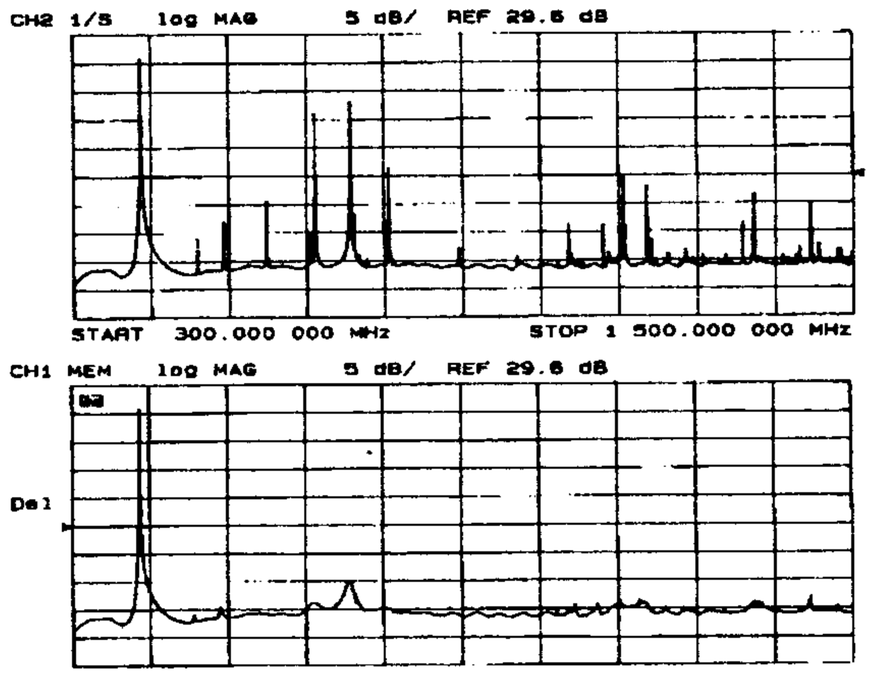

Figure 9 : Undamped (top) and damped (bottom) longitudinal spectra.

3.4 Longitudinal feedback

Even though the HOMs in the RF cavity are heavily damped the probability for a damped HOM to cross a coupled bunch mode frequency is not negligible and, due to the large total current, the growth rate of unstable modes can be stronger than the radiation damping rate even by two orders of magnitude. For this reason the required additional damping is provided by a time domain, bunch to bunch feedback system [7] largely based on Digital Signal Processors (DSP). It has been developed and tested [8] in the framework of a collaboration with SLAC/LBL PEP-II Group on feedback systems for the next generation of factories with intense beams and a large number of bunches.

The digital part is now under construction at SLAC, while the Kicker cavity for DAΦNE has been designed and built at Frascati.

3.5 Status of the collider construction

The procurement phase of all the major components has been completed. The installation inside the DAΦNE Hall has started in January 1996 (see Fig. 10). The completion of the installation phase is scheduled by the end of 1996 followed by the beginning of commissioning.

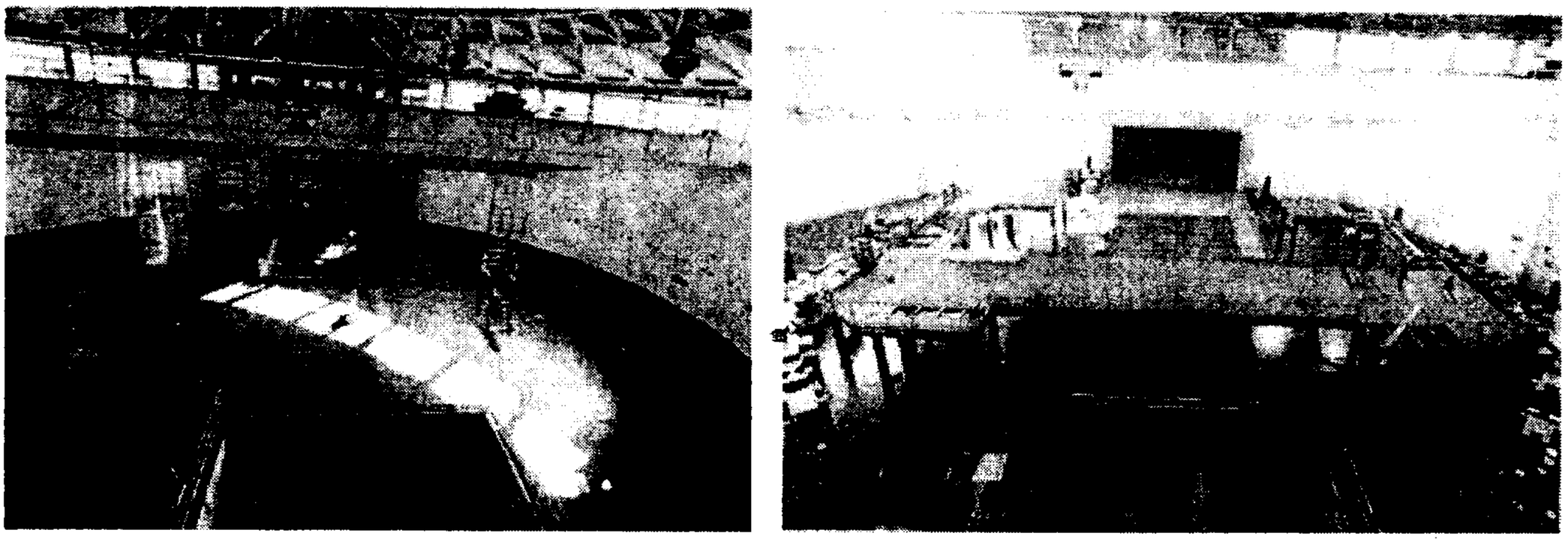

Figure 10 : DAΦNE installation progress. Status of the DAΦNE Hall in January 96 (left) and May 96 (right).

4 ACKNOWLEDGMENTS

I like to thank the DAΦNE Machine Review Committee (A.Hutton, Chairman, F.Bonaudi, D.Boussard, G.Brianti, J.P. Delahaye, H. Hsieh, A. Wrülich) for their constant advice; E. Iarocci and P. Laurelli, former and present LNF Directors, and the LNF Administration for their continuous support to this Project.

I am also pleased to acknowledge all the personnel of LNF Accelerator Division for their enthusiastic and professional commitment.

Special thanks to Pina Possanza not only for editing this article, but mainly for her outstanding and invaluable secretarial skills which constitute a reference point for everybody working in this Project.

5 REFERENCES

[1] PEP-II Status and Plans - J.T: Seeman , 1995 PAC and ICHEA Proceedings.

[2] KEK-B Status and Plans - S. Kurokawa, 1995 PAC and ICHEA Proceedings.

[3] R. Boni, "Hom-Free Cavities", these Proceedings.

M. Serio et al., "Multibunch Instabilities & Cures", these Proceedings.

M. Bassetti, C. Biscari, "Fringing Fields in Low-Beta Magnetic Elements", these Proceedings.

S. Guiducci, "Background Calculations for the DAΦNE Experiments", these Proceedings.

S. De Santis, M. Migliorati, L. Palumbo, and M. Zobov, "Impedances of a Hole in Coaxial Strctures", these Proceedings.

K. Hirata and M. Zobov, "Beam-Beam Interaction Study for DAΦNE", these Proceedings.

A. Gallo, A. Ghigo, F. Marcellini, B. Spataro M. Zobov, and L. Palumbo, "Impedance of DAΦNE Shielded Bellows", these Proceedings.

G. Di Pirro, A.Drago, A. Ghigo, F. Sannibale, M. Serio, "The DAΦNE Timing System", these Proceedings.

R. Boni, A. Gallo, F. Marcellini, "Experimental Tests of the DAΦNE RF Feedback System", these Proceedings.

R. Boni, A. Gallo, F. Marcellini, "High Power Test of the Waveguide Loaded RF Cavity for the Frascati Φ-Factory Main Rings", these Proceedings.

R. Boni, A. Drago, A. Gallo, A. Ghigo, F. Marcellini, M. Serio, M. Zobov, "Kickers and Power Amplifiers for the DAΦNE Bunch-by-bunch Longitudinal Feedback System", these Proceedings.

G. Di Pirro, C. Milardi, A. Stecchi, "First Operational Experience with the DAΦNE Control System", these Proceedings.

H. Hsieh, M. Modena, M. Preger, C. Sanelli, S. Vescovi, and Tesla Engineering, "Measurements of the Dipole, Quadrupole and Sextupole Prototypes for the Accumulator of DAΦNE, the Frascati Φ-Factory", these Proceedings.

M. Preger, C. Sanelli, "The DAΦNE Main Ring Magnet Prototypes", these Proceedings.

The DAΦNE Project Team, presented by F. Sannibale, "First Results of the DAΦNE Injection System Commissioning", these Proceedings.

A. Clozza, V. Chimenti, C. Vaccarezza, "An UHV Vacuum System for DAΦNE", these Proceedings.

[4] The KLOE collaboration, "KLOE, a general Purpose Detector for DAΦNE", Frascati Internal Note LNF-92/109, April 1992.

Physics at DAΦNE, J. Lee- Franzini, Proceedings of XXVI ICHEP - Dallas 1992.

[5] The FINUDA collaboration, "FINUDA, a detector for nuclear physics at DAΦNE", Frascati Internal Note LNF-93/021, May 1993.

[6] M. Bassetti et al., "DAΦNE interaction region design", Proceedings of 1993 Particle Accelerator Conference, Washington D.C., p. 2048.

[7] G. Oxoby et al., "Bunch by Bunch Longitudinal Feedback system for PEP-II", Proceedings of 4th European Particle Accelerator Conference, London 1994, p.1616.

[8] D. Teytelman et al., "Operation and Performance of the PEP-II Prototype Longitudinal Damping System at ALS", 1995 PAC and ICHEA Proceedings.

HOM-FREE CAVITIES

R. Boni, INFN-LNF, C.P. 13, 00044 Frascati, Italy

Abstract

Intense beam current and multibunch operation are the essential features for increasing the luminosity of the modern colliders or improving the performances of the synchrotron light sources. The high order modes (HOM)-free cavities can give the major contribution to these tasks since the beam current limit and the coupled-bunch mode instabilities mostly arise from the parasitic modes of the accelerating cavities. This article deals with the study and the designs which have led to the development of RF cavities with a low content of high order parasitic modes. Different techniques adopted in both superconducting and room-temperature radiofrequency are analysed. Drawbacks in the use of these special devices are also reviewed.

1 INTRODUCTION

The new generation of e^+/e^- colliders and light sources have required the development of several novel and unconventional devices to permit multibunch operation and high current beams. These features are indispensable to achieve the luminosity range of $10^{32} \div 10^{34}$ sec^{-2} cm^{-1} (in the factories and TeV linear colliders) or increase the photon flux in the synchrotron light sources.

Recently, RF experts of numerous accelerator laboratories have concentrated efforts and resources in the design and construction of HOM-free accelerating cavities. The motivation for this demanding job is to eliminate or reduce the interaction of the cavity HOMs with the particle beam spectrum, thus increasing the current threshold limited by the coupled-bunch instabilities and reducing the beam power losses. Even though the totality of the accelerator components contributes to increase the growth rate of both transverse and longitudinal coupled-bunch instabilities, the RF cavities are undoubtedly the major source of problems. This argument has been treated in many articles and technical papers and is still subject of discussions and experimentation.

The mechanism which can produce beam instability or power loss consists in the capability of the charged particles, to induce high order resonant fields in the RF cavities when passing them through. This is possible only for those cavity resonances which overlap beam Fourier harmonics or their sidebands. The HOMs have a decay time τ which can be much longer than the time gap between two neighbouring particle bunches, i.e.: $\tau = 2Q/\omega >> t_b$ where Q and ω are the quality factor and the angular frequency of the induced cavity HOM, t_b is the time interval between two successive bunches. In circular machines $t_b = To/n_b$ with To revolution time and n_b number of accumulated bunches. Particles which travel through the cavity on its longitudinal axis can generate TM0,n,m-like monopoles alone, whereas off-axis particles can generate both monopoles and dipoles. Due to the time persistence of the cavity HOMs, the resonant buildup of the parasitic fields may occur. Thus the beam can get unstable and the storable current severely limited if the instability growth rate is greater than the natural damping. In circular machines, the interaction of the beam spectrum sidebands with the cavity spectrum is responsible for longitudinal and transverse instability [1]. Beside this, power losses are associated to interaction of the main beam Fourier lines with the cavity HOM impedances. These losses can be evaluated by summing [2] the possible contribution for each beam line and cavity mode: $Z \cdot I_b^2/2$, where I_b is the beam line amplitude and Z is the real part of the cavity mode impedance at the beam line frequency. In linear colliders, the beam-cavity interaction can cause the so called beam blow-up (BBU).

The beam/cavity spectra overlapping can be faced by detuning the dangerous HOM frequencies. However, this may not be considered as a real way to render HOM-free the RF cavities. This method consists in the modification of the cavity temperature, for shifting the frequency of the potentially dangerous modes in order to avoid overlapping with the beam spectrum lines. This HOM detuning is an experimental approach for fighting coupled-bunch mode instabilities and in some cases it has been used successfully [3,4,5,6]. An alternative way of HOM detuning, based on the Slater's perturbation theory [7], is analysed and proposed in [8]. Anyway, HOM detuning can help in small rings only, since the particle revolution frequency is high and the beam Fourier components are largely spaced.

2 THE CONCEPT OF HOM-FREE CAVITIES

To counteract more rigorously the effect of the HOMs, the exponential growth of the parasitic fields must be reduced within the range that makes feasible the use of broadband feedback systems [9,10], that is the HOM impedances R and quality factors Q must be reduced the most. To achieve this result, it is necessary to remove the HOM power from the cavities and dissipate it with high RF losses materials or external loads. Several techniques have been proposed to suppress cavity HOMs depending on the accelerator requirements and the cavity frequency. Super-conducting (SC) and normal-conducting (NC) resonators require diverse HOM damping systems as well. In SC radiofrequency it is essential to avoid cavity quenching or strong degradation of the accelerating mode Q since this overloads the refrigeration systems and does not permit to achieve the design accelerating gradients. For these reasons in SC cavities, it is preferred to extract the HOM power from the cavity beam tube instead of from the accelerating cell. Also, low values of the [R/Q] ratios are helpful to minimize the cavity contribution to the broadband impedance of the ring and can be obtained by

properly shaping cavity and beam pipe profiles [2]. It is also wise to design the cavity shape so that the worst HOMs lie as far as possible from intense beam Fourier components. Therefore, the beam-cavity overlapping is unlikely in an undamped cavity but can lead to excessive instabilities and power losses. On the other hand, in a heavily damped cavity, the interaction is very probable but more easily controllable.

The concept of "HOM-free cavities" derives from the above considerations.

3 COUPLING OUT THE HOMs FROM THE RF CAVITIES

A detailed and very fine basic description of the HOM damping methods can be found in the ref. [11]. The most used HOM damping systems can be classified in three main categories, i.e. the coaxial couplers, the beam tube damping loads and finally, the waveguide couplers.

3.1 HOM couplers with coaxial structure for application in room temperature resonators

Narrow band and tuned devices belong to this group of couplers. They consist in coaxial structures with LC distributed elements, which penetrate the cavity with antennas (E-probes) or loops (H-probes). The damper position is chosen to couple the most dangerous parasitic fields and the HOM power is carried out and dissipated on external dummy loads. To avoid extraction of the principal mode, such dampers need a filter that can be achieved by means of transmission line techniques. Fundamental mode (FM) decoupling can be also obtained with a correct choice of the damper position.

Loop and antenna couplers were applied to the PETRA NC cavities [12] and used in DORIS e^+/e^- storage ring. The coupling impedance of the most troublesome TM011 has been reduced by several factors. The dampers had FM filtering and water cooling (Fig. 1).

The CERN SPS 100 MHz NC cavity [13] is equipped with three $\lambda/4$ coaxial lines ending with E-probes. Damping of some HOM impedances as much as 30 dB is obtained. Tuning, bandwidth and mode coupling are made by adjusting the length of the coaxial sections. The load resistor is connected at some distance of the line short and determines the coupler Q. Rod-antenna dampers (Fig. 1) have been operating on TRISTAN NC cavities at KEK since 1989 [14], providing significant reduction of the coupling impedance of the TM011 and TM111 modes. This permitted to increase the instability beam current threshold over 20 mA. The antenna is followed by a coaxial line with a short end tuned to reject the cavity FM. The HOM power is extracted at a mid point with a vacuum feedthrough and dissipated on a resistive metal film. E-probes and H-probes dampers have been developed at Argonne for the APS 352 MHz NC cavity [15]. The HOM power dissipation is achieved with vacuum compatible AlN ceramic materials and the damping factors are satisfactory for the machine operation. Installation on APS is foreseen early the summer 1996 [16]. Other similar damping systems have been proposed or developed elsewhere [17,18].

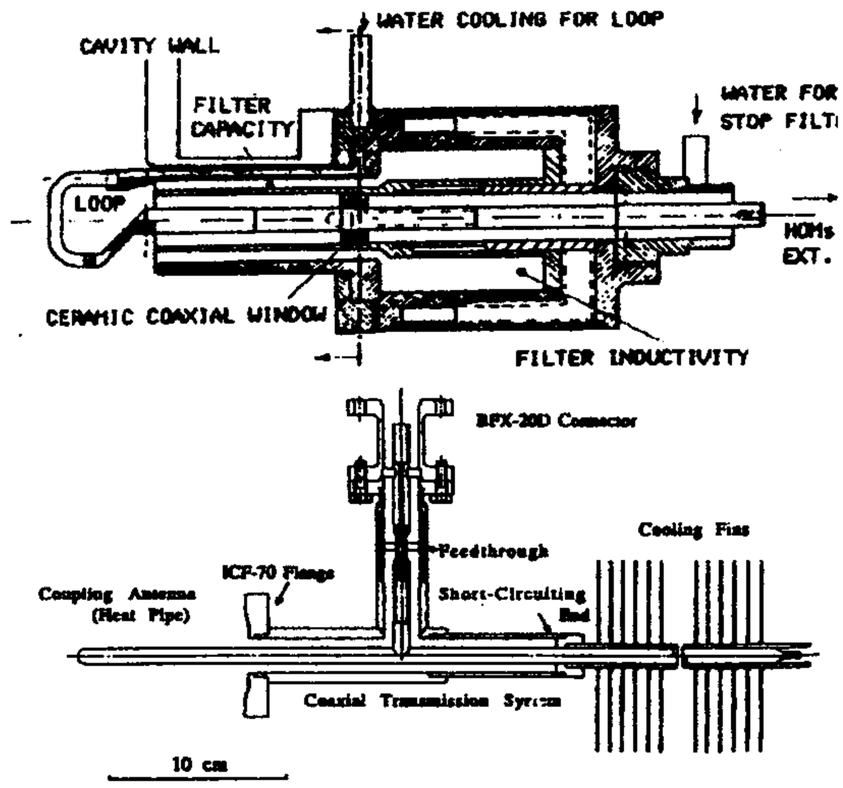

Figure 1 - Coaxial HOM couplers developed for normal conducting cavities technology at DESY (up) and KEK.

3.2 Coaxial HOM couplers for application in SC cavities

Coaxial HOM dampers are essential components of the multicell SC cavities operating at LEP, HERA and TRISTAN colliders and developed for the TESLA project too. Positioning the dampers at the equator of the cavity cells [19,20] has been in general avoided since it can cause multipacting and thermal-magnetic breakdowns. Thus, it has been chosen to put the couplers on the beam tubes [21,22,23] at both the ends of the cavity providing that the HOM wake fields propagate out by opening enough the pipe diameter as proposed in ref. [24]. Usually they are set with azimuthal angle of 90° to damp both polarizations of the dipole modes. The HOM power is extracted with vacuum feedthroughs and dissipated on 50 Ω resistors.

The LEP 352 MHz SC cavities are equipped with HOM couplers evolved through several projects to the final configuration [25] shown in Fig. 2. The original design is due to CEN-Saclay [26] and consists basically in an LC series to ground, intercepting the HOM magnetic fields (the so called "hook type" coupler). The HOM external Qs are in the range of a few thousands [27]. This model presents important features as dismountability, easy FM tuning, simple manufacturing and cooling. HOM coaxial couplers are used in the sixteen 500 MHz SC resonators of the HERA electron ring [28]. The couplers, based on two inductive stubs, have broadband response and tunable FM filtering. Beam energy upgrading has been achieved at TRISTAN main ring by installing 32 SC 508 MHz cavities equipped with beam tube HOM couplers [29]. FM rejection is achieved with a $\lambda/4$ resonator and an output T stub allows the inner conductor cooling. The HOM couplers for the nine-cells 1.3 GHz SC cavities of the TESLA project [30] are also demountable loops and have been developed and tested at Saclay.

Filtering of the cavity accelerating mode is very important in coaxial HOM couplers, especially in SC cavities where FM Q strong degradation is unacceptable.

The HOM Qs are damped down to $10^4 \div 10^5$ without perturbing the SC cavity performances. In NC resonators damping of single HOMs can be excellent. The reduced number of the damped modes is the main limitation of the coaxial HOM couplers and also their cooling in cryogenic environment presents some risks.

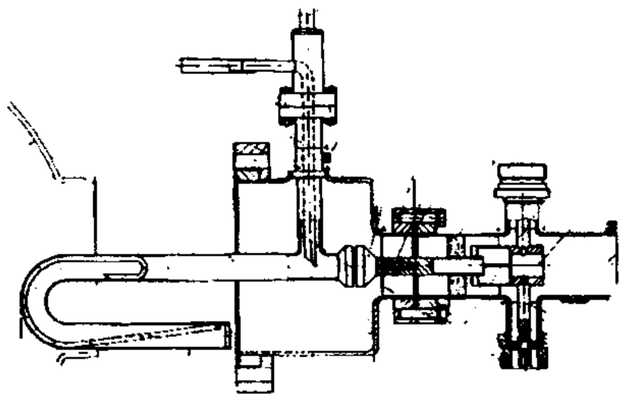

Figure 2 - The "Hook type" HOM Coupler.

3.3 Beam tube HOM damping loads

Single cell SC cavities will be used on CESR at Cornell University to upgrade the luminosity [31]. Also SC resonators are being developed for the KEK-B Factory [32]. In the two cases, the HOM power will be dissipated by means of RF lossy ferrites bonded to the inner surface of both cavity beam tubes. The loads are located at room temperature outside the cryostat. The cavity beam tubes are enlarged enough to permit the HOMs, but the FM, to propagate throughout. However, to ensure the propagation of the lowest dipoles (i.e. the TM110-like and TE111-like) the pipe cut-off is further lowered at one cavity side. At Cornell, a grooved pipe is adopted [33], whereas an extra-large tube of 300 mm diam. is used for the KEK-B SC cavity. Figure 3 shows a sketch of CESR-III and KEK-B cavity modules. The 500 MHz CESR-III cavity uses RF lossy ferrite tiles to dissipate the HOM power. The tiles are bonded on water cooled copper plates radially applied to the inner surface of a beam pipe section. Ferrite damping and power handling capabilities have been evaluate and a beam test of a fully equipped cavity has been performed [34]. The results are considered satisfactory for the full beam operation of CESR-III [35].

The KEK-B HOM loads are made by sintering a ferrite powder directly on the inner surface of a copper pipe with a special process developed at KEK [36]. The ferrite damping properties, measured on an cavity model, are excellent as reported in [32] and the bench power tests have proved the loads can withstand average power densities of 14 W/cm^2. A prototype ferrite load has been tested positively with the TRISTAN beam. Ferrites permit to damp the HOM Qs of large pipe single cell cavities down to a few hundreds or less over a 1.5÷2 GHz band without degradation of the FM features. Their outgassing rate seems compatible with the ultra vacuum of the accelerators. A very efficient cooling is necessary to avoid cracks of ferrites due to their low tensile strength and thermal conductivity. The beam line tests have not revealed, till now, other major drawbacks. Other dissipative materials, as the SiC ceramics, have been proposed [37] and their use is foreseen for the beam tube HOM loads of the ATF cavity at the Japan Linear Collider [38].

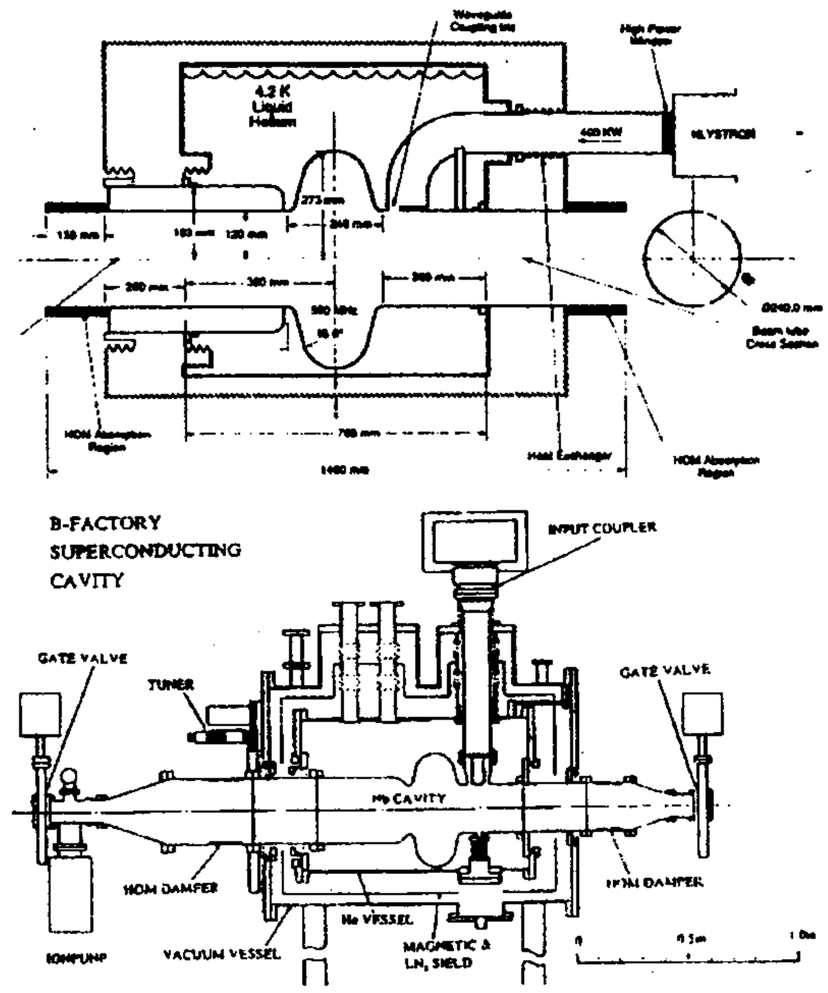

Figure 3 - The CESR-III (up) and KEK-B SC cavity modules.

3.4 Waveguide HOM Damping

S-band waveguides (WG) are used in the recirculating linac CEBAF to extract the HOM power from the beam pipes of 338 SC 1.5 GHz cavities. The cavity FM vanishes at the WG position so that its Q is unperturbed. The absorbing loads are made of an AlN based sintered ceramic which has good vacuum properties and thermal conductivity. They are brazed to the WG end flanges and operate in vacuum avoiding the use of a separation window. Because of the low HOM power, the WG dampers are inside the cryostat at 2°K [39]. The HOM Qs are brought down to $10^3 \div 10^5$ and the instability limit is raised over the 200 μA design value. The operation time accumulated till now in beam environment have not shown any drawbacks in the use of these HOM loads [40].

The WGs offer natural rejection to all the under cut-off frequencies and therefore their use in HOM extraction has the great advantage to stop the cavity FM. WGs were proposed in [41] already in 1988 for HOM damping in linear colliders.

The concept of using WGs in accelerating cavities has been stressed in ref. [42] with the proposal of a 3-WG loaded cylindrical resonator which is virtually free of HOMs. In that 3 GHz model, the WGs are considered integral part of the cavity rather than something added afterward. Three equally spaced square apertures are opened around the equator of a pill-box and convey out, by means of WGs, all the parasitic fields in the TE10 mode. The cavity FM, whose frequency is below the WG cut-off, is evanescent and remains trapped in. Terminating loads are placed at each WG short-end but the excellent wideband HOM damping is counterbalanced by a strong FM power loss because of an excessive dissipation in the WGs. A rather similar solution was initially investigated at Trieste for the ELETTRA synchrotron light source [43].

WG dampers have been adopted at SLAC for the PEP-II B-Factory project [44]. A total of 32 NC single cell 476 MHz copper cavities will be used. Since the accelerating voltage is more than 600 kV per cavity, the FM shunt impedance must be preserved as much as possible. Large WG apertures or wide beam tubes for housing lossy materials are therefore avoided. The PEP-II "nose-cone" resonator [45], shown in Fig. 4, is equipped with three WGs attached to rectangular slots opened 120° apart for symmetry reasons. The HOM load terminations [46] are made by brazing tiles of lossy ceramics (the same developed for CEBAF) on the WG broadwall near the short-end side. The RF characteristics and the load shape guarantee a VSWR less than 2:1 in a 700÷2500 MHz range. The calculated HOM power is about 10 kW per load. The WGs have 600 MHz TE10 cut-off and are located to couple strongly the worst parasitic modes. HOM longitudinal and transverse impedances have been significantly reduced over a large frequency band in a cavity prototype as shown in Fig. 5. A full power cavity model is being tested and one HOM load prototype has been powered to 4 kW separately [47].

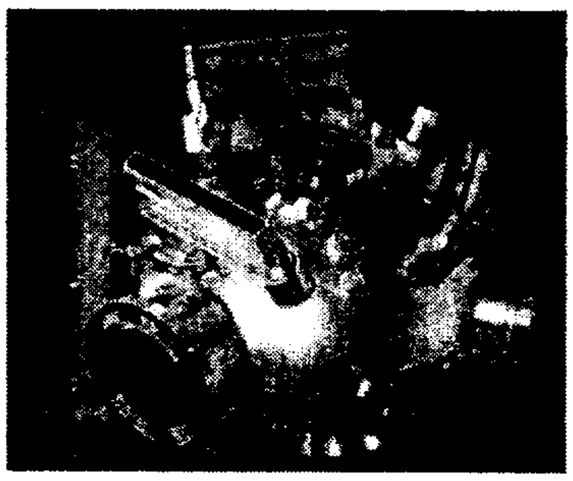

Figure 4 - The PEP-II Waveguide Loaded RF Cavity.

Figure 5 - Undamped (up) and damped spectra up to 1.4 GHz of the PEP-II cavity model [48].

Strong HOM damping is also required at the INFN-LNF e^+/e^- Φ-Factory DAΦNE [49] to reach the design luminosity. The machine is in construction at Frascati and consists of two intersecting rings for multibunch operation. One single cell room temperature 368 MHz copper cavity will be operating in each ring. Because of the low RF voltage required (250 kV peak), the FM impedance optimization was not of primary importance. A "door-bell" resonator with 80 cm long tapered beam pipes has been adopted. This shape, while keeping the FM impedance at an acceptable level, made possible to bring down substantially the r/Q values [2] and consequently, the HOM impedances are lowered by several factors, even without dampers, respect to more conventional solutions. Three rectangular 495 MHz cut-off WGs are applied to the cavity body for HOM coupling and other two with 1.2 GHz cut-off are connected to the tapered tubes to capture the parasitic modes propagating through the pipes. The WGs are then converted to coaxial lines with a gradual double ridge wideband low VSWR transition developed at LNF [50] which allows dissipation with commercial 50 Ω loads, via 7/8" coaxial vacuum feedthroughs. This design avoids the use of under vacuum brazed materials and permits to sample the HOM power. The overall estimated HOM power for a full beam (5 Amps) machine operation is lower than 3 kW and will propagate mostly throughout the larger WGs. The first cavity, equipped with HOM dampers, has been tested successfully to 30 kW that is about twice the nominal power. Figure 6 shows the DAΦNE cavity under test at Frascati.

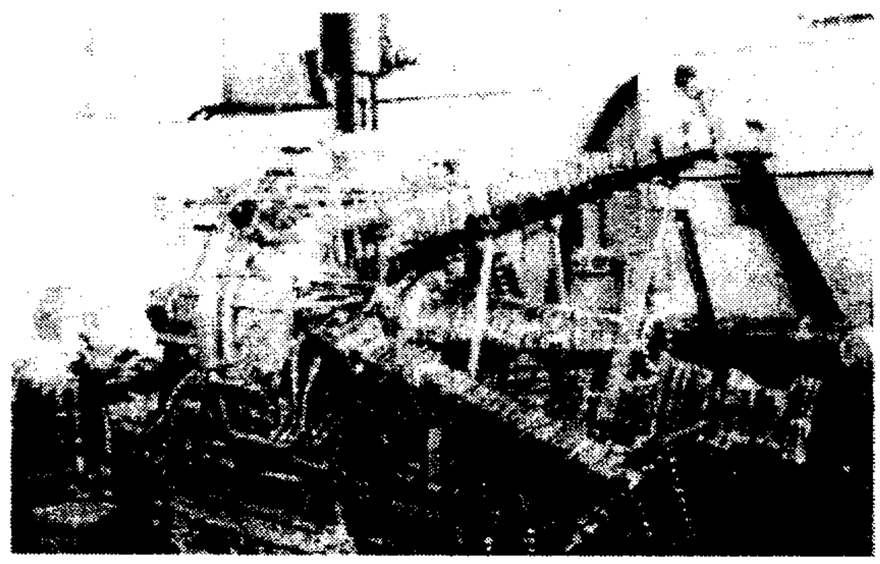

Figure 6 - The DAΦNE Cavity in the Power Test Hall.

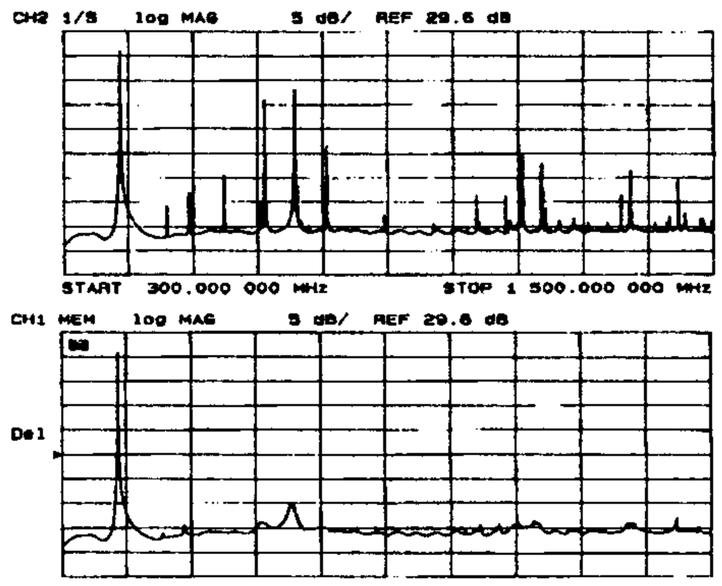

Figure 7 - Undamped (up) and damped longitudinal spectra of the DAΦNE Cavity.

Figure 7 shows the cavity longitudinal spectrum, measured with the "wire technique" [51], before and after connecting 50 Ω loads to the coaxial output of the WG transitions. The HOM impedances are damped to a few hundreds Ωs or less. The worst dipole mode Qs are also reduced to a few hundreds and have been evaluated by probe excitation. The additional power dissipation of the accelerating mode due to its penetration in the WGs is tolerable.

Among the HOM-free resonators, an important role plays the "choke-mode" cavity devised both for a damped linac structure [52] and a crab-cavity [53]. The concept has been applied to the room temperature KEK-B ARES resonator which is under test in Japan in parallel to the SC option [54]. It consists of a single cell copper cavity, sketched in Fig. 8, equipped with a large coaxial guide to extract monopole and dipole HOMs in the TEM and TE11 mode respectively. Since TEM mode has not cut-off, the coaxial guide requires a notch filter to block the cavity FM. However this is an advantage respect to WG loaded cavities where the RF currents are blocked by the WG slots. HOM power dissipation is achieved by 16 bullet shape sintered SiC absorbers inserted from the WG end. Recently [55], power tests have been made up to 150 kW-cw. The HOM damping performances [56] have been studied with simulation codes and found fully satisfactory.

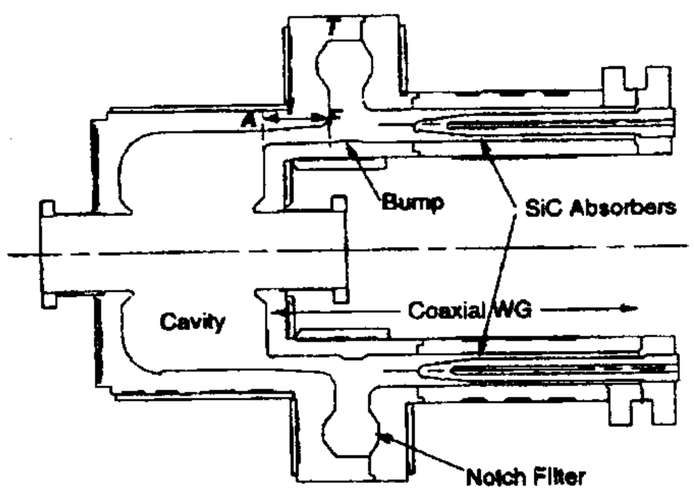

Figure 8 - Sketch of the NC Damped Cavity for KEK-B.

WG damped cavity design would have not been possible without powerful simulation codes (MAFIA, ARGUS) and post-processors [57]. The RF specialists get also great advantage in the use of the HFSS code [58] for designing three-dimensional electromagnetic devices as the Frascati WG-coaxial transitions or distributed structures like the FM notch filter of the KEK-ARES cavity.

Moreover, the HOM external Qs, due to damping WGs, can be predicted by means of methods based on the Slater's theory [59,60,61] and Kirchhoff's approximation [62] which are therefore helpful in the optimization of WG position and size. The author regrets not to have enough room to deepen this important aspect of the HOM-free cavities design. Other projects [63,64] are worthy of mention but they could not find space in this short note.

4 CONCLUSIONS

The HOM-free cavities are becoming real devices in accelerators for fighting beam instabilities and HOM power losses. Each solution offers its advantage depending upon the accelerator requirements. The use of WGs in NC cavities results in a satisfactory broadband HOM damping with a small cost in term of FM loss. Brazing techniques developed for the absorbing materials are getting reliable even though other original solutions, as the coaxial transitions, are worthy of consideration.

All the accelerator community is waiting impatiently full beam operations of the HOM-free cavities.

REFERENCES

[1] J.L. Laclare, CERN 87-03, 1987, p. 264
[2] S. Bartalucci et al., Part. Accel., 48-4, (1995), p. 213
[3] M. Thomas et al., Proc. 1989 PAC, p. 1859.
[4] M. Svandrlik et al., Proc. 1995 PAC, to be published
[5] D. Teytelman et al., SLAC-PUB 95-6879, May 1995.
[6] M. Izawa et al., KEK Report 88-7, 1988.
[7] L. Maier and J. Slater, J. Appl. Phys. 23(1), 1962, 68
[8] S. Bartalucci et al., NIM, A 309, 1991, p. 355.
[9] G. Oxoby et al., SLAC-PUB 6520, June 1994.
[10] M. Bassetti et al., Proc. 1992 EPAC, p. 807.
[11] E. Haebel, ibid. 10, p. 307.
[12] B. Dwersteg et al., Proc. 1985 PAC, p. 2797.
[13] D. Boussard et al., Proc. 1988 EPAC, p. 991.
[14] Y. Morozumi et al., Part. Accel., 29 (1990), p. 85.
[15] J. J. Song et al., Proc. 1994 EPAC, p. 1277.
[16] A.N.L., Y. Kang, private communication.
[17] P. Marchand, P.S.I. Int. Note, TM-12-89-06, 1989.
[18] V. Katalev et al., Proc. 1993 PAC, p. 916.
[19] P. Bernard et al, Proc. 1983 PAC, p. 3342.
[20] Y. Kojima, Proc.1984 Workshop on RF Supercond., p. 75.
[21] R. Sundelin et al., ibid. 19, p. 3336.
[22] B. Dwersteg et al., ibid. 19, p. 235.
[23] E. Haebel et al., ibid. 19, p. 281.
[24] T. Weiland, DESY 83-073.
[25] Ph. Bernard et al., Proc. 1991 Workshop on RF Supercond., p. 956.
[26] A. Mosnier, Proc. of the 1989 Workshop on RF Supercond., p. 377.
[27] CERN, D. Boussard, private communication.
[28] B. Dwersteg et al., Proc. of the 1987 Workshop on RF Supercond., p. 81.
[29] S. Noguchi et al, ibid. 26, p. 397.
[30] J. Sekutowicz, Proc. of the 1993 Workshop on RF Supercond., p. 426.
[31] J. Kirchgessner et al., Int. Note SRF950908-13, Lab. of Nucl. Studies, Cornell Univ., Ithaca, NY.
[32] T. Furuya et al., Proc. of the 1995 Workshop on RF Supercond.
[33] T. Kageyama, KEK P-133, 1991.
[34] W. Hartung et al., Int. Note CLNS 95/1339, Lab. of Nucl. Studies, Cornell Univ., Ithaca, NY.
[35] H. Padamsee et al., Int. Note SRF930527-09, Lab. of Nucl. Studies, Cornell Univ., Ithaca, NY.
[36] T. Tajima et al., KEK P 95-77, June 1995 A.
[37] T. Koseki et al., ibid. 15, p. 2152.
[38] F. Hinode et al., KEK P 95-45, May 1995 A.
[39] I. Campisi et al., ibid. 30, p. 587.
[40] A. Hutton, ibid. 15, p. 15.
[41] R. Palmer, SLAC-PUB 4542, July 1988.
[42] P. Arcioni et al., Part. Accel., 36 (1991), p. 177.
[43] A. Massarotti et al., Part. Accel, 35 (1991), p.167.
[44] "PEP-II Conceptual Design Report", June 1993, LBL-PUB-5379, SLAC-418.
[45] R. Rimmer et al., ibid. 15, p. 2101.
[46] R. Pendleton et al., ibid. 15, p.2013.
[47] LBL, R. Rimmer: private communication.
[48] R. Rimmer et al., ibid. 18, p 874.
[49] G. Vignola, "DAΦNE Status", Proc. 1995 PAC, to be published.
[50] R. Boni et al., Part. Accel., 45, 4, 1994, p.195.
[51] H. Hahn et al., BNL-50870, UC-414, April 1978.
[52] T. Shintake, Jpn. J. Appl. Phys., 31 L1567, 1992.
[53] K. Akai et al., Proc. 15th H.E.A.C., 757, 1992.
[54] T. Kageyama et al., KEK-P 95-52, May 1995, A.
[55] KEK, T. Kageyama: private communication.
[56] N. Akasaka et al., KEK-P 94-63, July 1994, A.
[57] P. Arcioni, SLAC-PUB 5444, March 1991.
[58] Hewlett Packard Part. N° 85180A., HP Corp.
[59] R.L.Gluckstern et al., Proc. 1988 Linac Conf. p. 356
[60] T. Kageyama, KEK Report 89-4, 1989.
[61] N.M. Kroll et al., SLAC-PUB 5171, Jan. 1990.
[62] S. De Santis et al., N.I.M. A 366 (1995), p. 53.
[63] D. Wisnivesky et al., ibid. 15, p. 1868.
[64] S. Sakanaka et al., ibid. 18, p. 1027.

MULTIBUNCH INSTABILITIES AND CURES

M. Serio, R. Boni, A. Drago, A. Gallo, A. Ghigo, F. Marcellini, M. Migliorati, M. Zobov
INFN-LNF, Frascati, Italy
L. Palumbo, INFN-LNF and Università La Sapienza, Roma, Italy
R. Claus, J. Fox, H. Hindi, J. Hoeflich, I. Linscott, J. Olsen, G. Oxoby, S. Prabhakar,
W. Ross, D. Teytelman, A. Young, SLAC, Stanford, USA
J. Byrd, J. Corlett, G. Lambertson, G. Stover, LBNL, Berkeley, USA

Abstract

The common approach to achieve the high luminosity needed for high precision measurements adopted by the particle factories now under construction consists in storing high current e^+e^- beams distributed in many bunches in separate rings. The beams are brought together to collide at one interaction point. An inconvenience of this strategy is that the performances can be seriously limited by unstable coupled-bunch oscillations excited by transients or noise and sustained by long-lasting parasitic resonating modes (high order modes-HOM) in the vacuum chamber, mainly in the RF cavities. Minimization of the HOM content and broad-band feedback systems together with the reduction of the driving transients are the complementary cures to this kind of disease. This paper introduces the subject with some examples and special emphasis on bunch-by-bunch feedback systems.

1 INTRODUCTION

All the e^+e^- particle *factories* aimed at high precision measurements now approved and under construction [1-3] have adopted a similar luminosity strategy that consists in resorting to "comfortable" single bunch beam-beam parameters and increasing as much as possible the number of colliding bunches.

The high current, multi-bunch approach moves the technical challenges elsewhere to the vacuum, RF and multibunch feedback systems. In fact, the operation is very critical with respect to longitudinal and transverse coupled bunch (CB) instabilities, caused by parasitic higher order modes in the ring, mainly in the RF cavities, and resistive wall impedance. These instabilities have been identified as a potentially severe limit on the ultimate achievable luminosity. The reduction of the beam-cavity interaction is of utmost importance and particularly demanding. The RF cavity designs have been aimed at reducing significantly the impedance of the high order cavity modes (HOM) by various means [4]. On the other hand, additional damping must be provided by a broad band feedback system capable of damping all coupled modes on a bunch by bunch basis. In this paper, after an introduction to the coupled modes terminology, we review the cures against multibunch instabilities with accent on time-domain digital feedback systems and we describe the first implementation at ALS.

2 MULTIBUNCH MODES

An ultra-relativistic beam in a storage ring of length $2\pi R$, with revolution time $T_0 = 2\pi R/c$ (c: speed of light) and revolution frequency $f_o = \omega_0/2\pi$, consisting of M equally-spaced bunches, can oscillate coherently in M different modes, depending on the phase relationship between the individual oscillations [5].

In order to look for suitable phase shifts between synchrotron oscillations (frequency = $\Omega_s/2\pi$) of adjacent bunches we consider the idealized situation of point-like bunches consisting of N particles of charge e on the same phase-plane orbit of radius τ_s . In the case of rigid bunch motion, the linear charge density is the sum of M periodic contributions :

$$\lambda(t) = \frac{Ne}{c} \sum_{b=1}^{M} \sum_{k=-\infty}^{\infty} \delta\left[t - \left(\frac{b}{M} + k \right) T_0 - \tau_b \right] \quad (1)$$

where

$$\tau_b = \tau_s \cos\left(\Omega_s t + \psi_b\right) \quad (2)$$

By expressing (1) as a Fourier series, we find non-zero terms at angular frequencies

$$\omega_{p,n} = \left(pM + n + mQ_s\right)\omega_0 \quad (3)$$

with Q_s the synchrotron tune, p running from -∞ to +∞, n = 0, 1, 2, .., M-1, defining the n-th mode of coherent CB motion and m = 1, 2, 3, ... , defining the phase-plane periodicity, provided the phase shifts between the perturbations of two adjacent bunches satisfy

$$\left(\psi_{b+1} - \psi_b\right) = \frac{2n\pi}{M}, \text{ modulo } 2\pi \quad (4)$$

With M equal bunches, M distinct longitudinal coherent CB modes can be excited. In Fig. 1 we show as an example a coherent synchrotron oscillation of six bunches, each oscillating with a phase advance of $2\pi/6$ with respect to the adjacent (mode number n = 1).

We see that the overall pattern of detected amplitudes can be fitted by two classes of sinusoidal signals, at positive and negative frequencies, equally spaced at M times the revolution frequency. Going to a representation with positive frequencies only, each coupled mode shows up as a pair of lines in the span Mf_0, i.e.: all modes appear once in any frequency span between pMf_0 and $\left(p+1/2\right)Mf_0$.

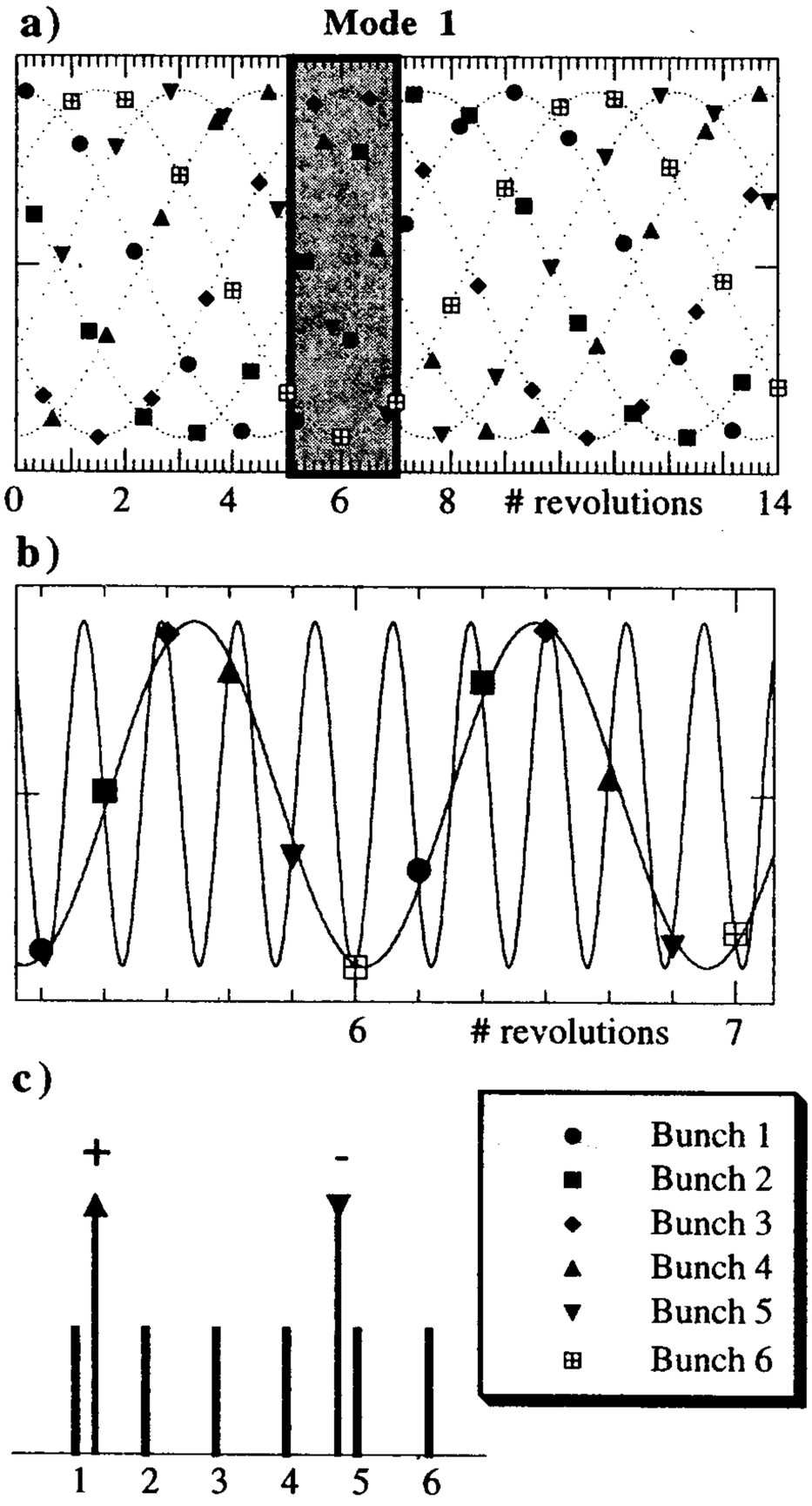

Figure 1: Example of a detected oscillation of $M = 6$ bunches executing coherent oscillations with $2\pi/6$ ($n = 1$) phase advance. **a)** Individual amplitude of oscillations for each bunch. **b)** Enlarged view of the shaded portion of a), with superimposed two high frequency modes at $(1+Q_s)\omega_0$ and $(-6+1+Q_s)\omega_0$. **c)** Spectrum analyzer representation (positive frequencies only) of modes b). The pattern repeats indefinitely every M-th revolution harmonics.

It is worth pointing out that among the sinusoids fitting the detected oscillation, those with ($p \geq 0$) present the same slope of the actual oscillation, while those with ($p < 0$) have an opposing slope.

We can now understand that if the real part of the impedance of a narrow band resonator crosses with a substantial value a CB mode frequency line, the bunch motion can be excited or damped, according to the relative slope of the motion and of the induced voltage in the resonator. In Fig. 1-c, we have labeled the stable line with "-" and the unstable one with "+". The situation is similar for all the other modes.

In the case of short (compared to the beam pipe radius) bunches, which is appropriate for high luminosity colliders, the growth rate of instability for each mode n can be computed approximately as [6]

$$\alpha_n = \frac{I_0\,\alpha_c}{4\pi Q_s\,E}\sum_p \omega_{p,n}\, e^{-\left(\omega_{p,n}\sigma_t\right)^2}\,\Re\left\{Z_l\left(\omega_{p,n}\right)\right\} \quad (5)$$

with I_0 the total current, α_c the momentum compaction factor, E the beam energy (eV), $\Re\left\{Z_l\left(\omega_{p,n}\right)\right\}$ the real part of the impedance and σ_t the rms bunch duration.

Since all coupled modes appear in a frequency interval $(M/2)f_0$, the growth rates α_n and the sum of offending impedances in (6) can be represented in an *aliased* way in the interval $0 \div (M/2)f_0$ [7]. Moreover, the minimum bandwidth required for an active feedback system to damp all the coupled modes must be half the bunch frequency.

In the high luminosity factories under construction it is very likely that undamped high order modes (HOM) in the storage ring, mainly in the RF cavities, give rise to growth rates much larger than the natural (radiation, Landau) damping rate because of the large total current and of the large number of possible CB modes, which are spaced at ~ the revolution frequency. In DAΦNE the line spacing is around 3 MHz, giving in principle some latitude to HOM displacement, but in larger rings (PEP-II, KEKB) the spacing of ~ 100 KHz is such that harmful interaction of some HOM impedance with CB modes is almost unavoidable: it is crucial to reduce the HOMs impedance as much as possible.

In addition, in large rings, the fundamental mode of the RF cavity itself can drive several CB modes and a feedback system around the cavity is needed.

It can be shown that for the transverse motion of M equally spaced bunches only every M-th line occurs for every n-th coupled mode:

$$\omega_{p,n} = \left(pM + n + Q_\beta + mQ_s\right)\omega_0 \quad (6)$$

where Q_β is the betatron tune and, again, $-\infty \leq p \leq +\infty$, $n = 0, 1, .., M\text{-}1$ and $m = 0, \pm 1, \pm 2, ...$, defining the m-th head-tail mode number.

Note that a coherent transverse mode $m = 0$ exists, corresponding to a dipolar transverse oscillation of the center of mass of a bunch with a stationary distribution in the longitudinal phase space; on the other hand, there are no longitudinal coherent modes at $m = 0$.

In the transverse case, multibunch motion can be driven by transverse HOMs in the cavities, but, in addition, modes at low frequency can be excited by the resistive wall impedance, which is large at low frequency. The bigger the size of the storage ring, the faster is the growth rate.

If the bunches carry unequal charges or they are not equally spaced we have a more complicated line pattern, but any motion can still be decomposed in terms of the orthogonal modes (3), (6).

3 HOM DAMPING

In synchrotron light facilities operating in the multi bunch mode, such as, for example, ALS (revolution frequency ~ 1.5 MHz) and Elettra (rev. freq. ~ 1.16 MHz) it has been possible to *park* the HOMs in *quiet* positions, by acting on the RF cavity temperature set point. In ALS it is possible to store 400 mA in 328 bunches without beam loss, but with self-limiting multibunch instabilities, both transverse and longitudinal. In Elettra, almost all longitudinal modes amplitudes can be reduced below 1° at 250 mA , with no sign of transverse effects [8].

The HOM shift approach above implies too many risks with respect to a predictable and consistent operation of a factory; therefore, extensive R&D work has been devoted to the development of HOM-free cavities. PEP-II and DAΦNE [4] adopt a similar design which consists of a room temperature resonator loaded with waveguides (WG) , whose cutoff frequency is higher than that of the accelerating mode. The WGs are connected to the cavity body to let the parasitic modes propagate out, with an effective reduction of their impedances by order of magnitudes.

In the PEP-II cavity the damping WGs are loaded with lossy ceramic tapers brazed inside [9]. In the DAΦNE cavity the WGs are terminated onto 50 Ω in air by means of broadband (0.5÷3 GHz) waveguide to coaxial transitions under vacuum, which have been developed at LNF to this purpose. This solution avoids the risks related to the heating of RF lossy materials brazed within the waveguides, in the ultra high vacuum environment of the accelerator.

The first DAΦNE cavity has been delivered and successfully tested at full power [10]. We have checked with a simulation program that the measured HOM Q are well within the capability of our bunch-by-bunch feedback system. In Fig.2 we show the measured spectrum of longitudinal impedance with and without the waveguide loads.

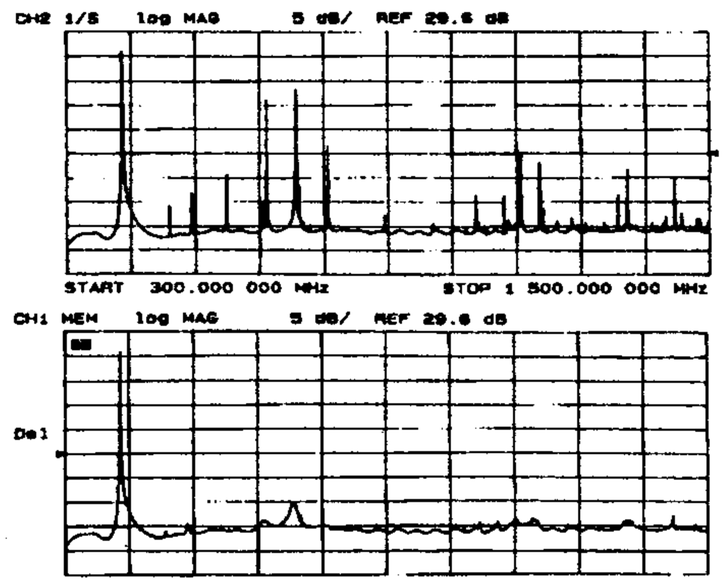

Figure 2: Spectrum of longitudinal HOM impedance of the DAΦNE RF cavity [10] with (lower) and without (upper) 50 Ω loads on the waveguides.

KEK has developed two designs for the B-Factory [3]. One, at room temperature (ARES), is based on a "choked" accelerating cavity coupled with an energy storage cell, and the other, superconducting, is a high gradient single cell with large aperture beam pipes to allow the propagation of HOMs outside the cell, where they are absorbed by ferrite loads.

4 FEEDBACK

In the presence of heavily damped HOMs in the accelerating cavity, the chance for a HOM to interact with a CB mode frequency becomes large and, because of the large total current, the growth rate of unstable modes can still be stronger than the natural damping rate. The complementary cure is an active feedback system capable to damp all the CB modes.

In principle the system can be equivalently realized in the frequency domain (mode feedback), or in the time domain (bunch by bunch). Regardless of the type of realization, as we have seen in section 3, the minimum bandwidth requirement is half the bunch frequency.

The mode feedback has been used successfully with few bunches [11] or in cases where a few dangerous cavity modes have been identified.

4.1 Bunch by bunch feedback

The bunch by bunch approach is more attractive since an *a-priori* knowledge of the endangered CB modes is not required. However, because of the HOM damping, they are likely to be evenly distributed over the spectrum.

In this system each bunch is treated as an individual oscillator. The basic components are: a time gated phase detector capable of continuous single bunch measurement; a bank of M parallel filters producing the correction kick signals, phase shifted by $\pi/2$ [12]; a broad-band power amplifier and a broad band kicker. See for example PEP [13] and UVSOR [14] with three and four bunches.

With a number of bunches of the order of thousand, as in the case of the B Factories, the parallel filter approach is of difficult realization. Fortunately, the electronic technology now available allows the realization of a mixed microwave-analog-digital system employing fast (≥ 500 Msamples/sec) analog to digital and digital to analog converters (ADC - DAC) and fast Digital Signal Processors (DSP) as filters. In Fig. 3 we illustrate the architecture of the DSP system adopted for PEP-II, ALS and DAΦNE, based on the results of considerable R&D work on feedback systems for the next generation of electron-positron colliders, carried out at SLAC.

The filter response is realized with an FIR (finite impulse response) band-pass filter, with peak gain at the base-band synchrotron frequency. It has to be software tunable in order to maintain the right phase shift over the range of the allowable synchrotron tunes.

The design specifications are such to meet the ultimate performance specifications of ALS, PEP-II and DAΦNE. Several components are the state of art of microwave and digital electronics, but all of them are commercially available.

A detailed description can be found in [15] and references therein. The first complete system is now running at ALS [16], where stable operation with 400 mA in 320 bunches has been routinely obtained. The capabilities of this system to collect and record data while operating can be exploited to carry on interesting machine studies, which are presented in [17].

The main advantage of such a system is that the same DSP can process several bunches, thus reducing the hardware complexity. Moreover, it is possible to take advantage of the relatively low synchrotron frequency and reduce substantially the sampling rate at which the synchrotron phase is detected. This results in less complex filters and reduces the overall data rate and computational load in the DSP section [18].

Table I below shows the relevant parameters for feedback systems at various machines. We remark the similarity of synchrotron damping times, bunch frequencies and data rate requirements. The approach taken by KEKB results in a similar architecture, with the important exception that it does not make use of down-sampling. The digital filter is implemented as a two-taps FIR with taps of value ±1 at 90° and 270° of the synchrotron oscillation [3,19]. This type of filter requires only a signed addition, but no multiplications, thus it is very fast. The DSPs are realized with CMOS memories and programmable logic. Each one is capable of dealing with 320 bunches. The fast data stream at the front-end is demultiplexed onto a parallel bank of 16 such DSPs by means of two custom GaAs fast demultiplexer chips. The processed data are multiplexed into the back end with a similar pair of fast GaAs multiplexers specially developed by OKI for KEK.

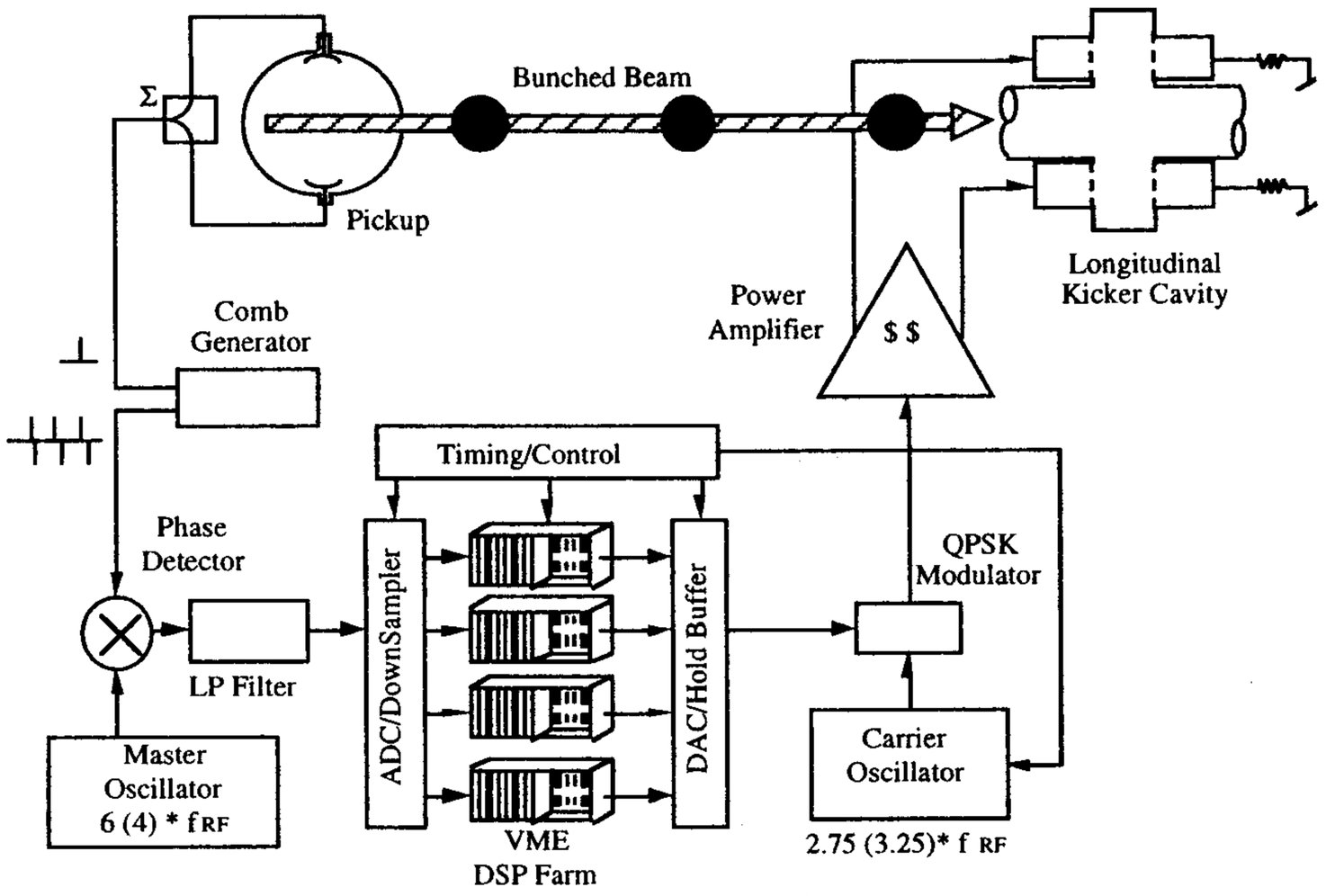

Figure 3 : Block diagram of the DSP based feedback system.

Table I - Summary of feedback related parameters of multi-bunch machines [1-3]

	PEP-II		KEKB		ALS	DAΦNE
	HER	LER	HER	LER		
Energy (GeV)	9	3.1	8	3.5	1.5	0.511
Revolution frequency (KHz)	136.3		99.39		1523.3	3068.8
Average current/bunch (mA)	0.59	1.29	0.22	0.51	1.22	43.7
Total beam current (A)	0.99	2.14	1.1	2.6	0.4	5.24
RF Voltage	14	5.5	10-20	5-10	1.5	.25
Number of cavities	20	6	36	10-20	2	1
Synchrotron damping time (ms)	19.8	26.4	23		10.7	17.8
Harmonic number	3492		5120		328	120
RF frequency (MHz)	476		508.9		499.6	368.3
Number of bunches	1658		5000		328	120
Bunch spacing (ns)	4.2		1.97		2.0	2.7
# revolutions per synchrotron period	22	28	50-100		138	56
Down-sampling factor	4	5	1		21	12
Next kick computation time (μs)	1.5		0.031		1.5	1.5
Data rate (MBytes/s)	56	45	500		24	31
# DSPs	80	64	16	16	40	60
Modular VXI/VMEArchitecture	√	√	"Single Board"		√	√

4.2 Longitudinal Kicker

The maximum power at the kicker is determined by the energy gain needed to achieve the required damping rate and the maximum synchrotron phase error allowed. The design of the kicker structure must be optimized in terms of shunt impedance and bandwidth in order to reduce the power requirement on the final stage, because broadband power is very expensive.

PEP-II and ALS [20] use two full coverage 25 Ω striplines connected in series by $\lambda/2$ lines to increase the shunt impedance (nominal value 400 Ω). In principle, this device is a matched load for the power amplifier and, being directional, no power from the beam is directed to power amp. On the other hand, proper tuning of this device is not easy. According to simulations and laboratory measurements, the stripline kicker is rich in HOM content and requires additional damping loops.

In order to increase the kicker shunt impedance and decrease the HOMs, a longitudinal kicker based on a WG loaded pill-box cavity has been designed for the DAΦNE feedback system [21]. A sketch is shown in Fig. 4.

The large bandwidth required to fill the cavity to any kick value in a time interval corresponding to the bunch time spacing is obtained by loading the accelerating mode with three single-ridged waveguides placed 120° apart on each pill-box side. Broadband waveguide-to-coaxial transitions similar to those in the RF cavity allow external connections to the power amp and loads.

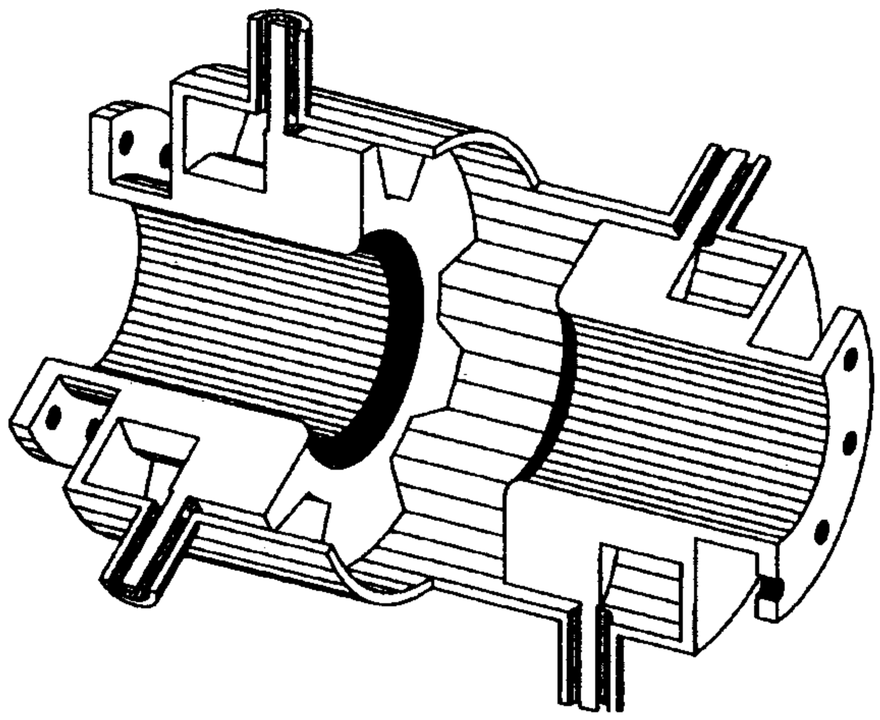

Figure 4: CAD view of the DAΦNE kicker cavity.

The measured shunt impedance is 620 Ω, with a half power bandwidth of 250 MHz, centered at ~ 1200 MHz, i.e. (3+1/4) times the RF frequency. According to simulations with the values of the RF HOM impedances, a large bandwidth power amplifier of ~ 200 Watt is enough to damp an initial offset of 100 ps with operation at 30 bunches. Two kicker cavities per ring will eventually be installed for operation at the full nominal current with 3x200 Watt power amplifiers per cavity, each feeding separately a waveguide coupler.

Being broadband, the kicker cavity does not need to be tuned in operation, nor cooled, since almost all the power is dissipated in the external loads. Moreover, the damping waveguides couple out the HOMs as well. However, the overloaded cavity is not a directional device like the stripline kicker: it extracts power from the beam. Ferrite circulators are then necessary to isolate the output section of the power amplifier.

REFERENCES

[1] G. Vignola: "DAΦNE, the first Φ-Factory", this Conference.

[2] J. T. Seeman: "PEP II Status and Plans", Proceedings of 1995 PAC and ICHEA, Dallas.

[3] S. Kurokawa: "KEK-B Status and Plans", Proceedings of 1995 PAC and ICHEA, Dallas.

[4] R. Boni: "HOM Free Cavities", this Conference.

[5] M. Serio, M. Zobov, "Measurement of Transverse and Longitudinal Spectra", Proceedings of the 1st DIPAC, Montreux, CERN SL/93-35 (BI), pp. 74-82 (1993).

[6] F. Pedersen: "Multibunch instabilities", in: Factories with e^+e^- Rings, Lecture Notes in Physics 425, Springer Verlag, pp. 269-292 (1994).

[7] J. Byrd et al.: "Study of Coupled-bunch Collective Effects in the ALS", Proceedings of 1993 PAC, Washington D.C., p. 3318.

[8] M. Svandrlik, private communication.

[9] R. Pendleton et al.: "PEP-II B-Factory Higher Order Mode Load Design", Proceedings of 1995 PAC and ICHEA, SLAC-PUB 95-6864 (1995).

[10] A. Gallo et al.: "High Power Test Of The Waveguide Loaded RF Cavity For The Frascati Φ-Factory Main Rings", this Conference.

[11] A. Renieri, F. Tazzioli: "The Longitudinal Feedback System in Adone", Proceedings of 1974 ICHEA, SLAC - Stanford, p.370 (1974).

[12] M. Bassetti et al.: "DAΦNE Longitudinal Feedback", Proceedings of 3-th EPAC, Berlin 1992, p. 807.

[13] M.A. Allen et al.: "A Longitudinal Feedback System for PEP", IEEE Transactions on Nuclear Science, Vol. NS 26, No 3, p. 3287 (1979).

[14] T. Kasuga, H. Yonehara: "Suppression of Longitudinal Coupled-Bunch Instability in UVSOR", Proceedings of 1989 PAC, Chicago, p. 918 (1989).

[15] G. Oxoby et al., "Bunch by Bunch Longitudinal Feedback System for PEP-II", Proc. of 4-th EPAC, London 1994, p. 1616.

[16] D. Teytelman et al.: "Operation and Performance of the PEP-II Prototype Longitudinal Damping System at the ALS", Proc. of 1995 PAC and ICHEA, Dallas.

[17] J. Fox et al.: "Observation, Control and Modal Analysis of Coupled-Bunch Longitudinal Instabilities", this Conference.

[18] H. Hindi et al.: "Down Sampled Signal Processing for a B Factory Bunch-by-Bunch Feedback System", Proc. of 3-th EPAC, Berlin 1992, p. 1067.

[19] M. Tobiyama, E. Kikutani et al.: "Development of a Two-Tap FIR Filter for Bunch-by-Bunch Feedback Systems", Note KEK 95-104 (1995).

[20] J.N. Corlett et al., "Longitudinal and Transverse Feedback Kickers for the ALS", Proc. of 4-th EPAC, London 1994, p. 1625.

[21] A. Ghigo et al.: "Kickers And Power Amplifiers For The DAΦNE Bunch-By-Bunch Longitudinal Feedback System", this Conference.

FRINGING FIELDS IN LOW-BETA MAGNETIC ELEMENTS

M. Bassetti and C. Biscari, INFN-LNF, Frascati, Italy

Abstract

The effect of the fringing fields in the low beta regions of DAΦNE are investigated. Due to the crossing angle the beam trajectory passes off axis in low beta quadrupoles and detector solenoids. The modification of the linear optics due to the magnetic field profile and to the linear expansion around the trajectory of the field components is considered. The non linear fringing field multipolar expansion is deduced from the longitudinal behaviour of quadrupole field gradients and solenoidal longitudinal magnetic field. Its effects on the beam dynamics are studied.

1 INTRODUCTION

DAΦNE, the Frascati Φ-factory [1], is a double ring e^+-e^- collider. The two rings share two Interaction Regions (IRs) where the opposite beams travel off-axis and cross at the Interaction Point (IP) at a tunable horizontal angle of θ_{cross} = ±10-15 mrad. Three experiments, DEAR [2], KLOE [3] and FI.NU.DA. [4], will be installed at different times in the IRs. While the DEAR experiment is transparent from the optics machine point of view, the presence of solenoids in the other two experiments is a strong lattice perturbation and the corresponding IR lattice designs [5] are determined by each detector characteristics.

The first approach to the IR linear optics was done with the usual rectangular model for solenoids and quadrupoles. To improve the model we use a very powerful and already known property: the knowledge of the fundamental functions on the axis of a magnet, i.e. the gradient for a quadrupole and the longitudinal field for a solenoid, is enough to deduce the off axis field components at all higher order terms. This global approach embraces what is usually referred to as the 'fringing field' problem, from the point of view either of the linear optics and of the non linear effects.

Using largely the theory developed in a recent paper [6], analytical functions, deduced from cylindrical current models, have been used to fit the longitudinal behaviour of the fundamental functions and analytical descriptions of the fields satisfying Maxwell equations inside the cylinder at any order are therefore available.

The magnetic field in the IRs is a superposition of quadrupolar and solenoidal field. The Rotating Frame Method (R.F.M.) [7] is applied to compensate the coupling and to produce uncoupled beams at the IP and outside the IRs: the quadrupoles immersed in the solenoid are tilted following the rotation of the transverse plane introduced by the longitudinal magnetic field. The integral of the longitudinal component of the magnetic field is cancelled by two superconducting solenoids placed in the IRs outside the detector. The residual coupling due to the fact that the quadrupole tilts do not follow continuously the longitudinal magnetic field component integral is corrected by using four parameters per each side around the IP: three additional quadrupole tilts of the order of few mrad and a correction on the field integral of the compensator.

2 POTENTIAL AND FIELD REPRESENTATION

We describe the IR magnetic fields deducing them from the expressions of the scalar potential of each magnetic element, and adding the contribution of the different element acting on each point. The scalar potential of a solenoid in cylindrical coordinates is:

$$P_0(r,z)=\left\{G_{00}(z)+G_{02}(z)r^2+G_{04}(z)r^4+\ldots\right\}$$

G_{00} is the integral of the longitudinal component on the axis and the functions G_{02k} are related to it by:

$$G_{02k}(z)=(-1)^k\frac{1}{4^k(k!)^2}\frac{d^{2k}G_{00}(z)}{dz^{2k}}$$

The scalar potential of a quadrupole is:

$$P_2(r,\theta,z)=\frac{r^2\sin 2\theta}{2}\left\{G_{20}(z)+G_{22}(z)r^2+\ldots\right\}$$

while the one corresponding to a quadrupole tilted by an angle θ_T is:

$$P_2(r,\theta,z)=\frac{r^2\sin 2(\theta+\theta_T)}{2}\left\{G_{20}(z)+G_{22}(z)r^2+\ldots\right\}$$

G_{20} is the gradient on the axis and G_{22k} are given by:

$$G_{22k}(z)=(-1)^k\frac{2}{4^k k!(2+k)!}\frac{d^{2k}G_{20}(z)}{dz^{2k}}$$

The fundamental functions $B_z(0,z)=\frac{dG_{00}(z)}{dz}$ and $G_{20}(z)$ describe the fringing field behaviour at lower order. Functions $G_{n2k}(z)$, $m>0$ describe the higher order

fringing fields. B_z and G_{20} are deduced from magnetic code calculations in the design stage of the magnet and from measurements on the real magnet.

3 ON-AXIS LINEAR OPTICS

For every IR magnetic component we have fitted the available measures or the magnetic computations with analytical and differentiable expressions, which can be found in [6]. Fig. 1 shows as an example the superconducting compensator measured field and the corresponding fitting function, which in this case was originated by two superimposed cylindrical currents differing in radius, length and intensity.

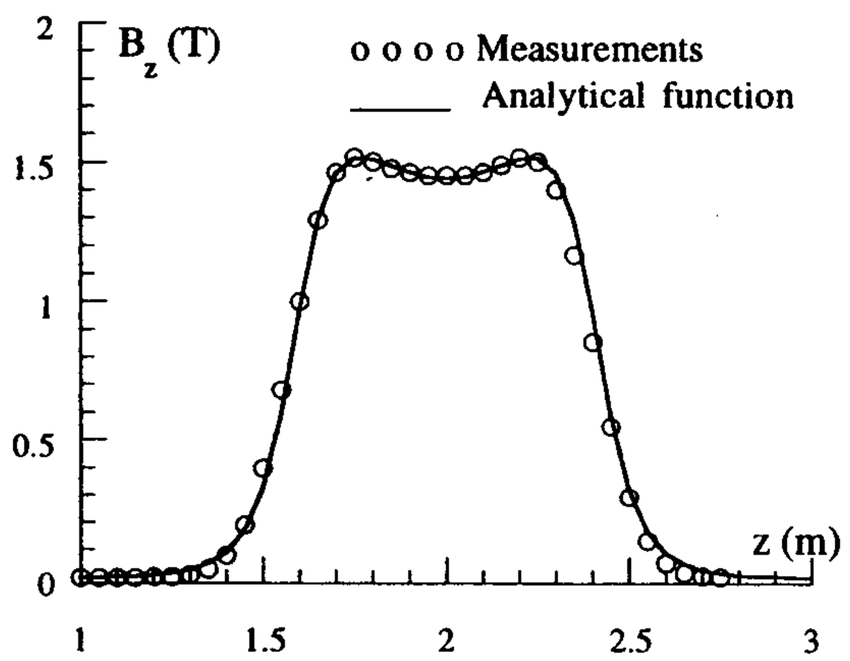

Figure 1 : B_Z on the axis of the compensator solenoid.

Figure 2 shows the fundamental functions of quadrupoles and solenoids along half IR for the design corresponding to KLOE experiment.

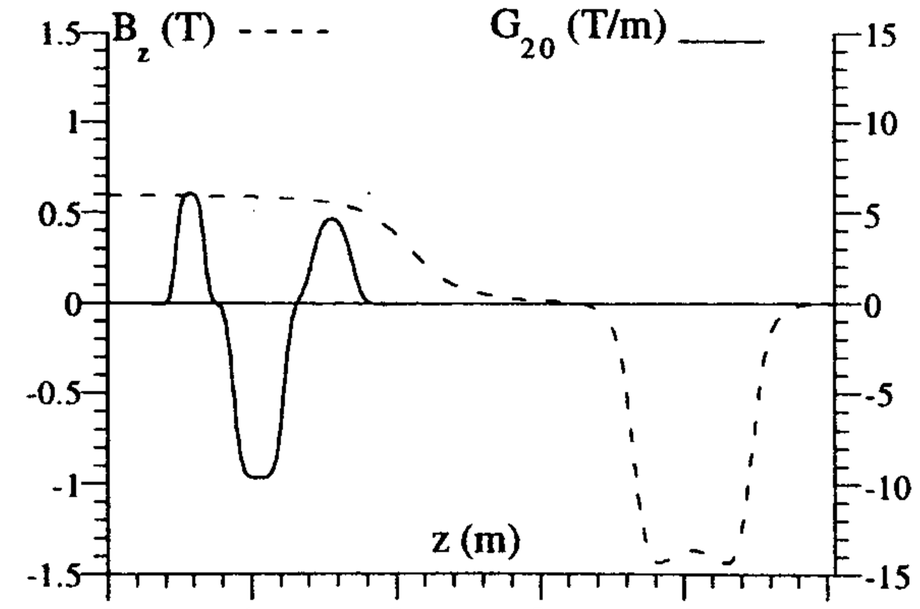

Figure 2 : KLOE IR solenoidal and quadrupolar fundamental functions.

As a first step to improve the rectangular model, the 'sliced' model [8] has been applied, which consists in computing the total IR transport matrix as the product of N linear rectangular model transport matrices, whose characteristic parameters follow the quadrupole and solenoid fundamental functions.

An analysis on the DAΦNE different types of quadrupoles and solenoids has been done separately on each element, before using the method on the whole transport matrix. For quick optical calculations, as for example control system codes, the transport matrix obtained with the sliced model can be still written on each plane as a quadrupole matrix, with the two characteristic parameters different in the two planes, their difference increasing with the fringing extension and with the gradient. In the focused plane the quadrupole strength decreases if compared to the rectangular model strength with the same integrated gradient; in the defocused one it increases.

The solenoid rectangular model transport matrix can be written as the product of a rotation matrix and of a focusing in both planes quadrupole matrix. The rotation matrix corresponding to the sliced model is equal to the rectangular model one, while the focusing matrix corresponds to a weaker focusing strength.

The differences between the rectangular and the sliced model are in general negligible in the overall optics of a ring, and can be summarized as a negative tune shift. They become relevant when quadrupoles with large aperture and strong gradient are placed in high beta position, as is the case of DAΦNE low beta quadrupoles. In KLOE and FI.NU.DA the quadrupoles are permanent magnet ones, and their specifications have been defined by applying the sliced model to the preliminary magnetic calculations. In fact by applying the sliced model to the DAΦNE optics we have found tune shifts of - 0.01 in both planes due to the quadrupoles outside the IRs, while the differences in tunes when the IR quads are included increase up to (-0.03,-0.07).

4 OFF-AXIS LINEAR OPTICS

Beams travel off-axis in the IRs. The nominal trajectory has been computed integrating the equations of motion from the IP to the IR end. The linear jacobian around the trajectory has been successively computed. Let's remind that if a magnetic vector potential **A** is present, the generalized canonical variables associated to x, y are $P_{x,y} = p_{x,y} + eA_{x,y}$, instead of the variables $p_{x,y}$, normally used in optics calculations. We have integrated the motion in the usual variables and transformed them to the generalized ones knowing the vector potential at the initial and final point of our system. At the IP, which corresponds to the center of the detector solenoid, the magnetic vector potential is [9]:

$$A_x = -\frac{1}{2} y B_z$$

$$A_y = \frac{1}{2} x B_z$$

while it is of course negligible at the IR end. We checked that the jacobian computed as the transformation between the generalized canonical variables is simplectic.

As expected, there is a very good agreement between the linear IR transport matrix computed with the 'sliced' model and the jacobian computed around the axis.

Information about the phase advance and the optical functions at the IR end are deduced from the jacobian. The jacobians computed at trajectories crossing at different angles are slightly different: for the nominal optical parameters at the IP (β_x = 4.5 m, β_y = 4.5 cm), as θ_{cross} increases the phase advance along the IR increases, especially in the vertical plane. In fact around the off axis trajectory the quadrupoles add an alternate bending action, like a wiggler, which, as it is well know, gives a vertical focusing. In the presence of solenoids this focusing acts in the direction perpendicular to the trajectory plane point by point. At the IR end, where the normal modes become horizontal and vertical because of the RFM method, the increase in phase advance appears in the vertical plane.

There is also another change in the off-axis linear optics due to the pseudo-octupole (G_{22}) appearing in the quadrupole fringing, which expanded around the off-axis trajectory modifies the linear quadrupole gradient. While the integral of G_{22} on the axis is zero, it is non null when integrated on the off-axis trajectory. Its influence on the IR optics is however much smaller than the previous effect.

The dependence of the machine tune on the crossing angle is shown in Fig. 3, for the DAΦNE configuration corresponding to KLOE + DEAR experiments.

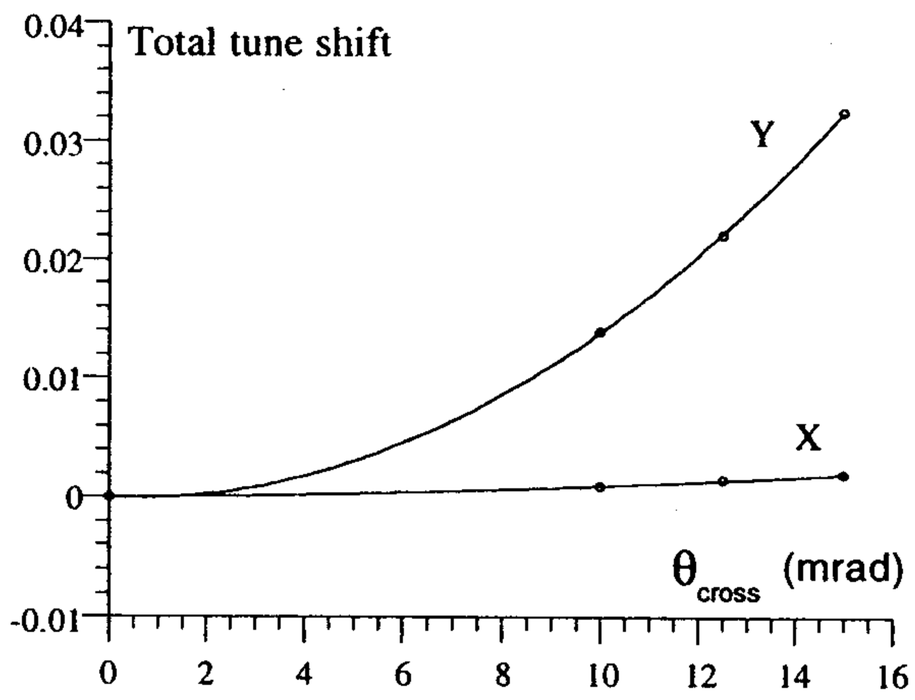

Figure 3 : Tune shift with crossing angle due to linear optics modification.

The R.F.M. had been applied up to now only on axis, and in fact if only linear terms of the field are included, the on-axis or off-axis methods are equivalent.

The four parameters which are used for decoupling the motion between the IP and the IR end, i.e. the three quadrupole tilting angles and the integral of the longitudinal magnetic field on the compensator solenoid depend in principle on the crossing angle.

Using the linear terms of the jacobian computed around the trajectory, it is possible to readjust the values of the decoupling parameters by minimizing the non diagonal elements of the jacobian, i.e.:

$$\frac{\partial x}{\partial y}, \frac{\partial x}{\partial P_y}, \frac{\partial P_x}{\partial y}, \frac{\partial P_x}{\partial P_y}, \frac{\partial y}{\partial x}, \frac{\partial y}{\partial P_x}, \frac{\partial P_y}{\partial x}, \frac{\partial P_y}{\partial P_x}$$

Since the jacobian is simplectic, vanishing four elements implies the vanishing of the remnant ones.

The differences between the decoupling parameters with θ_{cross} in the nominal range have resulted smaller than the alignment tolerances, which are set to 0.1°.

5 CONCLUSIONS

The fringing field effect due to the IR quadrupoles and solenoids on the linear optics has been investigated with the 'sliced' model.

The main trajectory in presence of all significant higher order terms and the jacobian around it has been computed. The dependence of the RFM parameters on the crossing angle has been studied, and shows to be negligible if compared with the coupling tolerances requested.

Presently multiturn tracking is being performed by integrating particle motion along the IR and applying the linear matrix from the IR end to its beginning, matched to the values obtained from the jacobian computation. First results show the appearance of resonances due to the non-linear fringing terms, which give rise to emittance exchange between the two transverse modes, with a strength which depends of course on the tune values. When far from the resonances the coupling parameter is kept under the design values (κ=1%). To understand deeply the real extent of the phenomena more investigation is needed.

REFERENCES

[1] G. Vignola and DAΦNE Team, 'DAΦNE, the First Φ-factory, this conference.

[2] The DEAR collaboration, The DEAR Proposal, LNF-95/055 (IR), Oct.1995.

[3] KLOE collaboration, KLOE, LNF-92/019(IR), Apr.1992.

[4] FI.NU.DA. collaboration , FI.NU.DA., LNF-93/021(IR), May 1993.

[5] M.E. Biagini, C. Biscari, S. Guiducci, DAΦNE Techical Note L-22, April 1996.

[6] M. Bassetti, C. Biscari, Analytical Formulae for Magnetic Multipoles, Particle Accelerators, to be published.

[7] M.B assetti, M.E. Biagini, C. Biscari, The compensation of Solenoidal Perturbation, to be published.

[8] C. Biscari, Quadrupole modelling, DAΦNE Technical Note L-23, June 1996.

[9] M. Bassetti, First order compensation of solenoidal field by skew quadrupoles (SQ), CERn-ISR-TH/79-41.

AN UHV VACUUM SYSTEM FOR DAΦNE

V. Chimenti, A. Clozza, C. Vaccarezza, INFN-LNF, Frascati, Italy

Abstract

A 510 MeV high luminosity Φ-Factory is under construction in Frascati. The main goal of the vacuum system is to maintain a mean pressure of $1 \cdot 10^{-9}$ Torr, after conditioning, with a stored current of 5.3 A per beam. The vacuum chamber is almost entirely made of aluminum. The inner surface of the chamber has a roughness of about 0.1 - 0.2 μ R_a. The vacuum system is completely oil free and all the vacuum components are all metal type. Special RF shielded bellows were designed avoiding any sliding contact. The synchrotron radiation produced by bending magnets and wigglers is intercepted by water cooled copper synchrotron light absorbers. The design of the pumping system is optimised in order to install the required pumping speed, about $1.2 \cdot 10^5$ l/s, on a 100 m long ring. A combination of titanium sublimator pumps, sputter ion pumps and non evaporable getter pumps as been chosen.

1 INTRODUCTION

The DAΦNE Φ- Factory [1] is a twin ring 510 MeV e^+e^- collider facility under construction at INFN-LNF in Frascati. A mean pressure of $1 \cdot 10^{-9}$ Torr with a stored beam of 5.3 A is required in each ring. A 10-meter long vessel constitutes the vacuum chamber of the eight bending sections. One of the bending sections of the positron ring is shown in Fig. 1. The selected material is Al 5083-H321 and the vacuum chamber is milling machined in two halves and welded along the perimeter. Special care has been taken in order to lower as much as possible the desorption yield from the vacuum chamber walls.

The procedure for the aluminum surface treatment is reported in section 2. Special RF shielded bellows were designed in order to follow the longitudinal expansions and the offsets of the vacuum chamber (section 3). Water cooled absorbers are employed to cope with the Synchrotron Radiation (SR) produced in the wigglers and dipoles, as reported in section 4. The total gas load in each of the electron/positron ring is $Q \approx 1.2 \cdot 10^{-4}$ Torr l/s for CO, with a photodesorption rate of $\eta \approx 1 \cdot 10^{-6}$ molec/ph [2], after ≈ 40 Ahr of conditioning. The required pumping speed for each ring is $\approx 1.2 \cdot 10^5$ l/s, and is achieved using Titanium Sublimation Pumps (TSP), Sputter Ion Pumps (SIP), and Non Evaporable Getter Pumps (NEG), (see section 5).

2 VACUUM CHAMBER

2.1 Vacuum chamber design

Both the two rings of the DAΦNE collider can be mainly divided into three parts: bending sections, straight sections, with injection and RF cavities, and interaction regions. In the bending sections, arcs, the main concern is the high and concentrated photodesorbed gas load due to the synchrotron radiation emitted in the two dipoles and the wiggler. The arc vacuum chamber is designed in such a way that the most of the synchrotron radiation is stopped by water cooled copper absorbers. A 10÷ 20 mm slot divides the beam channel from an antechamber where the absorbers and the pumping stations are located. In Fig. 2 two arc cross sections, with beam chamber and antechamber and pump ports, are shown, referring to the dipole and wiggler vacuum chambers respectively.

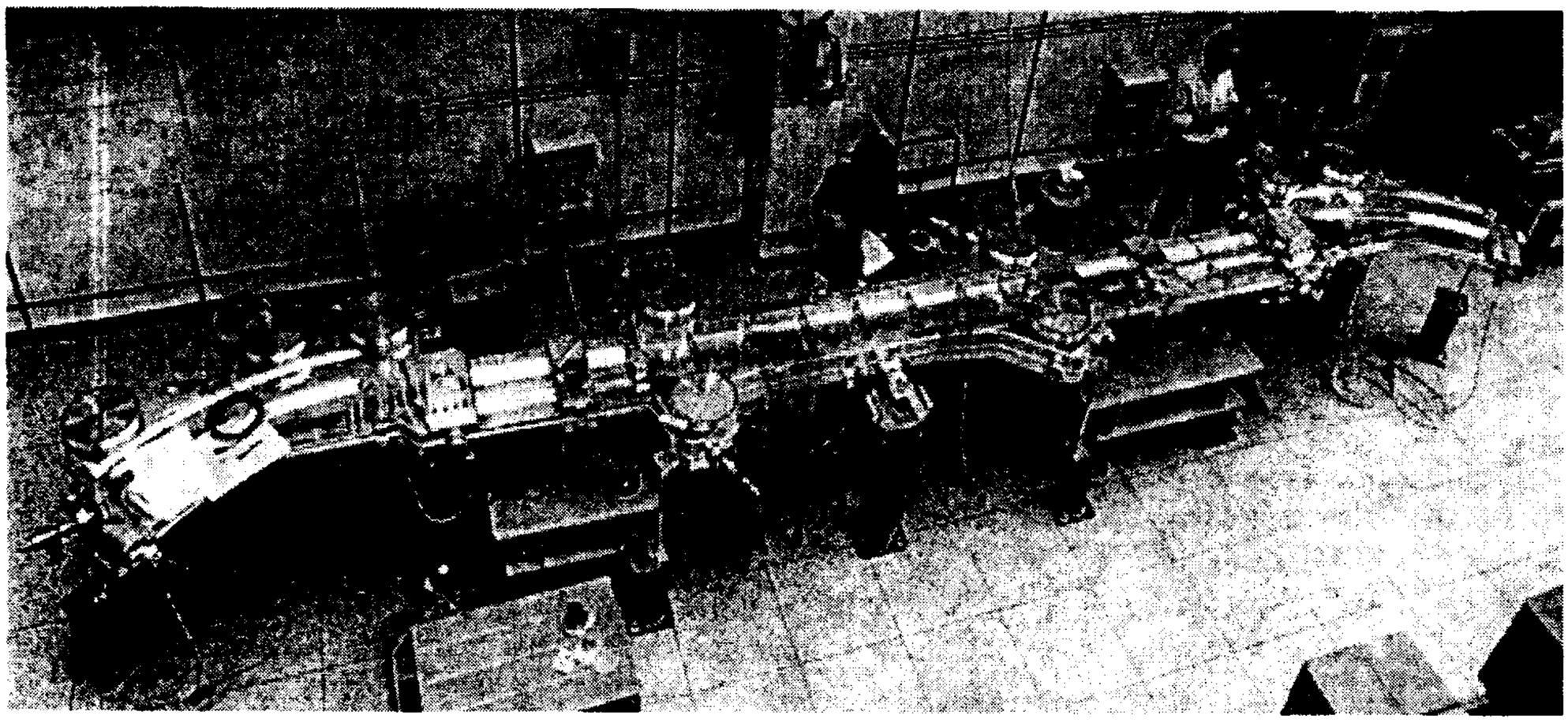

Figure 1: One of the arcs of the DAΦNE positron ring, under testing at the LNF vacuum laboratory.

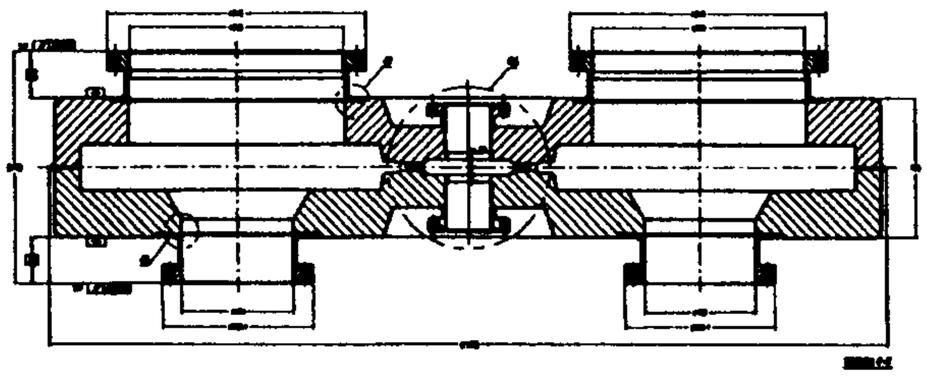

Figure 2: Two cross sections of the arc vacuum chamber, are shown. The first on top corresponds to the wiggler, the second below to the dipoles.

For the straight sections, (injection and RF cavities), a circular Al 6082 vacuum pipe is provided, tapered to match the vacuum chamber cross section of each lattice element, in order to reduce the impact of the vacuum chamber impedance on the beam dynamics. The two interaction regions of the DAΦNE Φ-Factory, consist of a stainless steel AISI 304L (with copper coating) tapered pipe up to the interaction point where two thin Be vacuum chambers (500 μ thick), are provided according to the experiment requirements.

2.2 Machining and cleaning

Each of the arcs is a 10-meter long aluminum vessel milling machined in two halves from a 120 mm thick Al 5083-H321 plate, (1.6 m width, 10 m length), thoroughly ultrasonic tested. In order to lower as much as possible the surface desorption yield the roughness of the surface has been limited to an average value $R_a \leq 0.2$ μ. The measured value in the most critical points, i.e. the beam closest zones, is $R_a \approx 0.15$ μ.

Considerable care has been taken of the Al surface contamination during the machining. The CIMSTAR MB-602 has been employed as cutting liquid, avoiding any contamination with sulphur or silicone compounds. For the Aluminum surface cleaning a detergent solution with Almeco 18 (HENKEL) at 50 °C has been used [3], followed by rinse with distilled water; reducing in this way the aluminum three-hydroxide formation on the surface.

The first four positron arcs have been tested. After few cycles of 150 °C bake-out for 48 hours each, the measured specific outgassing rate is: $q_d \leq 1 \cdot 10^{-14}$ Torr l s^{-1} cm^{-2}, obtained both dynamically and with the rising pressure method.

The ultimate pressure (with one pump of $S = 200$ l/s) turned out to be $P \approx 4 \cdot 10^{-11}$Torr, close to X-Ray limit of $2 \cdot 10^{-11}$ Torr of the ionisation gauge.

2.3 Gaskets and bolts

For the mixed joints aluminum-stainless steel of the DAΦNE ring vacuum chamber, the Helicoflex gaskets will be used; Al diamond type gaskets will be used for the aluminum-aluminum joints. (The Al diamond gaskets result to be reliable also for the mixed joints with a lower bake-out temperature, e.g. T ≈ 120 °C). In order to avoid the use of any lubricant, many self-lubricant alloys have been tested for the bolts production. The Cu-Al bronze turned out to have the best mechanical properties, but it is slightly magnetic and it results to affect the nominal value of the magnetic field of the main ring dipoles, if close to the flanges. The Cu-Sn bronze will be adopted. Prolonged bake-out tests showed that these bronze bolts maintain their reliability at least up to 200 °C.

3 RF SHIELDED BELLOWS

Between the DAΦNE arcs and the straight section vacuum chambers, special RF shielded bellows will be mounted [4]. They must allow 35 mm longitudinal expansion and 10 mm horizontal offset, mainly during the bake-out. Any sliding contact will be avoided to prevent the burning out due to the high current flowing on the bellows screen, and the creation of dust particles between the sliding surfaces. The bellows screen consists of thin CuBe-C17000 waved strips, (150 μ thick, 5 mm wide) vertically oriented and separated by small gaps. The strips will be hot formed and connected to the stainless steel AISI 316L bellows by brazing or mechanical clamp.

4 SYNCHROTRON RADIATION ABSORBERS

The DAΦNE synchrotron radiation absorbers are realised in one monolithic object (including the flange), from a bar of OFHC Copper.

In order to avoid any water-vacuum joint, the cooling channel is entirely machined as one path from the outside water inlet/outlet. Detailed calculations, together with laboratory tests, of the absorber deformation under the radiation load, show that any distorsion remains in the tolerances of the project.

5 PUMPING SYSTEM

The arc pumping system is designed to guarantee a mean operating pressure of $1 \cdot 10^{-9}$ Torr with a circulating current of 5.3 A.

The total photon flux per arc is :

$$N_{tot} = 8.8 \cdot 10^{20} \ \text{ph/s}. \qquad (1)$$

The resulting gas load is:

$$Q = \frac{N_{tot} \cdot \eta}{3.4 \times 10^{19}} = 2.6 \times 10^{-5} \ \text{Torr l s}^{-1} \ (20\ ^\circ\text{C}), \qquad (2)$$

where η (molec/ph) is the phodesorption rate of the Al vacuum chamber after conditioning [2].

The synchrotron radiation (SR) is almost entirely intercepted by the copper absorbers located in the antechamber, leading to a high and concentrated photodesorbed gas load. Close to the copper absorbers nine pumping stations per arc are located, each one consisting of a Titanium Sublimator Pump (TSP) on top, and a Sputter Ion Pump (SIP) below, see Fig. 3.

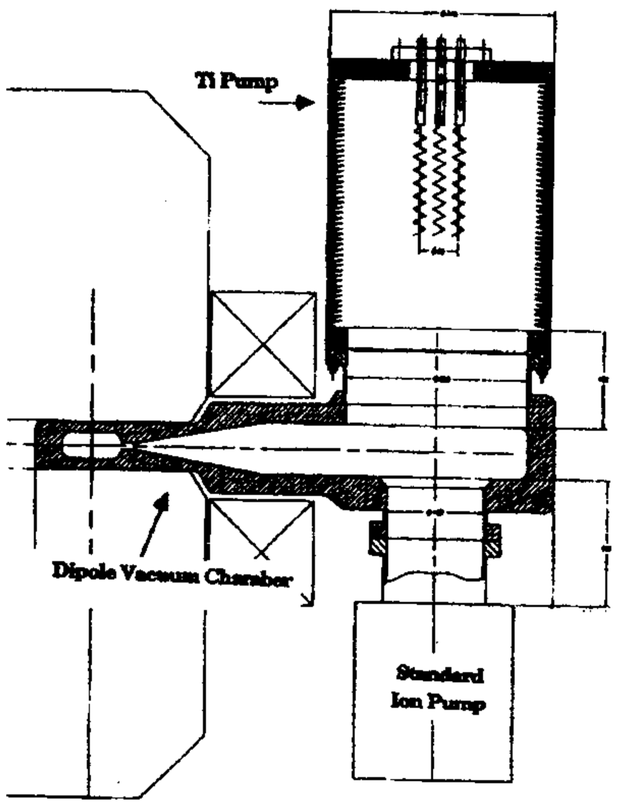

Figure 3: Final full scale prototype of DAΦNE TSP-SIP pumping station and Dipole vacuum chamber.

Combined with a SIP (200 l/s), each TSP has to provide:

$$S = \frac{2.8\times10^{-6}}{2\times10^{-9}} \approx 1.4\times10^{3} \ \text{l/s} \ , \qquad (3)$$

where the value $2\cdot10^{-9}$ Torr is the maximum pressure allowable in the arc to maintain a mean pressure of $1\cdot10^{-9}$ Torr in the ring. In Fig. 4 the performance of one Ti filament is reported.

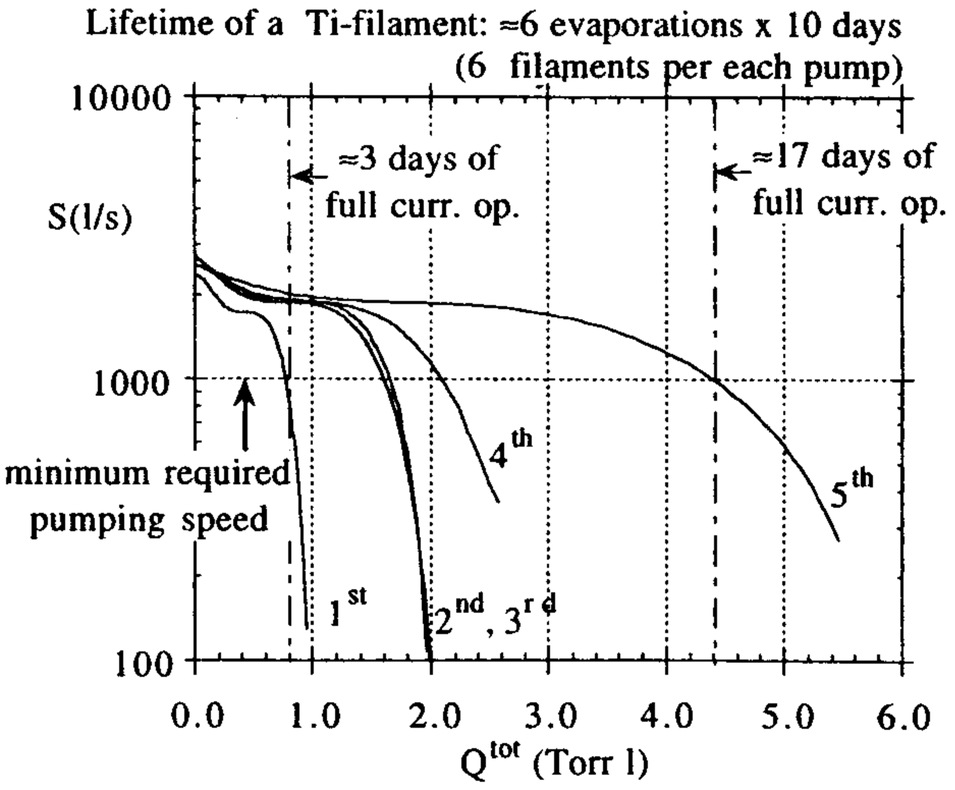

Figure 4: The pumping speed S (l/s) of the DAΦNE TSP with one Ti filament is reported vs. the total pumped gas load Q^{tot}(Torr l). Each filament allows 6 sublimation covering ≈ 60 days of full current operation (after conditioning). Each TSP cartridge provides 6 filaments.

In each TSP a cartridge of 6 filaments will be mounted, which is supposed to cover 6x60 days of full current operation, after conditioning. In the straight sections conventional Sputter Ion Pumps (Starcell, 200 l/s) are employed. For the interaction region Non Evaporable Getter (NEG) pumps have been chosen. In the experiment detectors design no room is available for lumped pumps set-up, therefore the NEG elements are arranged around the beam pipe, separated from the beam by a proper RF shield. A new high capacity composition of the getter Capacitorr™ has been tested at the Frascati Labs for the first time.

In Fig. 5 the performance of the new getter in its final configuration has been reported. The gas load of this section is $Q \approx 1\cdot10^{-7}$ Torr l/s, the required pumping speed is $S \approx 1000$ l/s, the test results indicate for this pump a duration time of tenth of years before re-activation (500 °C).

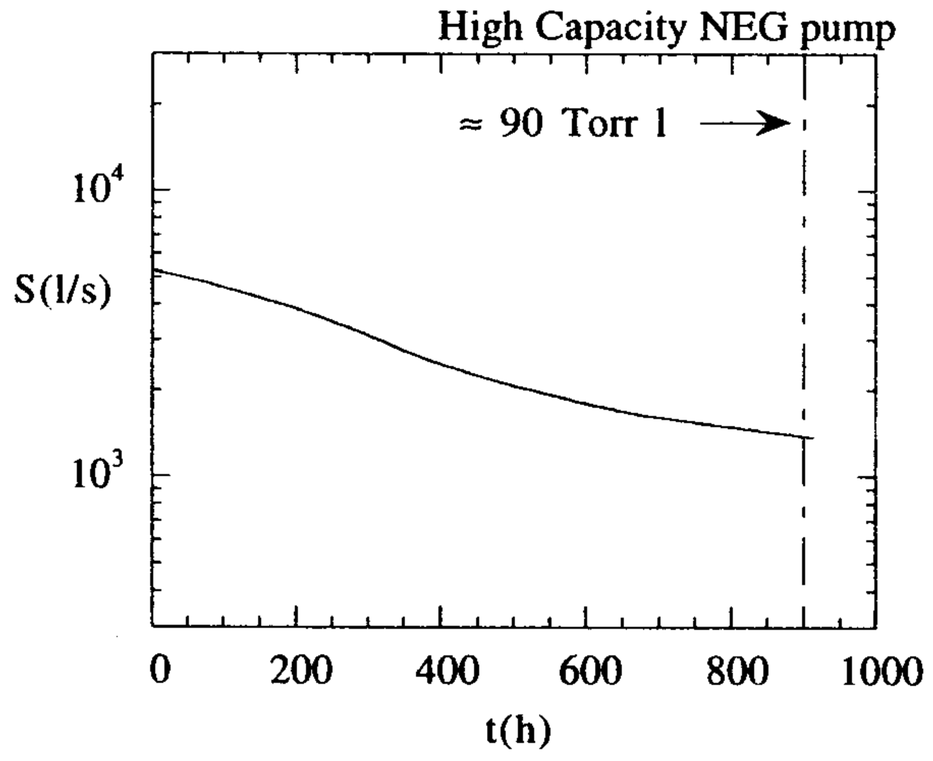

Figure 5: The result of the test on the final configuration of the DAΦNE High Capacity NEG is reported. The pumping speed S (l/s) vs. time is shown. The testing conditions relate 900 hr to ≈ 90 Torr l of pumped gas.

CONCLUSIONS

A UHV vacuum System for DAΦNE has been designed. The first arc vacuum chambers have been tested matching the specified project requirements. The different pumping system elements in their final configuration have been tested together with the performance of the Synchrotron Radiation absorbers, giving satisfactory results.

REFERENCES

[1] "DAΦNE, the first Φ-Factory", by G. Vignola, this Conference.

[2 Foerster C., Halama H., Vaccarezza C., to be published.

[3] R.A. Rosenberg, M.W. McDowell, J.R. Noonan, Jou. Vac. Sci. & Tech. A, vol.12, no.4, pt.1, p. 1755-9, Aug. 1994.

[4] "Impedance of DAΦNE shielded bellows", by M. Zobov, this Conference.

BEAM - BEAM INTERACTION STUDY FOR DAΦNE

K. Hirata, KEK, Tsukuba, Japan
M. Zobov, INFN-LNF, Frascati, Italy

Abstract

The right choice of a working point is very important for good collider performance.

We use a recently developed beam - beam simulation code in order to find a suitable working point for DAΦNE [1].

The performed tune scan shows reasonably large "safe" area around working points $(\nu_x, \nu_y) = (0.09, 0.07)$ and (0.53, 0.06), which both have an optimum luminosity, acceptable tail growth and satisfactory dynamic aperture. The possibility to employ the two interaction points in DAΦNE is also analyzed.

1 INTRODUCTION

The working points situated close and above integer (half-integer) tune values seem to be preferable for satisfactory collider performance, of course, if this choice does not lead to degradation of a machine dynamic aperture. The main reasons for that are following:

- the smaller beam-beam tune spread, i. e. the smaller number of resonance lines crosses a beam footprint;
- the lower order resonance lines are less dense there;
- close (above) integers, dynamic beta [2] and dynamic emittance [3] effects play a significant role in the beam-beam interaction. The emittance grows slower than the beta function decreases as the tune gets closer to an integer. This leads to the beam size shrinking which can partly compensate the beam blow up.

Here, in order to find a suitable working point for DAΦNE we perform a scan in the tune areas close (above) to the integer (half-integer) tunes by using a recently developed beam-beam simulation code [4]. The simulation algorithm is fully symplectic in the 6-dimensional phase space, and includes all the known effects as the effects of the crossing angle, finite bunch length, variation of β along the bunch during collisions, energy loss due to the longitudinal electric fields etc.

Finally, we simulate the case of DAΦNE operating with two interaction points having the different horizontal betatron phase advance between them.

Table 1 summarizes the main DAΦNE parameters used in the beam-beam simulations.

Table 1. DAΦNE parameters relevant for simulations

Energy, E	510	MeV
Circumference, C	97.69	m
β_x at IP	4.5	m
β_y at IP	0.045	m
Emittance, ε_x	10^{-6}	m·rad
Emittance, ε_y	10^{-8}	m·rad
Bunch length, σ_z	0.03	m
Synchrotron tune, ν_z	0.012	
Particles/bunch, N	$9 \cdot 10^{10}$	
Crossing angle, ϕ	±12.5	mrad
Tune shifts, ξ_x/ξ_y	.04/.04	
Damping time:		
horizontal	110540	turns
vertical	109650	turns
longitudinal	54620	turns

2 COLLISIONS AT A SINGLE INTERACTION POINT (IP)

2.1 Working point (0.09; 0.07)

We find the dependence of beam sizes and the luminosity on the tunes by scanning ν_x - ν_y plane in the range of $0.01 < \nu_{x,y} < 0.21$. In order to examine the equilibrium beam sizes the beam-beam collisions and revolutions through the ring are simulated for up to 10 radiation damping times. Because of the rather long damping time in DAΦNE in terms of the revolution turns (about 10^5 turns) in order to save CPU time the scan is rather rough with a step of $\Delta\nu_{x,y} = 0.01$. The strong bunch is longitudinally sliced into 5 slices, and the weak one is represented by 50 superparticles. The luminosity is estimated by a convolution of the distribution function of the two beams.

Figure 1 shows a luminosity contour plot in the ν_x — ν_y plane. The darker areas correspond to the higher luminosities with the design luminosity being the maximum value. The contour spacing is 10% in luminosity reduction.

On the contour plot we can clearly see the reduction of luminosity due to various resonances: $\nu_x = \nu_y, \nu_x = 2\nu_y$, $6\nu_y = 1$ and others. The absolute minimum of the luminosity in the given tune region is near the intersection of the beam-beam resonances of the sixth order and the resonance $\nu_x = \nu_y$. The number of areas where the luminosity can reach the design value is limited: there are two areas near the vertical integer tune, one area is close to the horizontal integer tune and another one is situated between the resonances $\nu_x = \nu_y$ and $\nu_x = 2\nu_y$. Numerical simulations have shown that the three former areas have a very small dynamic aperture, while for the working points in the latter one a satisfactory dynamic aperture can be found [5].

In particular we consider a point $\nu_x = 0.09$; $\nu_y = 0.07$ as a possible candidate for the DAΦNE working point. For this working point the luminosity reaches 95% of the nominal value.

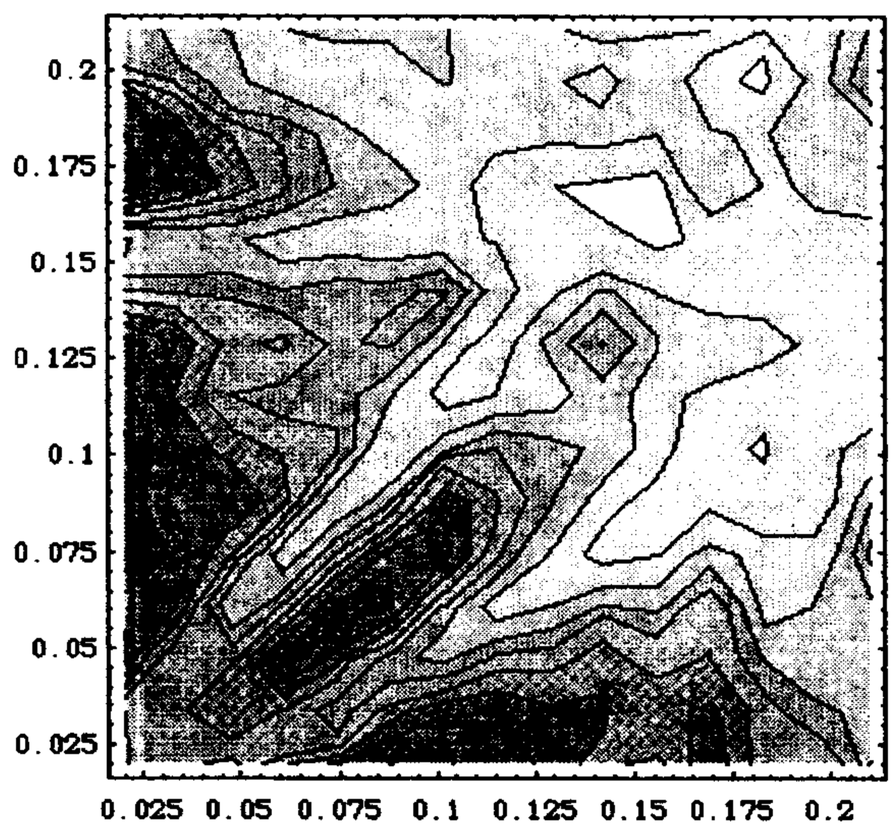

Figure 1 - Luminosity contour plot (scan). The abscissa and ordinate are the horizontal and vertical tunes, respectively.

For the chosen working point we repeat simulation with 500 particle in the weak beam and 10 slices in the strong one. The results do not differ substantially from those with 5 slices and 50 particles. After 10^6 turns the luminosity is equal to 95.3% of the design value.

The finer tune scan with a step of $\Delta\nu_{x,y} = 0.0025$ has been done in the vicinity of the working point which confirms that the tune area with an acceptable beam-beam performance is reasonably large.

2.2 Working point (0.53; 0.06)

Our main concern about the working point (0.09; 0.07) consists in the fact that it is situated rather close to the main diagonal ($\nu_x = \nu_y$) which could perturb the control of the coupling between transverse planes.

From this point of view a horizontal tune slightly above half integer would be preferable. The working point (0.52; 0.08) of the KEK B-factory is a good example [6].

We could expect also a better dynamic aperture for such a point. The working point (0.09; 0.07) lies near the strong resonance $\nu_x = 2\nu_y$ excited by sextupoles and appearing in the first order in perturbation, while the points above half integer are near the resonances appearing in the second order in the perturbation.

Hopefully, the DAΦNE lattice with the momentum compaction $\alpha_c = 0.02$ [5] is rather flexible giving the possibility to change the working point from (0.09; 0.07) to the working points above the half-integer in the horizontal plane by simple tuning of the magnet strengths without any mechanical adjustment.

We explore the tune region above the horizontal half-integer by performing the numerical tune scan in the range $0.51 < \nu_x < 0.6$; $0.01 < \nu_y < 0.1$.

Figure 2 shows the corresponding luminosity contour plot.

We can see a relatively large safe area near the vertical half-integer tune. In particular, the simulation for the working point (0.53; 0.06) with 500 particles in the weak beam and 10 slices in the strong one gives the luminosity which is equal to 98% of the design value, the maximum vertical amplitude of 24.6 σ_y and the maximum horizontal amplitude of 4 σ_x.

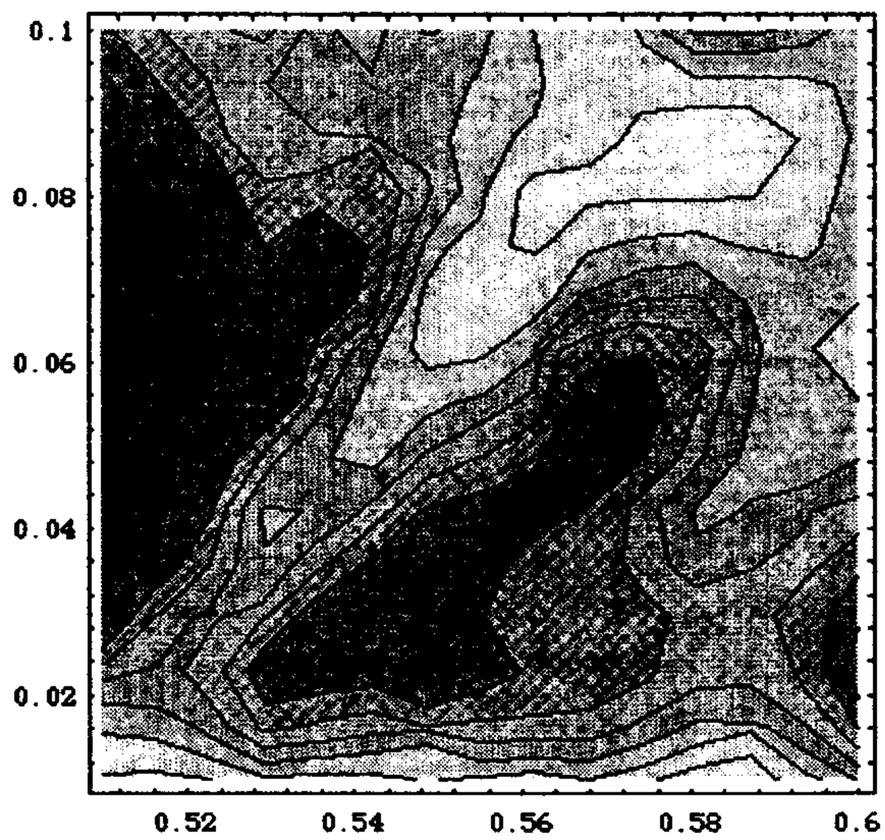

Figure 2 - Luminosity contour plot above horizontal half-integer. The abscissa and ordinate are the horizontal and vertical tunes, respectively.

3 ESTIMATES OF TAIL GROWTH

The growth of bunch tails due to beam-beam interactions for the two chosen working points, (0.09; 0.07) and (0.53; 0.06), has been studied with a long-term strong week calculation. The simulation have been done by tracking 50 superparticles over 10^8 turns.

Figures 3 and 4 show the calculated vertical particle distributions $\rho(I_y)$ as a function of the action variable I_y. Here we define the normalized vertical amplitude as $A_y^2 = 2I_y$.

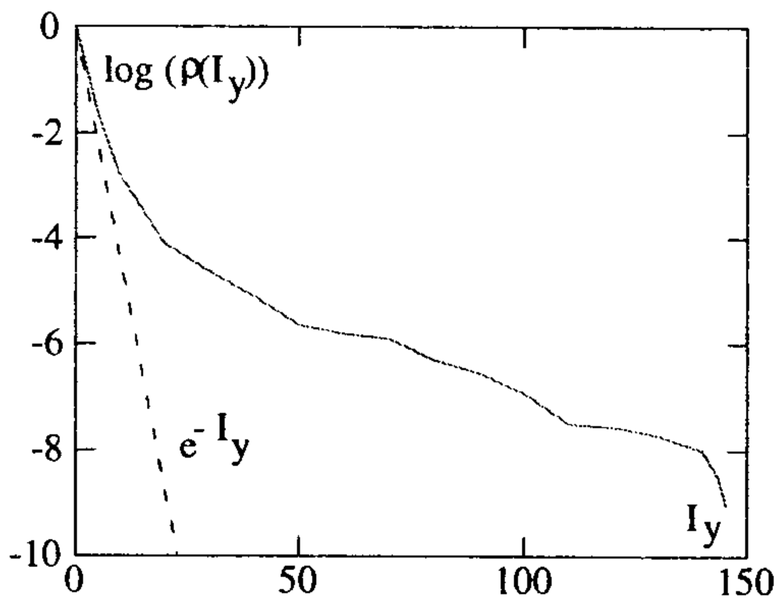

Figure 3 - Particle distribution in the vertical plane (working point (0.09; 0.07)).

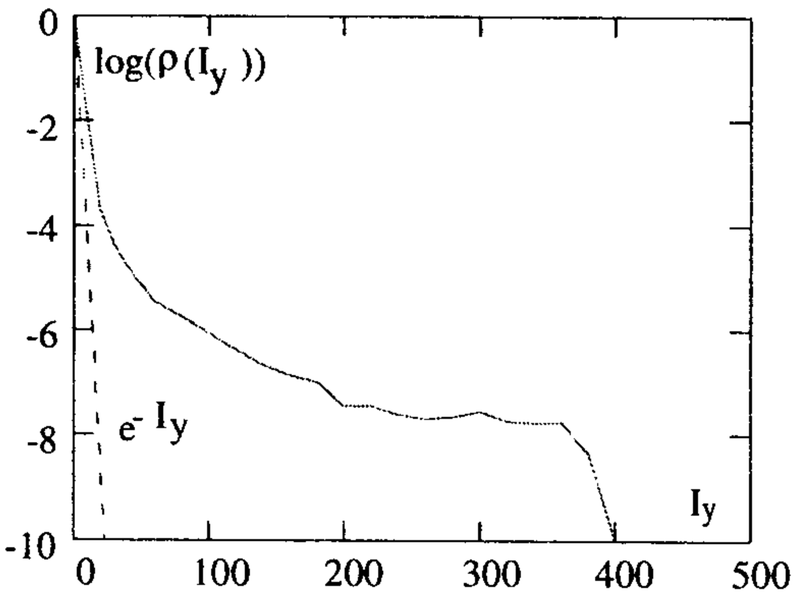

Figure 4 - Particle distribution in the vertical plane (working point (0.53; 0.06)).

The very core of the distributions has the nominal Gaussian distribution, while the non-gaussian tails are observed for the higher particle amplitudes. As it can be seen, only a very small fraction of the bunch population with $\log \rho(I_y) < 10^{-8}$ has vertical amplitudes beyond 17 σ_y for the working point (0.09;0.07) and 28 σ_y for the point (0.53; 0.06). The growth of horizontal bunch tails is much slower than in the vertical direction.

In order to get more precise information on the distribution at the higher amplitudes we are planning to use a recently developed code [7], allowing considerable reduction of the necessary CPU time, which showed a good agreement with the tracking for KEKB parameters [8]. However, since DAΦNE dynamical and physical apertures are larger than 70 σ_y at the coupling k = 0.01 [5], any substantial particle losses and background problems due to the beam-beam induced tails are not expected.

4 COLLISIONS AT THE TWO IP

The DAΦNE main rings consist of two rather different arcs ("Short" and "Long") having different horizontal phase advances between the two IPs.

It is known that phase advance differences between IPs break the symmetry of a collider, i. e. introduce new, low order resonances thus deteriorating the collider performance. In order to investigate a possibility to employ both IPs for the experimental study in DAΦNE we have simulated beam-beam collisions at these two IPs.

Table 2 and Table 3 show the tune advance between the two IPs in DAΦNE for two different working points.

Table 2. Tunes between IPs for the point (0.09;0.07)

	Short	Long	Total
ν_x	2.279	2.811	5.09
ν_y	3.035	3.035	6.07

Table 3. Tunes between IPs for the point (0.10;0.14)

	Short	Long	Total
ν_x	2.324	2.776	5.10
ν_y	3.070	3.070	6.14

Despite the differences in the horizontal tunes between IPs the weak-strong simulation for the nominal working point (0.09; 0.07) shows only a slight reduction in luminosity to 86% of the design luminosity value per each IP. For the other working point (0.14; 0.10), chosen for a comparison, luminosity drops from 61% with a single IP to 21% per each IP in the two IP collisions.

4 CONCLUSIONS

Simulations of the beam-beam interaction with an ideal linear lattice have shown that the two proposed working points both have an optimum luminosity close to the design value and acceptable tail growth.

However, the beam-beam study will continue in order to include the nonlinearities of the machine lattice and explore the bunch distribution tails at large amplitudes.

ACKNOWLEDGEMENTS

The authors would like to thank prof. L. Palumbo for useful discussions. Dr. M. Migliorati is acknowledged for his assistance in installing the simulation code at LNF INFN. One of the authors (K. H.) thanks the hospitality extended to him during his stay in LNF INFN.

REFERENCES

[1] "DAΦNE Machine Project", LNF-94/055, 1994.
[2] B. Richter, Proc. Int. Sym. Electron and Positron Storage Rings, Saclay, 1966.
[3] K. Hirata and F. Ruggiero, Particle Accelerators 28,-137 (1990).
[4] K. Hirata, Phys. Rev. Lett. 74, 2228 (1995).
[5] M. E. Biagini, C. Biscari, S. Guiducci, DAΦNE Technical Note: L-22, 1996.
[6] "KEKB B - Factory Design Report", KEK Report 95-7, August 1995 (A).
[7] D. Shatilov, to be Published in Particle Accelerators.
[8] D. Shatilov, "Beam-Beam Tail Simulations for KEK B - Factory", to appear as a KEK report.

MAGNETIC MEASUREMENTS OF THE DIPOLE, QUADRUPOLE AND SEXTUPOLE PROTOTYPES FOR THE ACCUMULATOR OF DAΦNE, THE FRASCATI Φ–FACTORY

H. Hsieh, M. Modena, M. Preger, C. Sanelli, S. Vescovi, INFN-LNF, Frascati, Italy
TESLA Engineering Limited, Water Lane, Storrington, Sussex, RH20EA, England

Abstract

DAΦNE is a Φ-Factory, presently under construction at INFN-LNF in Frascati. Injection is performed through a Linac and an intermediate damping Accumulator. The Dipole, Quadrupole and Sextupole magnets of the Accumulator have been designed at LNF. Prototypes of each kind of magnet have been built by TESLA Engineering (UK) and magnetically characterized at LNF before series production. Construction of 8 dipoles, 12 quadrupoles and 8 sextupoles has been completed and each magnet measured at LNF before complete machine assembling. The results of point by point (Hall probe system) and integrated measurements (rotating coil system) are presented.

1 INTRODUCTION

DAΦNE [1] is a Φ-factory, expected to be completely assembled in the Frascati National Laboratory (LNF) at the end of 1996. Its injector consists of a 800 MeV electron (550 MeV positron) Linac and a 32 m long damping/storage ring (Accumulator) [2].

The contract for the construction of the Accumulator Ring has been awarded to Oxford Instruments (UK) [3] in July 1993, on the basis of an international tender. TESLA Eng. has been appointed by Oxford as a subcontractor for the construction of the magnets. All the Accumulator magnets have been completely designed by LNF in order to set a sound Specification for the tender. However, the seller was responsible for the magnet performances, and therefore free to make changes to the basic design (with LNF approval). Only minor changes have been proposed by the manufacturer.

Series production of the magnets has been completed, and systematic magnetic measurements to characterize mechanical and magnetic properties of each magnet have been performed. Here we present the results obtained on the dipole, quadrupole and sextupole prototypes.

2 DIPOLE

The Accumulator dipole is an "H" type solid steel magnet with a bending radius of 1.1 m, a nominal field of 1.55 T and 0.5 field index. Its magnetic parameters are listed in Table 1.

Preliminary tests performed on the prototype showed good agreement between measured and calculated parameters. As an example, the current required to reach the nominal field was only 1.7% larger than expected. However, the harmonic analysis of the field at the magnet center showed a dominant octupole component, which is hard to correct and harmful to the beam dynamics. For this reason, the final choice for the pole profile was a simple, flat one; in this way a better field quality with a sextupole-like major high order contribution was obtained. Figure 1 is a sketch, on a vertically enlarged scale, of the shapes of the first and second pole profiles.

Table 1 - Magnetic parameters of the dipole

Quantity	8
Nominal Magnetic Field (T)	1.545
Maximum Magnetic Field (T)	1.66
Gradient (T/m)	0.657
Bending Radius (m)	1.1
Deflection Angle (deg)	45
Magnetic Arc Length (mm)	864
Magnet Gap at center (mm)	42
Good Field Region (mm)	±30
|ΔB/B| at magnet center (%)	0 ÷ -0.08
Nominal Current (A)	590
Maximum Current (A)	700

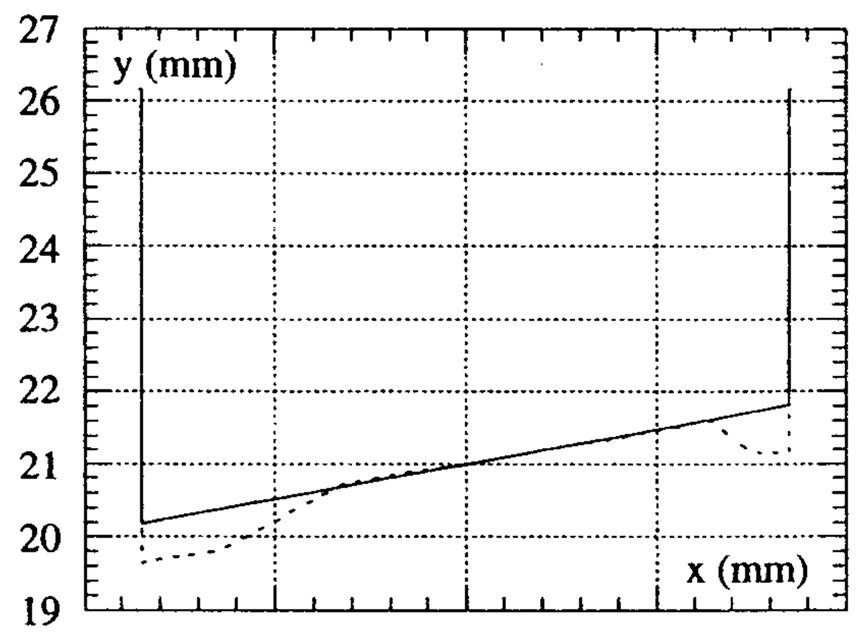

Figure 1 - Shimmed (dotted) and flat (full) pole profiles.

Figures 2 and 3 show the two measured fractional deviations from the ideal linear field. Note that the two plots have different vertical scales and that the solid vertical lines represent the limits of the good field region. Both the measured and calculated (by means of 2-D FEM) deviations are referred to an ideal linear field with the slope of the measured field at the magnet center.

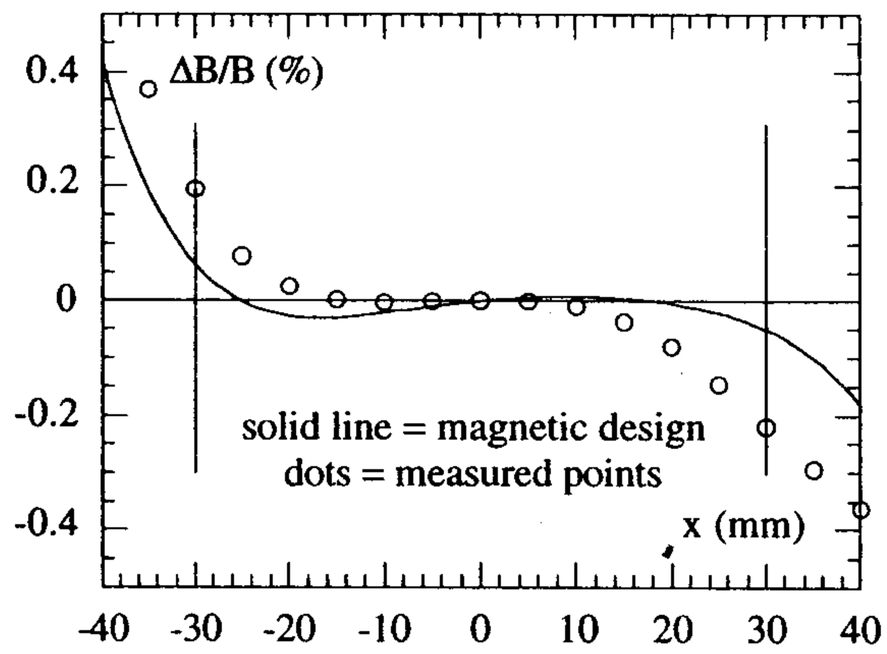

Figure 2 - Field quality with shimmed pole profile.

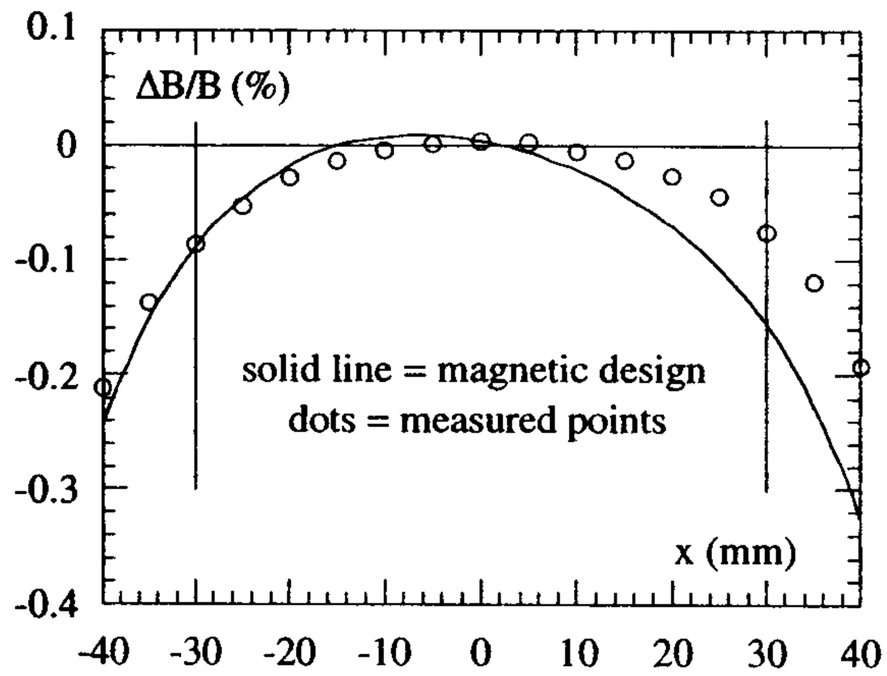

Figure 3 - Field quality with flat pole profile.

For such a short magnet, the contribution of nonlinear terms, mainly sextupoles, in the fringing field region is rather large, and needs to be locally corrected to keep the overall chromaticity of the machine within tolerable limits. We have therefore applied shims on the end caps, measuring the contribution of non linear terms with different geometries. Figure 4 shows the behaviour of the sextupole term along the magnet axis without shims and with two shim thicknesses.

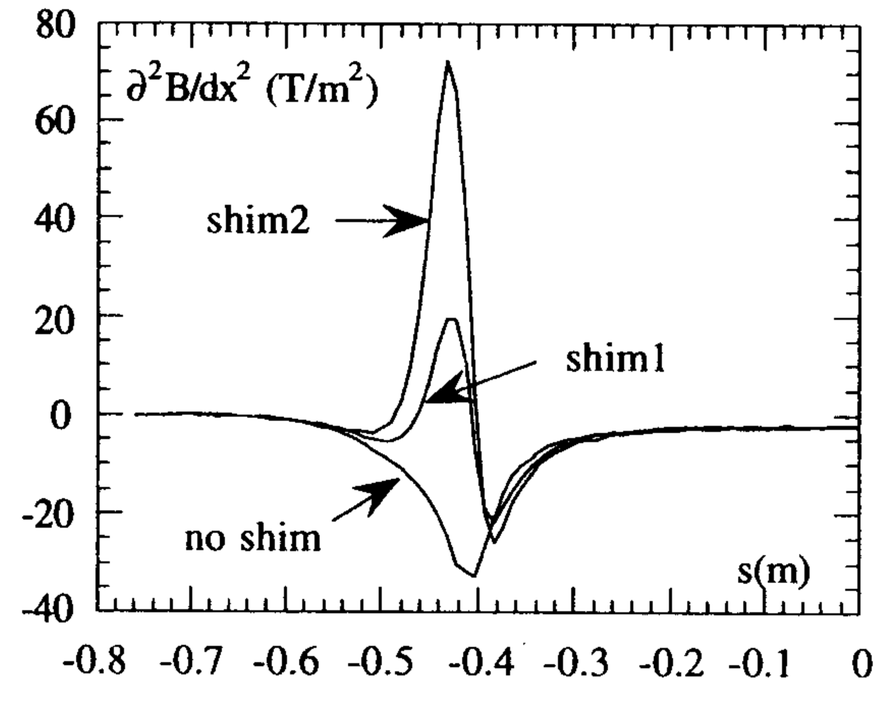

Figure 4 - Sextupole term along half magnet.

The configuration indicated as "shim1" was chosen for series production, as the result of a compromise between chromaticity correction and minimization of the 10-pole component introduced by the shims, given in Fig. 5.

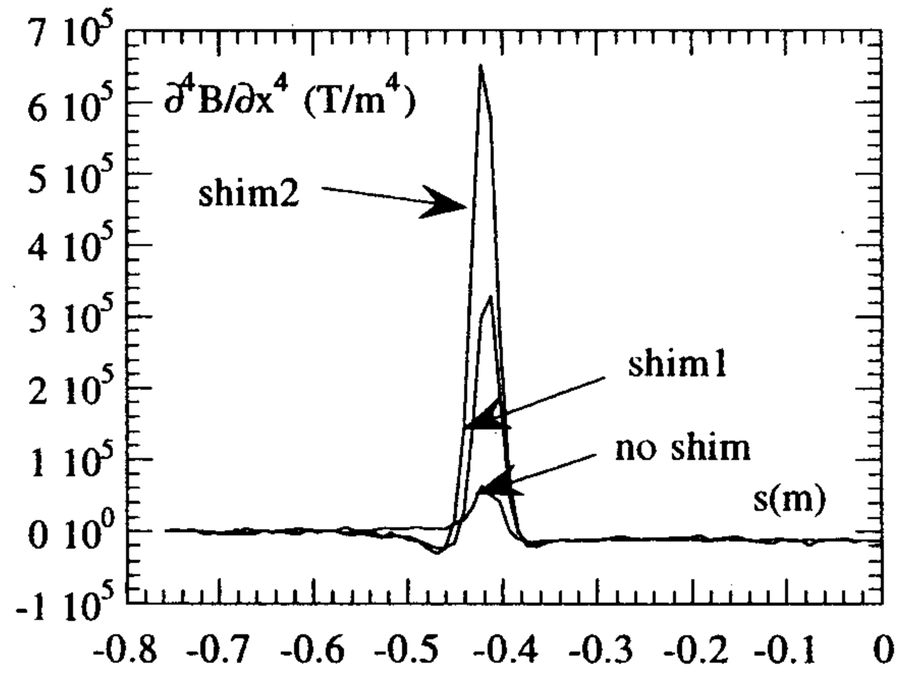

Figure 5 - Decapole term along half magnet.

3 QUADRUPOLE

The DAΦNE Accumulator Quadrupole prototype was delivered and fully tested at LNF during summer 1994. Its magnetic parameters are given in Table 2. Its pole shape is hyperbolic at the pole center with a straight line on each side.

Table 2 - Magnetic parameters of quadrupole prototype

Quantity	12
Nominal Gradient (T/m)	8
Maximum Gradient (T/m)	12
Magnet Bore Diameter (cm)	10
Good Field Region (mm)	±30
Integrated field quality |ΔB/B| (%)	±0.01
Magnetic Length (mm)	295.9
Nominal Current (A)	262
Maximum Current (A)	400

Also for this magnet the measurements were in good agreement with the expected values. The nominal gradient was achieved at 262 A (261 A computed by 3-D FEM). The overall high order contribution to the field, before any chamfer, defined as ΔB/B on a circle of 30 mm radius, is shown in Fig. 6. The measurement was performed by means of a rotating coil technique. The radial and azimuthal components of the error field are plotted together with their vector sum versus the azimuthal position, clearly showing a leading 12-pole term. Following a standard procedure, we have therefore chamfered the removable end caps, by applying a 45° cut of increasing depth.

Figure 7 shows the dependence of the main high order terms on the chamfer depth, demonstrating that the 12-pole contribution has been reduced by an order of magnitude, leaving the other terms almost constant.

Figure 8 shows, on an expanded scale, the final field quality: the overall high order contribution is $\approx 1 \times 10^{-4}$, well below the requirement of both the DAΦNE Accumulator and Main Rings.

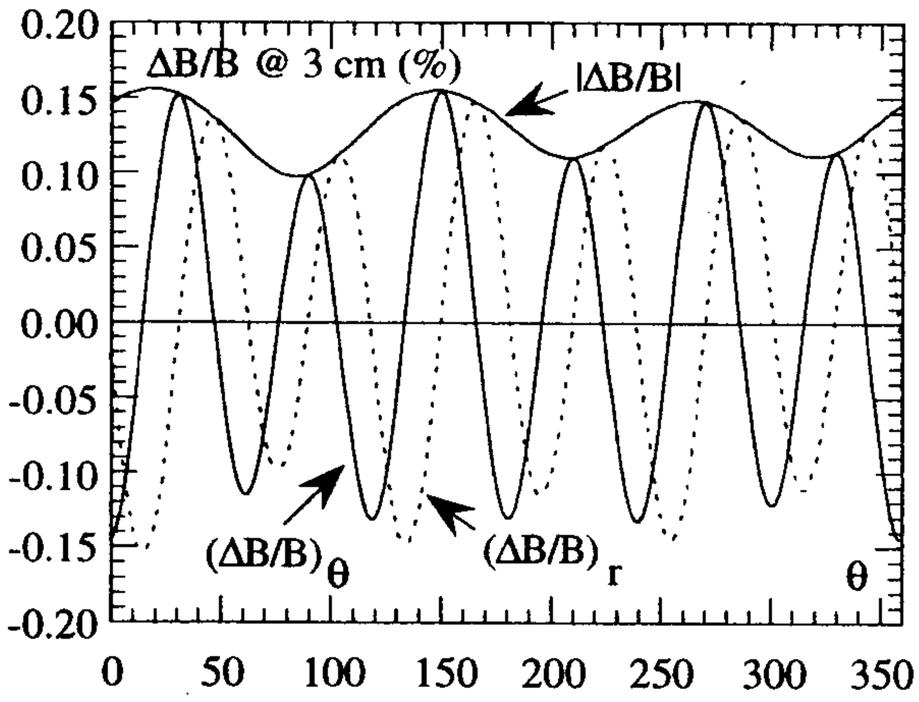

Figure 6 - Quadrupole field quality before chamfer.

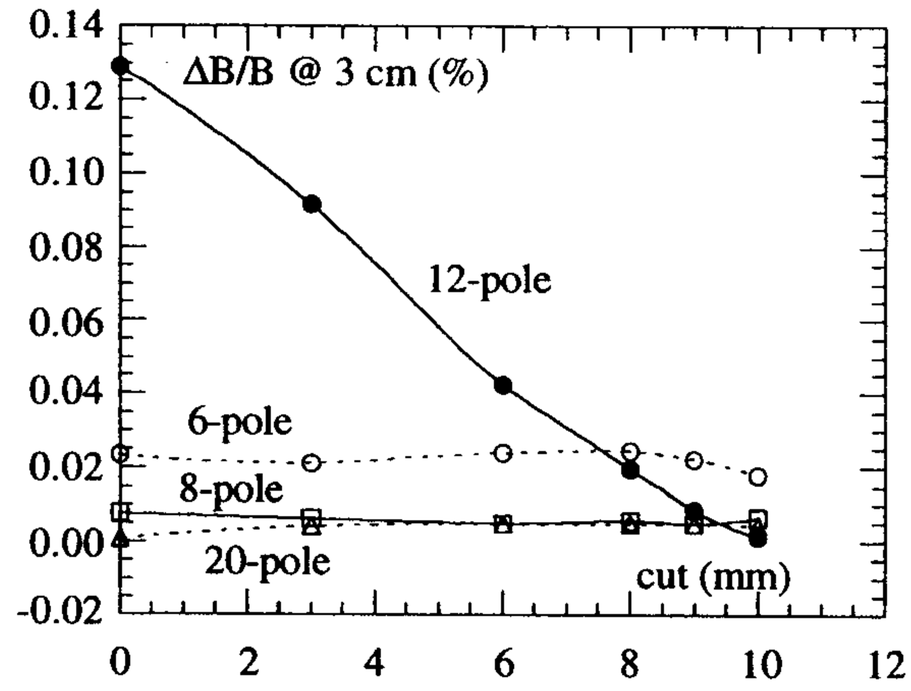

Figure 7 - Multipole contributions versus chamfer.

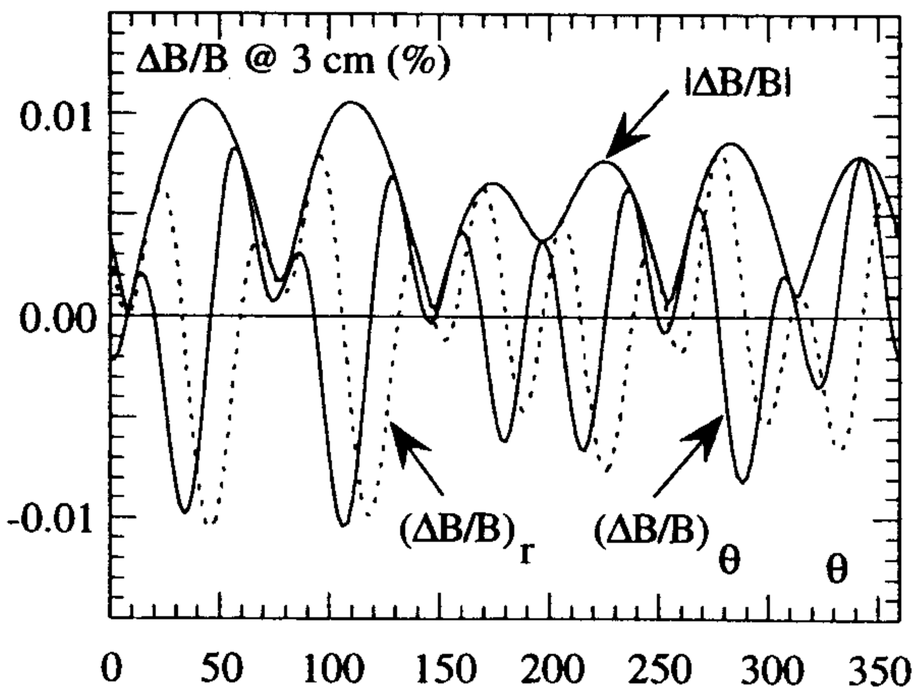

Figure 8 - Quadrupole field quality after chamfer.

4 SEXTUPOLE

Also the DAΦNE Accumulator Sextupole magnet prototype was delivered and fully tested at LNF during summer 1994.

Its pole shape is cubic at the pole center with a straight line on each side. Its main parameters are given in Table 3.

Table 3 - Magnetic parameters of sextupole prototype

Quantity	8
Gradient ($\partial^2 B/\partial x^2$, T/m^2)	135
Maximum Gradient (T/m^2)	180
Magnet Bore Diameter (cm)	10.8
Good Field Region (mm)	±30
Integrated |ΔB/B| (%)	±0.11
Magnetic Length (mm)	104.8
Nominal Current (A)	212
Maximum Current (A)	275

The deviation from the integrated ideal sextupole field is shown in Fig. 9, its maximum value being less than $\pm 1.1 \times 10^{-3}$. Tracking simulations showed that this field quality is acceptable, in spite of the very short yoke (67 mm): the longitudinal field profile does not exhibit any "flat top", and the integrated field quality is mainly determined by the fringing field at the magnet ends.

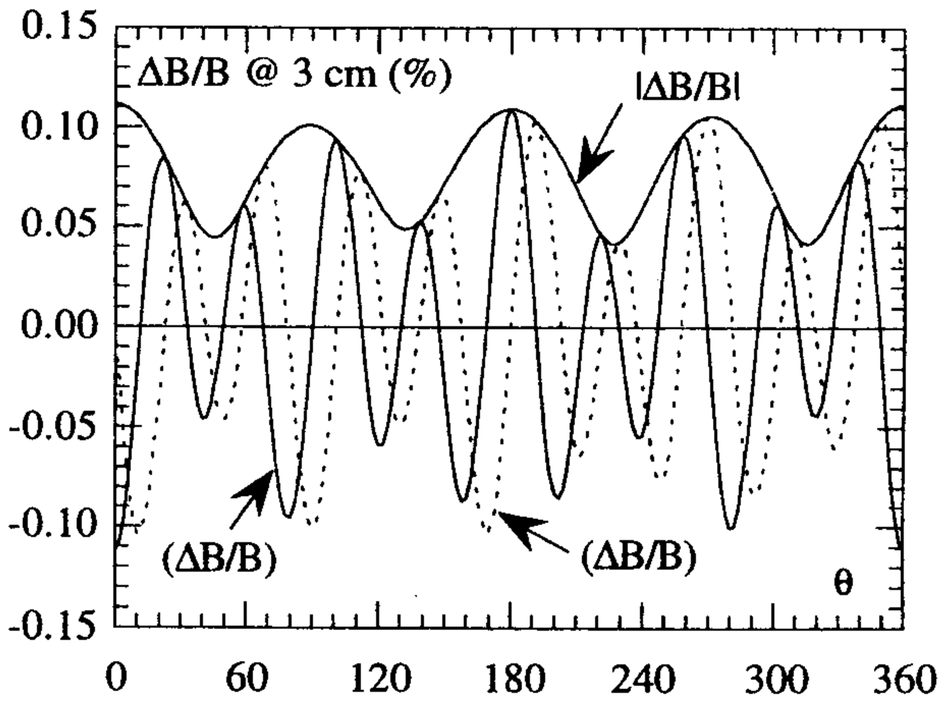

Figure 9 - Sextupole field quality.

5 CONCLUSION

Sixty quadrupoles (out of 96) and 14 sextupoles (out of 32) in the DAΦNE Main rings, where the field quality requirements are more severe than in the Accumulator, are of the same type of those described above. All these magnets have been built by TESLA and their field quality was found to be remarkably constant among the whole series production.

REFERENCES

[1] "DAΦNE, the first Φ-Factory", by G. Vignola, this Conference.

[2] R. Boni, S. Kulinski, M. Preger, B. Spataro, M. Vescovi and G. Vignola, "The Frascati F-Factory Injection System", 1991 Particle Accelerator Conf., S. Francisco, USA, p. 961.

[3] OXFORD Instruments, Accelerator Technology Group, Osney Mead, Oxford OX2 0DX, England.

THE DAΦNE MAIN RING MAGNET PROTOTYPES

M. Preger, C. Sanelli, INFN - LNF, Frascati, Italy

Abstract

The arcs of the DAΦNE Main Rings are equipped with bending magnets, quadrupoles, sextupoles and correctors of unconventional shape, in order to cope with the large size and peculiar design of the vacuum chamber, where the synchrotron radiation emitted by the high current electron beam is absorbed in a special antechamber isolated from the beam through a narrow slot. The magnets have been designed at LNF and the prototypes realized in Italy by Ansaldo Energia (dipoles, quadrupoles, sextupoles) and in France by Sigma-Phi (correctors). The paper describes the final adjustments on removable end caps and the results of magnetic measurements performed on the prototypes to check the field quality requirements.

1 INTRODUCTION

The two pseudo-elliptic, intersecting Main Rings [1] of DAΦNE are equipped, in the bending sections, with eight 9 m long aluminium vacuum chambers named "arcs". Two bending magnets, three large quadrupoles, two sextupoles and two corrector magnets are located around the vacuum chamber.

Two types of bending dipoles, each one having two different magnetic lengths, are under construction. Quadrupoles and sextupoles are expected to be delivered this summer. Corrector magnets have been delivered and are ready to be installed.

Eight out of sixteen dipoles have parallel ends (P.E. Dipoles) and the other eight are sector like shaped (S.L. Dipoles). Quadrupoles and sextupoles are fully symmetric. Large horizontal/vertical correctors are used for orbit correction. All magnets are laminated.

2 DIPOLE MAGNETS

Two dipole magnet prototypes, one for each type, have been built by ANSALDO Energia, Italy. The first one has been completely characterized. The second one, delivered at the end of May, is now under measurement. The series production of the P.E. Dipoles is in progress. Table I lists the main parameters of these magnets.

The construction of the first prototype was slower than schedule because the laminations were out of tolerance. After some attempts to recover the inconvenient, the decision was taken to machine with a suitable tool the pole surfaces, allowing for a gap increase of 0.6 mm. Accurate measurements were performed to verify the presence of short circuits among laminations on the machined surfaces and an extensive power up/down at the maximum ramp speed rate was accomplished to detect any possible degradation phenomena. The magnet was powered up to the maximum current, corresponding to a beam energy of about 715 MeV (@ 650 A, 1.8 T). Figure 1 shows a picture of the P.E. Dipole Prototype.

Table I - Design parameters of Main Ring dipoles

Dipole Type	Long		Short
Beam Energy (MeV)		510	
Nominal Field (T)		1.214	
Bending Radius (m)		1.4006	
Gap Height (mm)		75.6	
Magnetic Length (m)	1.21		0.99
Good Field Region (mm)		± 30	
ΔB/B @ 3 cm (%)		±0.015	
Turns per pole		144	
Nominal Current (A)		266	
P.E. Resistance (mΩ)	225.5		197.5
S.L. Resistance (mΩ)	197.3		175.5

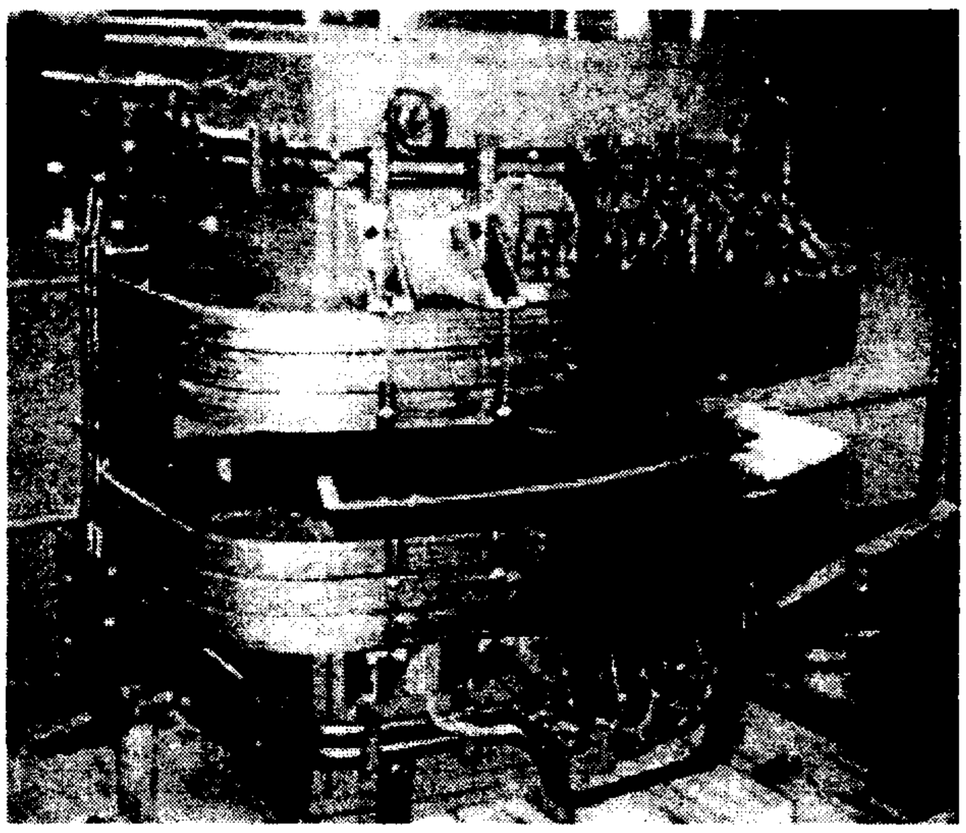

Figure 1 - The Parallel End Dipole Prototype.

A complete set of point by point magnetic measurements was performed using a Hall Probe mounted on a x-y-z computer controlled positioning system. The required transverse homogeneity was obtained without any shimming. The magnetic length, estimated on the beam trajectory calculated from the measured field, was obtained by adjusting the thickness of the end pole caps which were also iteratively shaped to minimize the natural integrated sextupole term of the magnet.

Figure 2 shows the integrated gradient due to the parallel ends and the sextupole term as a function of beam energy. Higher order terms are negligible. Figure 3 plots the field B on the ideal trajectory and the distance D between the real beam trajectory calculated from the measured field and the ideal one.

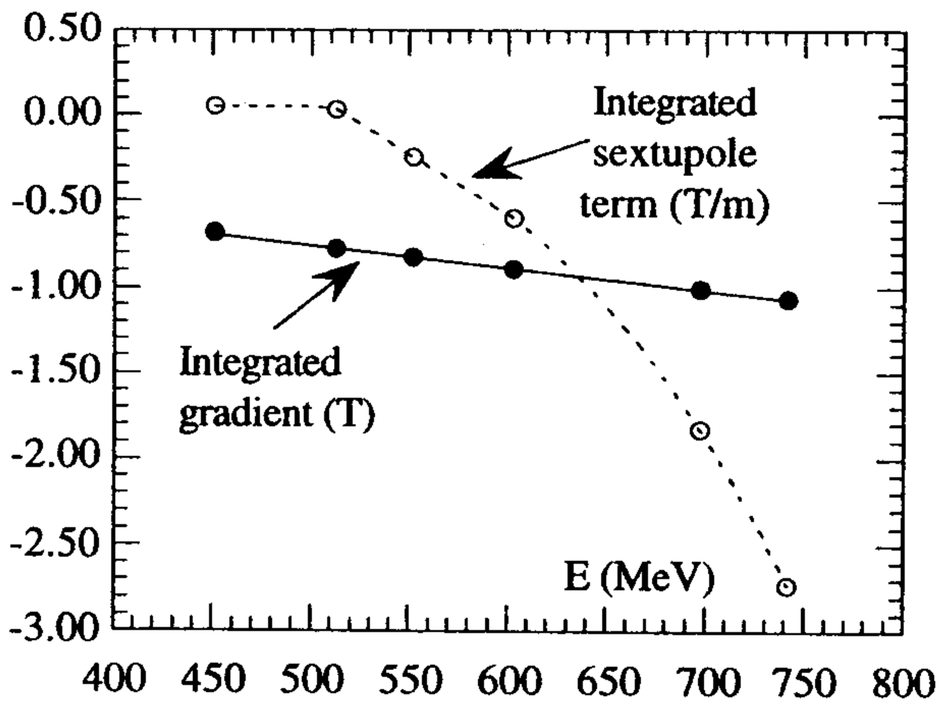

Figure 2 - P.E. Dipole integrated gradient and sextupole term as a function of beam energy.

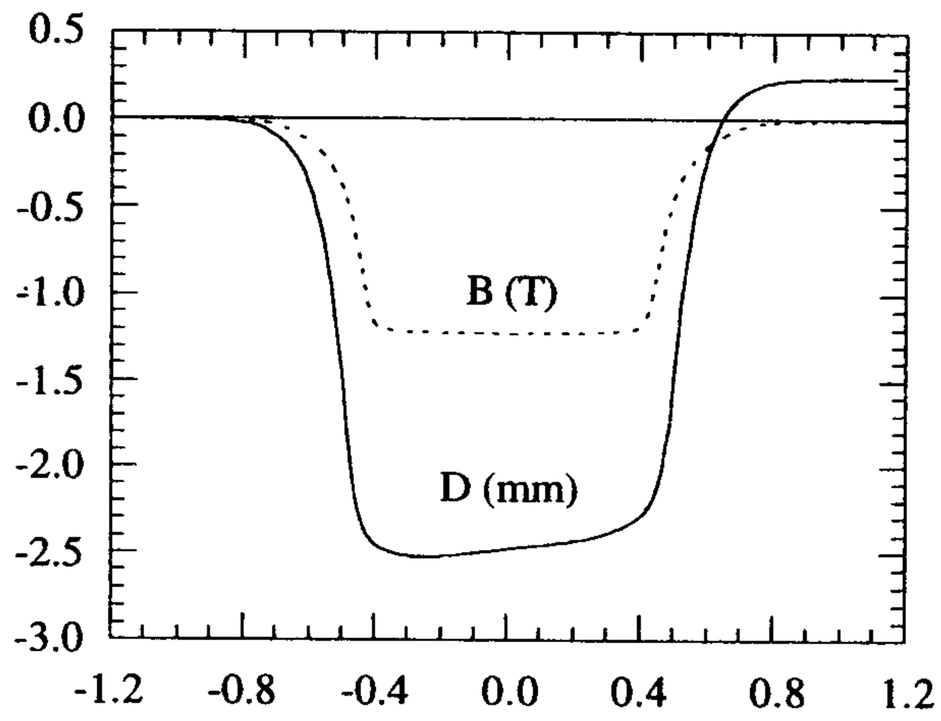

Figure 3 - Magnetic field on ideal trajectory (B) and distance (D) between calculated and ideal trajectories.

3 QUADRUPOLE PROTOTYPE

A first large quadrupole prototype was delivered by Ansaldo in May 1995 and a second one in February 1996. The main parameters are listed in Table 2 and a picture of the quadrupole is shown in Figure 4.

Table 2 - Large Quadrupole prototype parameters

	Nominal	Maximum
Energy (MeV)	510	750
Nominal Gradient (T/m)	3.6	8
Bore Diameter (mm)	108	108
Good Field Region (mm)	± 30	± 30
ΔB/B @ 3 cm (%)	≤0.05	≤0.05
Magnetic Length (m)	0.3027	0.3005
Nominal Current (A)	64.6	146
Resistance (mΩ)	115	118

The magnetic length (296 mm) was measured by means of the Hall Probe positioning system and the integrated field components with a Rotating Coil equipment built by Danfysik (Denmark). The 12-pole term was reduced by an order of magnitude by chamfering the removable end caps and Fig. 5 shows the resulting fractional deviation of the integrated field from the ideal quadrupole at 30 mm from the axis: the most relevant high order components are the sextupole (0.017%), the octupole (0.024%), the 12-pole (0.005%) and the 20-pole (0.003%).

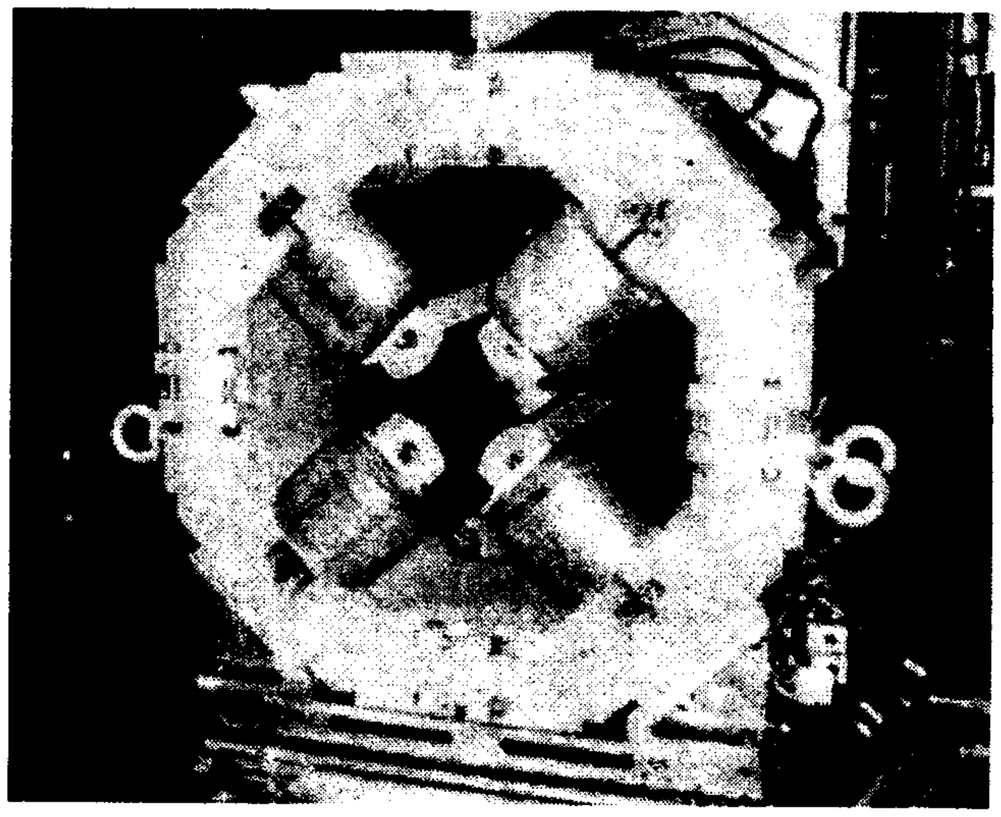

Figure 4 - Large Quadrupole Prototype.

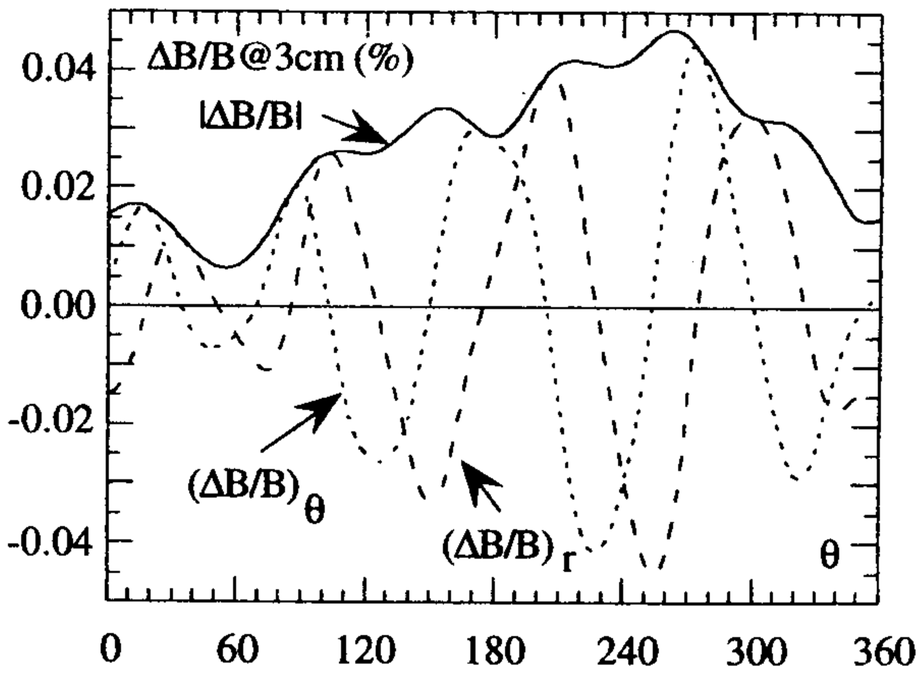

Figure 5 - Integrated field deviation from ideal quadrupole on a 30 mm radius circle around the magnet axis.

4 SEXTUPOLE PROTOTYPE

This prototype was delivered in December 1995. The main parameters are listed in Table 3 and a picture of the sextupole, assembled on the arc vacuum chamber, is shown in Fig. 7.

Table 3 - Sextupole prototype parameters

	Nominal	Maximum
Nominal Gradient (T/m^2)	90	234
Bore Diameter (mm)	108	108
Good Field Region (mm)	± 30	± 30
<ΔB/B> @ 3 cm (%)	0.11	0.11
Magnetic Length (m)	0.153	0.151
Nominal Current (A)	78.3	209.3
Resistance (mΩ)	41.6	41.6

The integrated field deviation from the ideal sextupole at 30 mm from the magnet axis is plotted in Fig. 8.

The dominant high order harmonic is the 18-pole (0.08% @ 3 cm, independent of the excitation current). There are also contributions from the 8-pole, 10-pole and 12-pole (≈0.015% @ 3 cm, independent of excitation current).

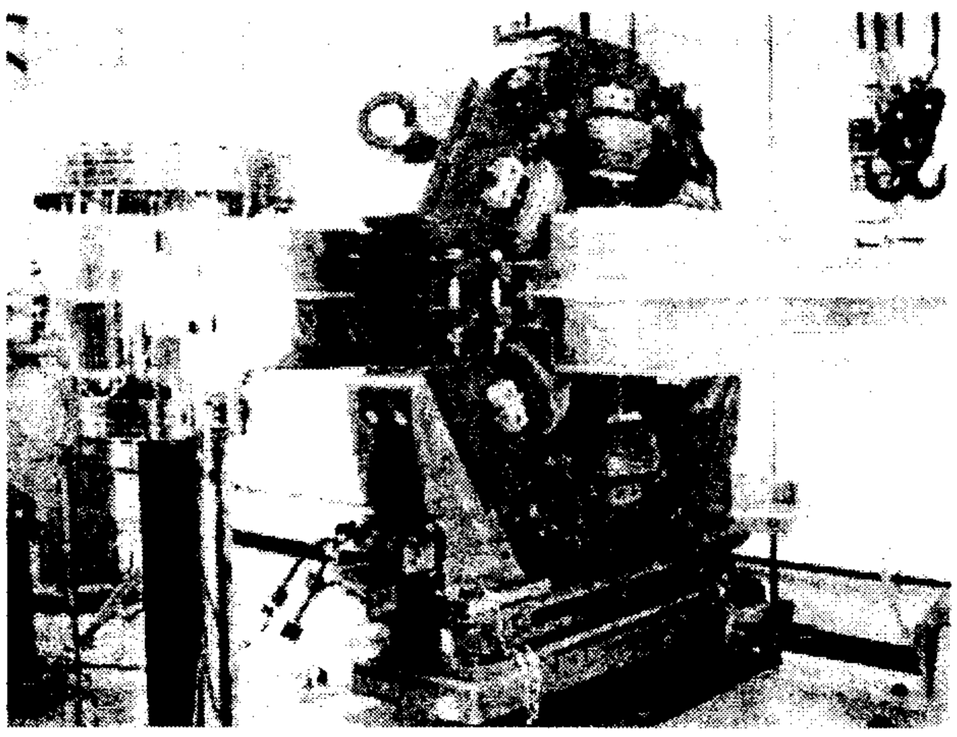

Figure 7 - The sextupole prototype assembled on the arc vacuum chamber.

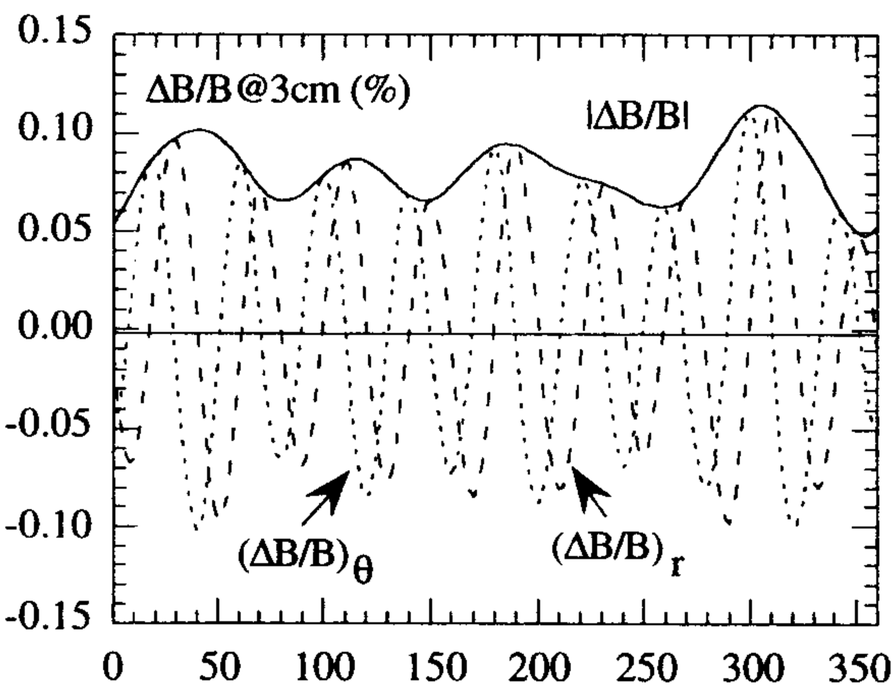

Figure 8 - Integrated field deviation from ideal sextupole on a 30 mm radius circle around the magnet axis.

5 RECTANGULAR CORRECTOR PROTOTYPE

Rectangular Corrector Magnets of large internal aperture (501 mm horizontal by 213 mm vertical) surround the arc vacuum chamber. The first prototype was delivered by Sigma-Phi (France) in March 1996, together with other 2 prototypes (the Square Corrector and the Horizontal/Vertical/SkewQuad Corrector) to be installed in the straight part of the rings. All remaining correctors (15 magnets) were delivered in May.

Figure 9 shows a picture of the Rectangular Corrector Magnet and Table 4 lists its main characteristics. In this magnet, a first coil (CH) creates a vertical field at the magnet center, which deflects the beam in the horizontal direction; the second coil (CV) acts as a vertical corrector.

Table 4 - Rectangular Corrector parameters

	CH	CV
Deflection Angle (mrad)	3	3
Nominal Field (G)	150	80
Magnet Gap (mm)	240	540
Magnetic length (mm)	362	456
Nominal Current (A)	8.78	6.36
Conductor Diameter (mm)	2.65	2.65

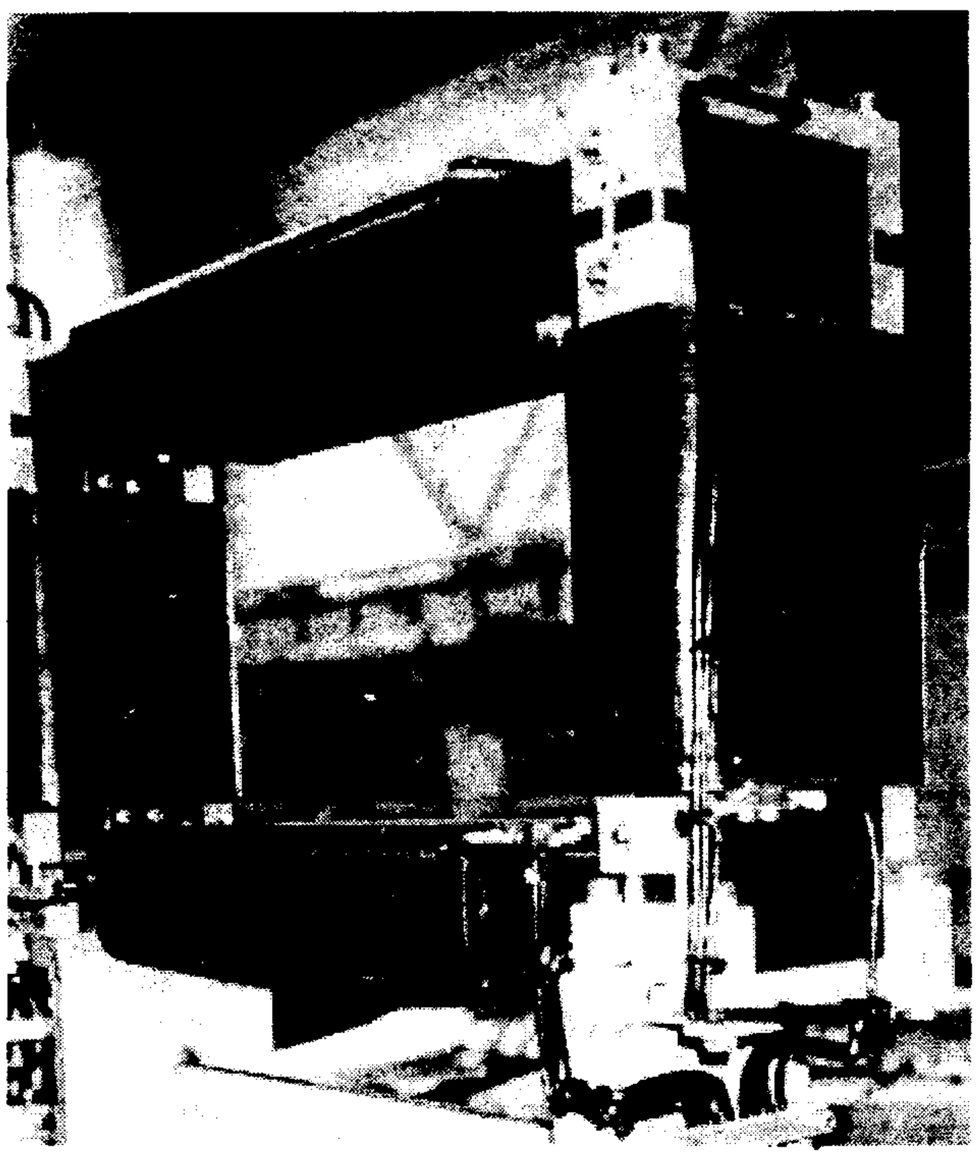

Figure 9 - The HV Rectangular Corrector Magnet

Due to the symmetry of the magnet, the vertical (horizontal) field component on the magnet axis does not change when CV (CH) is switched on. However, there is some interference between the two corrections when the beam does not pass in the center of the magnet. Being the magnet much larger in the horizontal direction, there is no influence of CH on the horizontal field component in the required operating range (±30 mm from the magnet axis). The vertical component instead changes up to ± 2% when CV is set to its nominal current, depending on the horizontal position of the beam. However the field at any point in the operating range is a linear combination of the separate effect of CH and CV, and this allows independent closed orbit corrections in the horizontal and vertical planes by means of a suitable correction algorithm.

REFERENCES

[1] G. Vignola, "DAΦNE, the First Φ-Factory", These Proceedings.

THE DAΦNE TIMING SYSTEM

A. Drago, G. Di Pirro, A. Ghigo, F. Sannibale, M. Serio
INFN-LNF, Frascati, Italy

Abstract

DAΦNE is a Φ-factory, presently under construction at INFN-LNF in Frascati. The electron / positron injection in the two main rings is performed through a Linac and an intermediate damping accumulator ring. The DAΦNE Timing System has been developed in the Frascati National Laboratory to synchronize many different devices distributed in more than 100^2 square meters area. The goal is to generate, under control of the general control system, the injection and extraction triggers related to the destination RF bucket in the main rings. All these outputs must have very low jitter. They are distributed to slow and fast pulsed devices such as, for example, Linac, injection / extraction kickers, diagnostic instrumentation and magnets. The timing system generates also the accumulator ring radiofrequency driver and various triggers for the detectors. Components and technologies used, modules description, control software and performances are presented.

1 INTRODUCTION

DAΦNE [1] is a Φ-factory, expected to be completely assembled in the Frascati National Laboratory (LNF) at the end of 1996. It consists of an 800 MeV electron (550 MeV positron) Linac, of a 32 m long damping/storage ring (Accumulator) and of two 100 m long main rings.

The DAΦNE Timing System has been developed in the Frascati National Laboratory to synchronize many different devices distributed in a more than 100^2 square meters area. Goal of this system is to generate, under control of the general control system, all the injection and extraction triggers related to the destination RF bucket in the main rings.

All these outputs must have very low jitter. They are distributed to slow and fast pulsed devices such as, for example, Linac, injection/extraction kickers, diagnostic instrumentation and magnets. The timing system generates also the accumulator ring radiofrequency driver and various triggers for the detectors.

Many different frequencies are involved in the DAΦNE accelerator: they are all generated from two main frequencies: 50 Hz and radiofrequency (around 368 MHz). From these, the other frequencies are derived and/or combined by digital hardware and software control devices. For every frequency it is possible also a phase control and this is performed through the software operator interface.

2 COMPONENTS AND TECHNOLOGIES

The Timing System is set up by more than half-dozen of different boards all designed at the LNF.

The higher frequency signals are managed through advanced ECL integrated circuits by the Motorola Eclinps (ECL in PicoSeconds) logic family [2]. These commercially available components have performances up to 1.1 GHz, very good stability in temperature and good compatibility with the other ECL logic families. Digital programmable delay components with steps of about 20 psec are included in this logic family: this is a flexible way to manage high frequency signals clocking flip-flops and latchs.

The lower frequencies signals are managed by TTL/CMOS logic family integrated circuits. VME bus interfaces [3], to the DAΦNE control system, permit to generate signals with different frequencies and phases from the software. These derived frequencies and all the enable/disable control bits are still locked with the master frequencies generators.

The shift in phase, both for the higher and lower frequencies, can be set by the software. This is done without missing trigger, i.e. in one revolution period. The synchronization between the high level software and the master frequency is performed through the low level timing software based on the AT&T DSP1610 [4], a 16 bits digital signal processor that is clocked at 80 MHz and can be used also as single-chip controller.

The distribution to local and remote devices is performed through 8-wires RS-485 synchronous connections transmitting 1 Megabit per second; with this speed it is possible to connect all the interested area without any auxiliary repeaters.

At crate level the synchronous transmission of the commands is made in compatibility with the VXI specification [5] through a local bus which uses the A and C rows of the lower 96 pins VME connectors.

In this way, it is possible to avoid the VME handshaking in order to minimize the jitter when the commands are released, and it is possible to simplify the receiving interface.

Large part of the printed circuit boards are designed with controlled impedance techniques, i.e. considering the wires as microstrip lines.

The PCB dielectric is FR4 (a low cost insulator) and the PCB conductors are copper based. Almost all the boards are multilayer, with up to eight layers; the CAD for the PCB design used can reach one thousandth of inch of precision in the trace layout.

3 MODULE DESCRIPTIONS

Many different frequencies are necessary in the DAΦNE accelerator: they are all generated from the two main frequencies: the 50 Hz, that is the external power supply frequency, and the RF (the Radio Frequency at around 368 MHz), that is the two main ring cavities frequency.

The first module is the master 50 Hz board: this is a device which, from the external 50 Hz frequency of the 220 Volts power supply, generates four master 50 Hz signals locked in phase with the external reference. This is made through a 74HCT4046 PLL (Phase Locked Loop). The four 50 Hz signals are 90 degree delayed each other and they are called Ø1, Ø2, Ø3 and Ø4. The 20 msec time slot is the discrete time unit which any timed operation in the accelerator must be performed in. Having four delayed timing signals is useful to timing slow devices on different 5 msec time subslot trigger. For example the injection kicker is charged itself on phase Ø1 and discharges itself on phase Ø4.

The second module is a fan out board that can accept four different TTL or differential ECL signals and fans them out through 4 TTL and 4 differential ECL output port for each input. The signals can be synchronized by an other external clock with frequency up to 100 MHz. This module is replicated in different zones of the plant to give remote triggers to many devices. Typically this module is useful to merge the low frequencies (50 Hz and 1 Hz) with one of the higher frequencies (RF/120 or RF/40).

Taking the main RF signals from a commercially available synthesizer, the fiducial generator module simply divides the frequency by 120 that is the harmonic number of the DAΦNE main rings. At full current it is expected that the machine will have 120 electron bunches and 120 positron bunches. The fiducial generator module is a RF/120 oscillator that give a trigger reference useful to label a bucket as the first bucket. The output signal levels are differential ECL and NIM.

The RF divider and bucket selector (or "fast timing") is a programmable module; it takes the RF as input and divides it by a dip-switch programmable value. In this way it is possible to produce three useful frequencies that are RF/120, RF/40 and RF/5.

All the modules accept the fiducial reference as input to synchronize the bucket count each other. To select the bucket the boards accept, through the local bus, a bucket number that is interpreted as a phase shift equal to the RF period times the input value. The phase shift is very critical and the error must be minimized to insure correct injection time to every bunch. The output levels are differential ECL and NIM.

The RF synch and fan out gives better RF synchronization and fans the signals out by four with differential ECL and NIM levels.

The connection with the control system is made by the state word dispatcher module that is provided by a VME bus A16 / D16 slave interface. This VME board is designed around an AT&T DSP1610 processor that makes very flexible the timed exchange of information between the timing system and the DAΦNE control system. This module takes as input two 50 Hz signals (Ø1 and Ø2) and it is provided, besides the VME interface, with a 1 Mbit/s RS-485 serial transmitter unit to broadcast the state word, a 31 bits pattern that contains the bucket number and the enable/disable bits for all the timed devices. The state word can be renewed every 20 msec and it is read from the control system that keep memory sequences of them stored in disk files (see Table 1). This module has also other interfaces as the local bus interface modelled on the local bus VXI specification, the JTAG interface to debug the software module and an auxiliary serial interface for remote serial connections, remote abort and remote reset.

Table 1 - DAΦNE timing state token

TOKEN	DESCRIPTION	APPLIES TO
LTO	Linac triggers off	Linac
LSB	Linac stand by	Linac
LSP	Beam from Linac to Spectrometer	Linac
LBT	Beam Linac to BTF	Linac
LAC	Beam Linac to Accumulator ring	Linac
AST	Accum.ring stored beam	Accumulator ring
AEX	Accumulator extraction	Accumulator ring
AMR	Accumulator extraction and main ring injection	Accumulator ring
EMS	Electron main ring stored beam	Electr. main ring
PMS	Positron main ring stored beam	Positr. main ring
VMP	Pulsed Magnet triggers	Various
VCA	Calibrations	Various
E+/E-	Electron/Positron	All
BCK	Bucket number selected	All

A twin module of the dispatcher is the state word receiver that receive remotely the state word and a 50 Hz phase trigger through the RS-485 serial link. This VME slave module is based on a DSP1610 and writes the state word to the local bus. The receivers are located in racks close to the devices to be controlled. Other modules have been designed in Frascati National Laboratories to receive the state word from the local bus and to execute the timed commands, for example to generate frequencies lower than 50 Hz and controlled in phase and duty cycle.

4 CONTROL SOFTWARE

The DAΦNE timing system software is composed by the low level software stored on eproms and by the high level software stored on the control system mass memory; they have assigned different tasks.

The low level software is a real time code that runs on the AT&T DSP1610 and it is written in assembler language. It consists of the state word dispatcher program that runs on one module and of the state word receiver program that runs on up to 128 connected modules. The dispatcher software is designed as a 4 state finite machine that switches from a state to the next one every 5 msec according to the 50 Hz input level signals phase Ø1 and phase Ø2. This finite state machine generates a two bits semaphore and puts it in the VME interface register. In this way, it is possible to synchronize the data flow from the control system. On the green light the control system writes the current 31 bits word, on the red light it retrieves the new word from a sequential table, checking an external condition and waiting.

The receiver real time software is also written in DSP1610 assembler, it is a two state finite machine based on the 50 Hz phase received from the RS-485 serial link together with a state word. It performs a delayed and timed writing on the VME interface and on the local bus to activate the command execution with a low jitter.

The high level software runs on commercial Apple MacIntosh computers and on special MacIntosh machines with a VME interface. Large part of the code is written in LabView, a language developed by National Instruments.

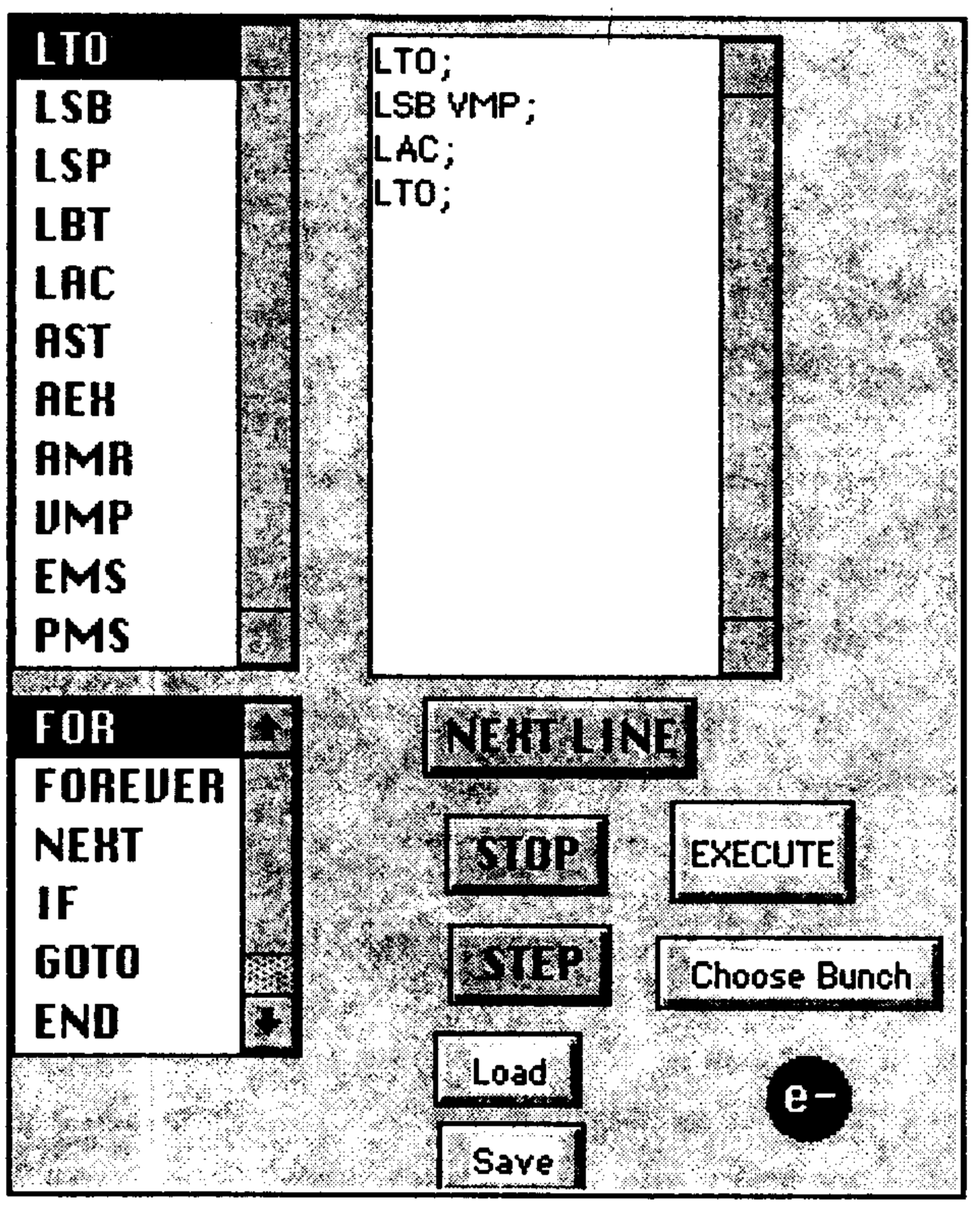

Figure 1 : Development of timing sequence.

The main task of the high level software is to create, to edit , to store and to retrieve different table files. These data are used for different injection and/or extraction schemes or for test and calibration purposes.

5 PERFORMANCES

The performances of the system have been measured in the laboratory, the main goals have been, at low frequency, to minimize the jitter on the remote distribution of state word, and, at high frequency, to minimize the displacement of the phase shift relatively to the bucket chosen.

Regarding to the first test, all the transmission chain of the state word from the operator interface to the remote devices has a measured jitter of 500 nsec without transmission errors over 128000 patterns.

The high frequency tests have been done in the laboratory using the automatic test set shown in Fig. 2.

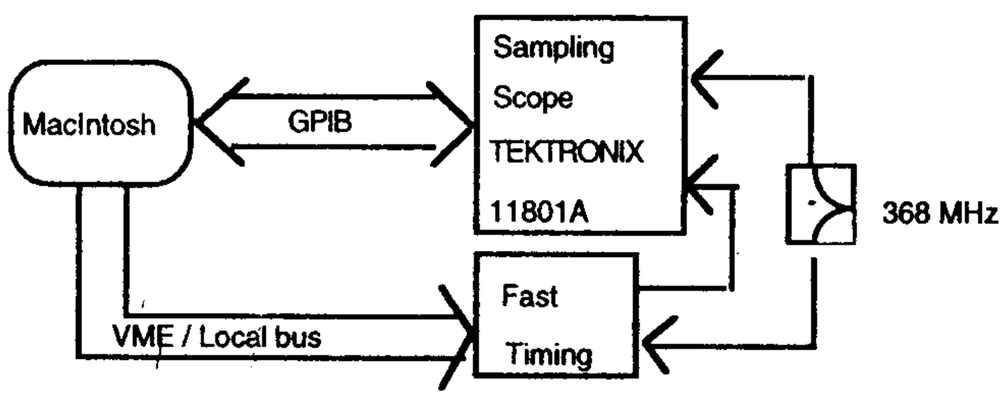

Figure 2 : Bucket phase shift test set.

Through the VME and the local bus interfaces it has been possible to modify the programmable delay in the fast timing module to best fit the desired output triggers. In this way it has been possible to reach for the 120 buckets selector a standard deviation of 1.6 picosec for the displacement from RF.

6 CONCLUSIONS

It has been presented an overall description of the DAΦNE timing system, that has been installed during the April 1996 on the DAΦNE complex.

All the laboratory tests are completed and the integration with the other accelerator subsystems is in progress.

REFERENCES

[1] "DAΦNE, the first Φ-Factory", by G. Vignola, this Conference.

[2] "Motorola ECLinPS Data", Motorola Inc., 1991.

[3] "VMEbus Specification", V.I.T.A., 1987.

[4] "WE DSP 1610 Digital Signal Processor Information Manual", AT&T Microelectronics, 1991.

[5] "VXI bus System Specification revision 1.4", VXIbus Consortium Inc., 1992.

FIRST OPERATIONAL EXPERIENCE WITH THE DAΦNE CONTROL SYSTEM

G. Di Pirro, C. Milardi, A. Stecchi, INFN-LNF, Frascati, Italy

Abstract

The DAΦNE Control System has been fully implemented for the accelerator complex component already operative. The architecture has been improved both from the hardware and from the software point of view. Control application for magnetic elements, vacuum equipment, RF cavity and diagnostics have been developed and debugged on line. Tools to include HLS (High Level Software) application in the Control System have been developed together with a dedicated Real Time database.

1 INTRODUCTION

DAΦNE [1] is the Frascati F-factory project and DANTE [2] is its Control System.

DAΦNE consists of an 800 MeV electron Linac, a 510 MeV damping ring, the Accumulator, and two colliding beam main rings. A Transfer Line, 156 m long, joins the different parts. At the present the Linac the Accumulator and the related Transfer Line are available and under commissioning.

DANTE is a three levels Control System, having a hierarchical communication structure and distributed intelligence. It is based on the VME bus and on the Macintosh personal computer, used as a console and as VME CPU.

2 SYSTEM OVERVIEW

The DANTE 3rd level, HELL, is made up by many different CPUs, DEVILs, each one controlling a specific class of element and updating the corresponding part in the RTDB (Real Time Data Base) [2]. The 2nd level, PURGATORY, includes two CPUs CARON and LOGGER. CARON forwards the command from the 1st level to the proper DEVIL and the 3rd level coming error messages and warnings to the running consoles. Moreover it checks continuously the DEVILs status. The LOGGER keeps trace and periodically saves all the communication between the 1st and 3rd level.

The 1st level, PARADISE, consists of several consoles providing a graphical access to the accelerator complex and of a Control System Server where the applications, the DEVIL start-up configuration and the DAΦNE data-set are stored.

The Link between PARADISE and PURGATORY is performed through the CES VMV bus interface (CES 7212-8250) [3], while between PURGATORY and HELL several optical point to point links have been implemented using the VME-VME LEXTEL LL2000 interface [4].

An Ethernet network connects all the Control System processors and it is used to download the DEVIL applications and the configuration data-sets. The Ethernet LAN is also used for debugging purpose.

It is worth noticing how using the same processor throughout the whole system permits to have the same Operative System [5] and the same development environment LabVIEW [6].

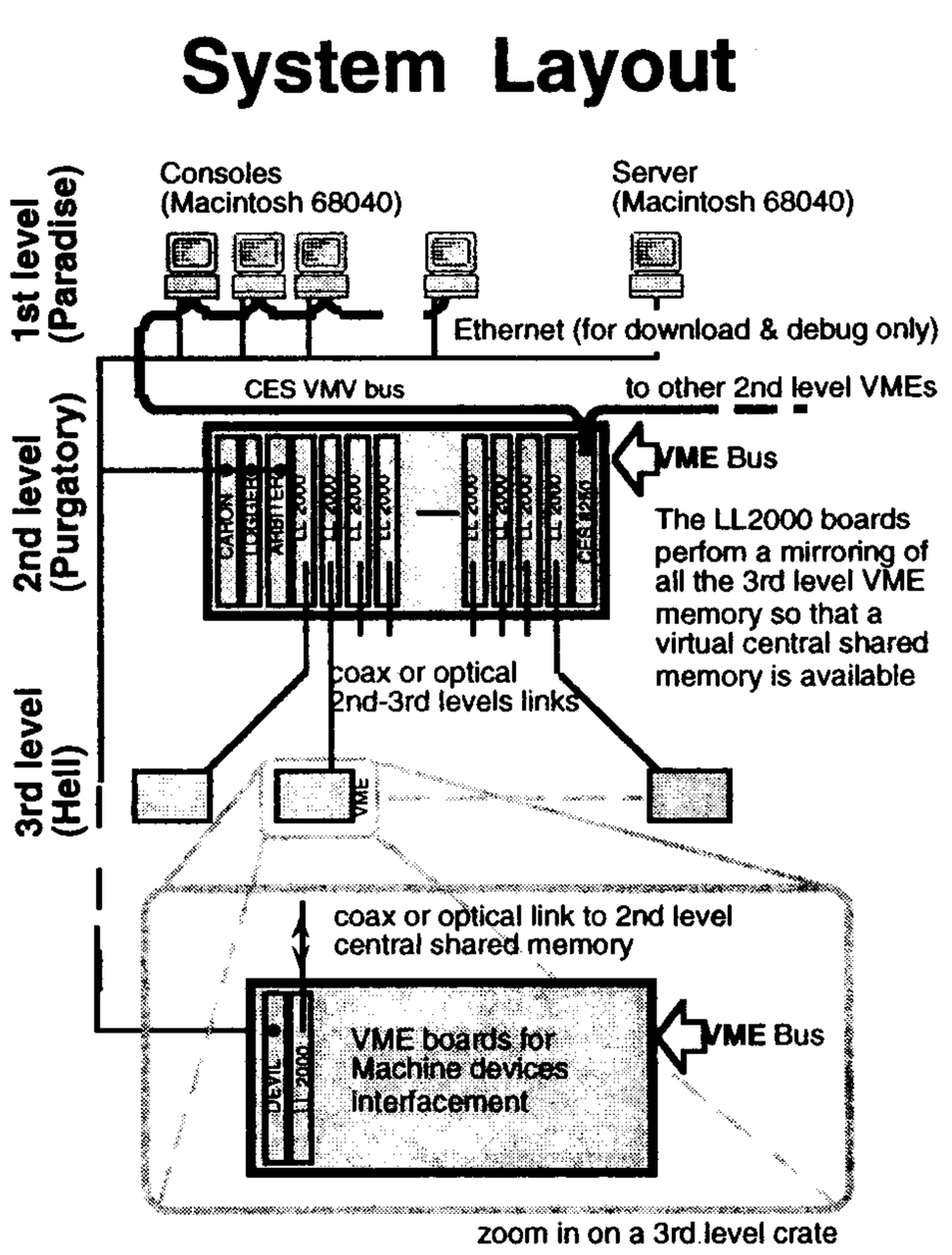

Figure 1 - General System architecture: all the distributed 3rd level VME crates contain one or more DEVILs (Macintosh LCIII with 68030, Math coprocessor, 8MB internal RAM, 4 MB VME RAM, Ethernet for diskless booting). All the DEVIL VME memories are mapped into the 2nd level VME address space. This virtual central shared memory is accessible from the consoles with a direct memory access.

3 DANTE IMPLEMENTATION

In this early stage of the DAΦNE complex commissioning the Control Group has been in charge of installing the hardware and providing the DEVIL applications for the primary devices. The first DANTE implementation, phase 0, started one year ago.

A control room was arranged in the Linac area, it has been used extensively to investigate in very deep detail the Control System main structure, and then also to commission the 20 m long first Transfer Line part. For this reason four consoles have been installed.

One month ago started the DANTE phase 1, it was supposed to control the Accumulator and the, 90 m long, Transfer Line, up to the Linac.

A new control room has been set up. This time all the efforts have been appointed in testing the Control System ability to drive the machine devices and defining the operating procedures.

The main Hardware components installed are listed in Table 1.

The total amount of software written and debugged for the controlled devices is greater then 150 Mbyte, 95% written in the native LabVIEW graphical language G and 5% written in a standard ANSI C and FORTRAN language.

Table 1 - Phase 1 hardware components

Console	2
Remote console	1
Server	1
Caron	1
Logger	1
Arbiter	1
Lextel coax link (pairs)	6
Lextel optical link (pairs)	4
DEVIL	15
Ethernet hub	1
VME crate	10

4 DANTE UPGRADE

The experience done with the DANTE phase 0 resulted in some modification of the Control System general scheme. An ARBITER has been introduced in order to rule the console data fetching from the 3rd level RTDB, because a 1st level VME access through the CES and LEXTEL boards produces seldom a time delay exceeding the NuBus time-out (25µs). This may result in a busError when two or more consoles try to get data from the RTDB concurrently.

The increasing number of installed DEVILs required a dedicated Server were to store the relative applications together with the start-up data-set files. The log files saved from the LOGGER, containing the list of command and error travelling between PARADISE and HELL, are housed on this server too.

A complete transition from coax LEXTEL point to point link to the optical one has been planned in order to face not only the problem of the long distance communication, but also the noise due to the harsh environment.

A description of the most important devices controlled by DANTE, in the phase 1, follows.

4.1 Magnets

All the accelerator magnets Power Supplies (more than 164 up to now) are *intelligent* devices. This means that they have an embedded micro controller which drives the current ramp with a pre-defined slew rate, monitors the interlock conditions and arbiters all the Power Supply status transitions.

The link with the Control System 3rd level (VME BUS) is done via many RS 422/485 4-wires multidrop busses at medium speed (from 9,600 to 57,600 bps). Not all the Power Supplies run the same communication protocol so that 4 different sets of drivers have been developed in order to control and read back all of them.

Dealing with "intelligent" devices made the control a matter of logic rather than of hardware. The concept of Power Supply element has been abstracted into a software object which contains virtual statuses and accepts always the same system commands.

The control applications running on the 3rd level DEVILs are in charge of updating continuously this software object representation into the RTDB and converting the system commands into a device dependent syntax.

The RTDB refresh rate depends on the baud rate and on the protocol going from 1 to 25 Hz.

All the 1st level user windows for the control of the Transfer Lines Power Supplies are completed and those for the Accumulator are on the way.

The control of the Accumulator and Main Rings *Kickers* magnets differs from the above general description. The *Kickers* magnets have been fully designed and built in house and required a strongly customised interfacement. In this case the command and control is performed through DAC, ADC, digital I/O and GPIB programmable delays. All this hardware is connected to the VME and controlled by a 3rd level DEVIL.

4.2 Radio Frequency

At this stage the Accumulator RF cavity control has been provided. It permits to visualise and to set the main cavity parameters.

An Industry Pack carrier, appointed for its reliability, has been used. It allows to house up to four, mixed type, I/O modules using a single VME slot. The carrier arrangement includes multiple channels DAC, ADC and digital I/O. The drivers for the hardware, the RTDB and the 1st level control window have been written and fully debugged. An operator window with less information and automatic start-up procedure is under development.

4.3 Vacuum

The Control System for the vacuum equipment has to deal with 24 SIP (Sputter Ion Pump) and 7 VUG (Vacuum Ion Gauge). Both of them are controlled, through the DEVIL serial port, using RS 485 4-wires multidrop busses.

Low level drivers, RTDB, 1st level control window and an overview window giving the vacuum general status at glance are available.

4.4 Diagnostic

The Control System for the diagnostic is in an early stage. Full remote control has been provided for the *Flags* and the related video camera, the (SEM) Secondary Emission Monitor and for a general purpose video and RF multiplexer.

VMEIO 1016 relai and VMEIO 1018 IO, by the OR Industrial Computer , have been used for the *Flags* control. A Video Multiplexer, controlled through the DEVIL serial port, permits the *Flags* remote view.

The 3rd level drivers, the RTDB and the 1st level control window have been written and are available for all the listed diagnostic element.

5 HIGH LEVEL SOFTWARE

The DANTE 1st level permits to include and to run HLS applications. They consist of codes, written using the FORTRAN compiler [7] available under the MPW development environment [8], integrated in the proper LabVIEW VI using the CIN (Code Interface Node) facility. A CIN allows to run a code written in C language which may itself calls a FORTRAN routine. To implement this mechanism a library to matching the C language data types with the corresponding FORTRAN ones has been developed.

Every HLS application must be able to access all the device read backs in the DANTE RTDB. Moreover it needs other information such as machine models, static lattice description, calibration and numerical constants. The last database part has been developed, it is housed at the 2nd level of the Control System on the LOGGER. RAM. It is initialised by the 1st level main program at the Control System start-up. Data are grouped according to the DAΦNE functional areas they refer to and may be read and modified at run time.

A HAL (High level software Application Library), 1 Megabyte large, has been written and debugged. It provides the basic machine oriented routines and meets the CIN requirements. The HAL library has been used to write the basic applications for the accumulator commissioning. Their integration into the Control System is on the way.

6 CONCLUSIONS

The DANTE phase 1 is running. It has been fundamental to drive the beam from the Linac into the Accumulator and to optimise the Accumulator lattice in order to get a *circulating beam.*

The Accumulator commissioning is a powerful bench test for a continuos Control System refinement. Nevertheless its general structure and the implemented software have not shown, up to now, any relevant problem and will be easily extended to the main rings control.

7 ACKNOWLEDGEMENTS

Thanks are due to Luciano Trasatti who inspired the DANTE Control System and worked on it up to the past year, as well as to Gianfranco Baldini and Mario Masciarelli who contributed, with their commitment, to the DANTE realisation.

REFERENCES

[1] "DAΦNE, the first F-Factory", by G. Vignola, this Conference.

[2] "DANTE: control system for DAΦNE based on Macintosh and LabVIEW", by G. Di Pirro, C. Milardi, A. Stecchi and L. Trasatti, Nuclear Instruments and Methods in Physics Research A 352 (1994) 455-475.

[3] Lextel, Inc. P.O. Box 306 Wakefield, Ma 01880 617-245-5017.

[4] Creative Electronic System S.A. Route du Pont-Butin 70 CH-1213 Petit-Lancy 1/Geneva Switzerland.

[5] Mac™ OS - Apple Computer, Inc., 20525 Mariani Avenue Cupertino, CA.

[6] LabVIEW® National Instrument Corporation, 6504 Bridge Point Parkway, Austin, TX 78730-5039.

[7] Language System FORTRAN 3.0 Reference Manual, Language System Corporation, 441 Charlisle Drive, Herndon, VA 22070-4802.

[8] MPW: Macintosh Programmer's Workshop Development Environment - Apple Computer, Inc., 20525 Mariani Avenue Cupertino, CA.

BACKGROUND CALCULATION FOR THE DAΦNE EXPERIMENTS

S. Guiducci, INFN-LNF, Frascati, Italy

Abstract

DAΦNE is an e^+e^- Φ-factory under construction at the Frascati National Laboratories. The project status is well advanced and commissioning of the main rings is foreseen for beginning of 1997 [1]. The beams will circulate in a double ring collider and cross, with a small horizontal angle, in two Interaction Points (IPs). A careful study of the loss rates due to Touschek scattering, which are the main source of background for the detectors, has been performed for both Interaction Regions (IRs) and a solution to strongly reduce them has been adopted.

1 INTRODUCTION

The IR1 interaction region is dedicated to the KLOE detector, mainly to study CP violation in neutral K decays [2]. The other one, IR2, will house the FINUDA detector for hypernuclei decays study [3]. A third experiment, DEAR, for exotic nuclear physics [4], will run at an early stage of machine operation.

In order to get the high luminosity required for the CP violation experiment ($L = 5 \cdot 10^{32}$ cm^{-2} s^{-1}) DAΦNE will operate with high current and many bunches: from 30 for initial operation up to a maximum of 120. Due to the low energy of the machine (.51 GeV) and the high current there will be a high rate of particle losses, mainly from Touschek scattering, which dominates the beam lifetime.

The different contributions to the DAΦNE single beam lifetime and the related design parameters are listed in Table I.

Table I - Single beam lifetime and related parameters

Particles/bunch	$8.9\ 10^{10}$
Emittance	10^{-6} m rad
Coupling factor	.01
Bunch length	.03 m
Relative energy spread	$5.5\ 10^{-4}$
RF Voltage	254 kV
Gas pressure (biatomic gas Z=8)	10^{-9} Torr
Quantum lifetime	$4.5\ 10^{31}$ hours
Gas bremsstrahlung	$2.0\ 10^{3}$ min
Coulomb gas scattering	$1.9\ 10^{3}$ min
Touschek scatterimg	160 min
Single beam total lifetime	135 min

For the three experiments the loss rates due to Touschek scattering have been computed. The results and a solution adopted to reduce the background rates are presented in the following.

An evaluation of the rates of particle losses due to Coulomb gas scattering and bremsstrahlung has been done for KLOE [5], [6] and is in progress for DEAR and FINUDA. The expected background level is low because special care has been taken in the design of the interacion regions vacuum system in order to get a low local gas pressure and to reduce the beam gas interactions.

2 TOUSCHEK SCATTERING BACKGROUND

Touschek scattering is an elastic Coulomb scattering between pairs of particles within a bunch. The result is a change of the longitudinal momentum of the two particles: one loses and the other gains the same fraction δ of momentum. If the momentum deviation exceeds the acceptance of the ring the particle is lost.

In the DAΦNE rings we distinguish two regions: straight sections with vanishing dispersion and arcs with high dispersion.

The particles scattered in the straigth sections undergo a momentum deviation but no betatron oscillation, and therefore cannot be lost in the IRs, where the dispersion is zero.

The particles scattered in the arcs gain an horizontal oscillation amplitude and can be lost on the vacuum chamber inside the IRs producing background for the experiments.

These particles follow similar trajectories, i.e. with the same phase of the betatron oscillation and an amplitude proportional to the momentum deviation δ. An example is given in Fig. 1

The number of particles hitting the vacuum chamber has been evaluated by tracking the Touschek scattered particles from the arc upstream to the end of each IR.

3 RESULTS

3.1 KLOE and FINUDA

After a detailed study of the particle losses in the KLOE and FINUDA IRs [7], [8], the following solution has been adopted to reduce the background rates:

- increase the vacuum chamber aperture inside the detectors
- insert two beam scrapers upstream the splitter magnet of each IR.

The scrapers are thick targets (3.5 cm tungsten ~ 10 radiation lengths) which can be inserted independently on both sides of the vacuum chamber reducing the horizontal aperture to cut the large amplitude particles upstream the IR.

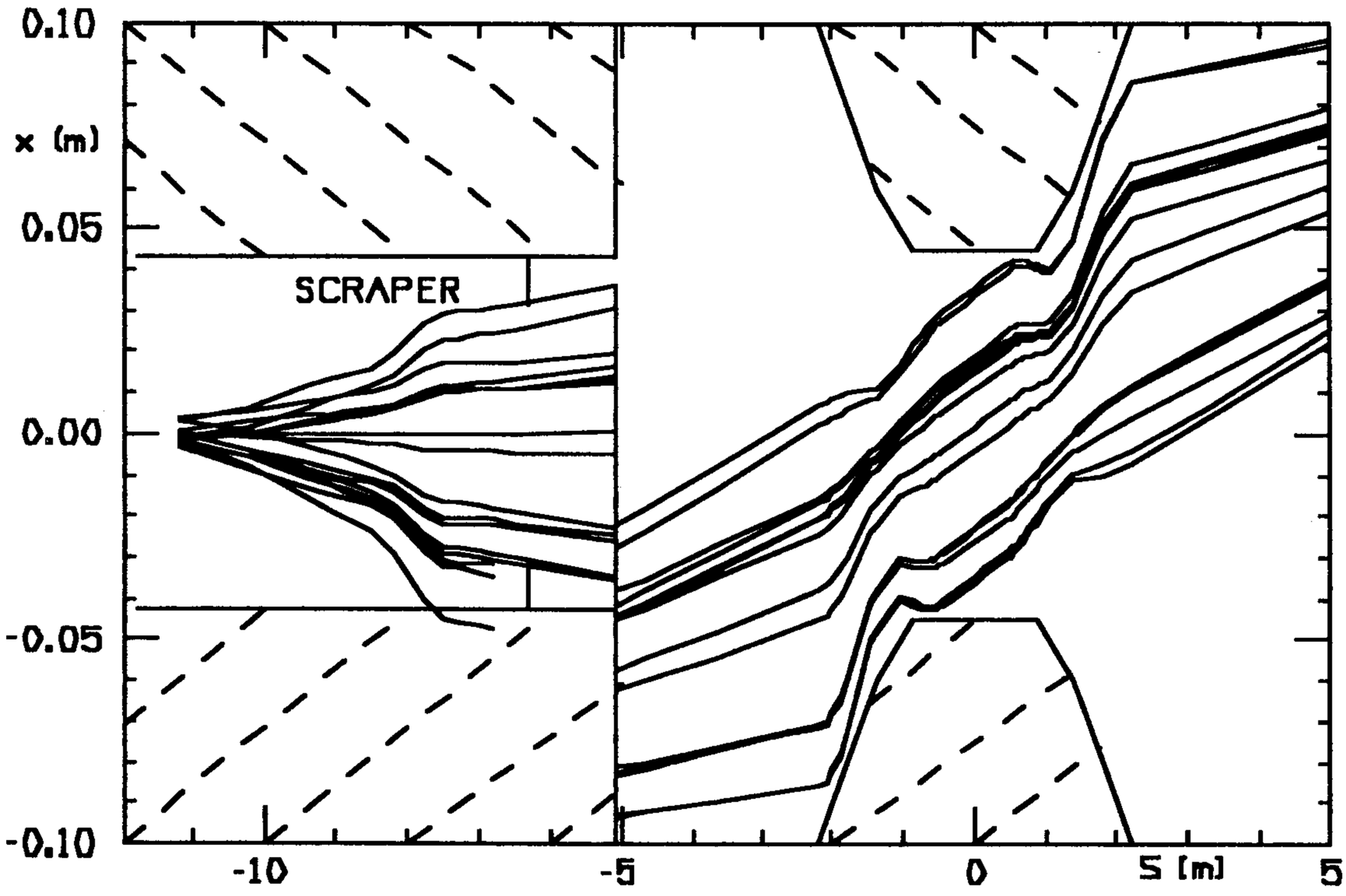

Figure : Horizontal trajectories of Touschek scattered particles from the last bending of the arc to the end of the DEAR IR2. The vacuum chamber apertures are shown in the picture. At the ends of the IR there is a change of the reference system, which is centered on the quadrupole axis.

TABLE II - Particles lost due to Touschek scattering in the KLOE and FI.NU.DA. detectors
N=8.9 10^{10} part./s/bunch/beam – θ = 12.5mrad

A_{sc}/σ_x	N, KLOE (s^{-1}/bunch/beam)	N, FI.NU.DA. (s^{-1}/bunch/beam)	τ_{tot} (min)
no scrapers	1.47 10^5	1.76 10^5	135.
10	695.	1.55 10^4	117.
9	0.	4.10 10^3	101.
8	0.	756.	84.

The results are shown in Table II for the nominal value of the half crossing angle θ and the maximum number of particles per bunch foreseen in DAΦNE.

The number of particles per bunch lost on the vacuum chamber inside the KLOE and FINUDA detectors is listed in the table for different values of A_{sc}, the scrapers' aperture in units of the horizontal beam size. The beam lifetime corresponding to different scrapers' apertures is shown in the last column. The calculations have been performed for the updated version of the DAΦNE lattices.

Due to the horizontal crossing angle, the layout of the machine is not symmetric with respect to the Interaction Point (IP). In the KLOE IR the beams come from the external (LONG) ring, while in the FINUDA IR come from the internal (SHORT) one.

The number of particles lost in the FINUDA IR is higher, anyway the rate calculated with a scrapers' aperture of $10\sigma_x$ is already acceptable for the detector.

3.2 DEAR

DEAR has more stringent requirements than the other experiments on the background rates because it uses a CCD camera and has no trigger. This experiment does not have a dedicated IR design but will be installed in one of the two IRs in the configuration designed for machine commissioning.

DAΦNE has a special IR design for commissioning with electromagnetic quadrupoles and no solenoids, while the KLOE and FINUDA IRs have permanent magnet quadrupoles and solenoids.

Table III - Particles lost due to Touschek scattering in the DEAR (IR1) detector
N=8.9 10^{10} part./s/bunch/beam – θ = 12.5mrad

A_{sc}/σ_x	A_{sc} (mm)	N_{DEAR} (IR1) (s^{-1}/bunch/beam)			τ_{tot} (min)
		δ<0.	δ>0.	total	
no scrapers	43	7.73 10^5	6.03 10^4	8.33 10^5	139
11	31	0.	323.	323.	138
10	28	0.	0.	0.	124

Table IV - Particles lost due to Touschek scattering in the DEAR (IR2) detector
N=8.9 10^{10} part./s/bunch/beam – θ = 12.5mrad

A_{sc}/σ_x	A_{sc} (mm)	N_{DEAR} (IR2) (s^{-1}/bunch/beam)			τ_{tot} (min)
		δ<0.	δ>0.	total	
no scrapers	43	8.77 10^4	1.10 10^5	1.97 10^5	97
10	31	7.45 10^3	2.71 10^4	3.46 10^4	96
9	28	725.	7.38 10^3	8.11 10^3	90
8	25	35.	1.01 10^3	1,05 10^3	77
7	22	0.	55.	55.	63

The two IRs are different and therefore the calculation has been performed for both, using different lattices to reduce the background.

The same quantities as in Table II are shown in Tables III and IV together with the rates for the positive and negative energy deviation. These are listed separately in the tables because the particles with negative energy deviation δ are lost in the quadrupole before the IP, and are the main source of background, while those with positive δ are lost in the quadrupole after the IP and have a very small probability of reaching the detector.

The DEAR experiment is compatible with both the IRs but will be most probably installed into IR1, which has a lower background rate.

The DEAR group is preparing a version of the experiment dedicated to background measurements to take data in a very preliminary stage of machine operation. This will be useful to have a precise estimate of background rates for all the experiments and to adjust the machine parameters in order to reduce the background.

4 CONCLUSIONS

To reduce the background rates due to Touschek scattered particles in the DAΦNE interaction regions the following solutions have been adopted: to increase the vacuum chamber aperture in the interaction regions and to install three beam scrapers in proper locations for each ring.

Two horizontal scrapers will be installed upstream the splitter magnet in both the IRs and a vertical one downstream the splitter in the FINUDA IR.

The horizontal scrapers help also in reducing the background coming from gas bremsstrahlung in the arcs; the vertical one reduces the number of lost particles generated by Coulomb gas scattering.

At a very early stage of machine operation it will be possible to measure the rate of particle losses in the DEAR IR. This will be very useful to improve the machine performance for all the experiments by adjusting the machine parameters to get a high average luminosity with low background rates.

REFERENCES

[1] 'DAΦNE: the first Φ-Factory', G. Vignola and DAΦNE Team, these proceedings.

[2] 'KLOE', KLOE Collaboration, LNF-92/019(IR), Apr. 1992.

[3] 'FINUDA', FINUDA Collaboration, LNF-93/021 (IR), May. 1993 .

[4] 'The DEAR Proposal', DEAR Collaboration, LNF-95/055(IR), Oct. 1995.

[5] 'Preliminary background calculations for DAΦNE', M. K. Sullivan, DAΦNE technical note IR-2, 1993.

[6] 'Beam-gas background calculations for DAΦNE', E. Gero, KLOE note 102, 1994.

[7] 'Background in the KLOE IR due to Touschek scattering', S. Guiducci, DAΦNE technical note IR-5, 1994.

[8] 'Background evaluation in DAΦNE', S. Guiducci, DAΦNE technical note IR-6, 1995.

IMPEDANCE OF A HOLE IN COAXIAL STRUCTURES

S. De Santis, M. Migliorati, L. Palumbo, Università di Roma "La Sapienza" and INFN-LNF
M. Zobov, INFN-LNF, Frascati, Italy

Abstract

We derive the impedance of a circular hole in the inner tube of a coaxial beam pipe. The method used differs from the classical Bethe's theory since, in the calculation of the electric and magnetic dipole moments, we take into account also the scattered fields in the aperture to match the power conservation law. The low frequency impedance shows a real contribution accounting for the TEM waves propagating within the coaxial waveguide. The method is also applied to the case of the outer tube closed at both ends by conducting plates, thus forming a coaxial cavity. The resistive part of the longitudinal impedance obtained can be predominant near the cavity resonances.

1 INTRODUCTION

The impedance of a hole in a beam pipe has been extensively analyzed for many hole shapes and distributions [1-4]. At low frequencies, when the wavelength is much larger than the hole dimensions, the classical method of study involves Bethe's diffraction theory [5], stating that the hole is equivalent to a magnetic and an electric dipole, which moments are related to the incident field. In the first order this method is insensitive of the structure surrounding the pipe and yields a pure imaginary impedance. More recently the real part of the impedance has been calculated considering the energy radiated into the pipe and in the free space [6-8].

We improve the impedance calculations giving a method applicable for any geometry. In particular we show the results in the case of an infinitely long coaxial beam pipe and of a coaxial resonant cavity.

2 IMPEDANCE OF A ROUND HOLE IN COAXIAL STRUCTURES

We assume a primary (incident) field $\mathbf{E}_0$, $\mathbf{H}_0$ produced by a charge travelling off-axis with velocity c and an offset r_1,φ_1 [9]. The scattered field in the beam pipe is represented as a sum of independent modes, each one propagating along both z directions after scattering occurs at the aperture [1]:

$$\begin{aligned}\mathbf{E}_i &= \sum_{n,m}\Big(a_{n,m}\mathbf{e}^{+}_{i(n,m)}e^{-jk_{z(n,m)}z}\theta(z)+ \\ &\qquad + b_{n,m}\mathbf{e}^{-}_{i(n,m)}e^{jk_{z(n,m)}z}\theta(-z)\Big) \\ \mathbf{H}_i &= \sum_{n,m}\Big(a_{n,m}\mathbf{h}^{+}_{i(n,m)}e^{-jk_{z(n,m)}z}\theta(z)+ \\ &\qquad + b_{n,m}\mathbf{h}^{-}_{i(n,m)}e^{jk_{z(n,m)}z}\theta(-z)\Big)\end{aligned} \tag{1}$$

2.1 Coaxial Waveguide

Similarly, the scattered field in an infinitely long outer pipe (Fig. 1) can be expressed as:

$$\begin{aligned}\mathbf{E}_e &= \sum_{n,m}\Big(c_{n,m}\mathbf{e}^{+}_{e(n,m)}e^{-jk_{z(n,m)}z}\theta(z)+ \\ &\qquad + d_{n,m}\mathbf{e}^{-}_{e(n,m)}e^{jk_{z(n,m)}z}\theta(-z)\Big) \\ \mathbf{H}_e &= \sum_{n,m}\Big(c_{n,m}\mathbf{h}^{+}_{e(n,m)}e^{-jk_{z(n,m)}z}\theta(z)+ \\ &\qquad + d_{n,m}\mathbf{h}^{-}_{e(n,m)}e^{jk_{z(n,m)}z}\theta(-z)\Big)\end{aligned} \tag{2}$$

where $\mathbf{e}_e$ and $\mathbf{h}_e$ are the normalized modal function of a coaxial waveguide [8].

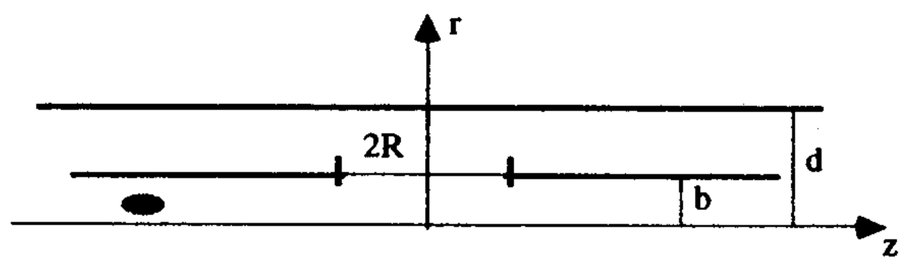

Figure 1 : Coaxial waveguide of radii b and d, with a circular hole of radius R on the inner tube.

The coefficients $a_{n,m}$, $b_{n,m}$, $c_{n,m}$ and $d_{n,m}$ can be found through the Lorentz reciprocity principle. Because of the orthogonality of the modal functions we get:

$$\begin{aligned}a_{n,m} &= \frac{j\omega}{2}\Big(\mu\mathbf{h}_{i(n,m)}e^{-jk_{z(n,m)}z}\cdot\mathbf{M}+ \\ &\qquad -\mathbf{e}_{i(n,m)}e^{-jk_{z(n,m)}z}\cdot\mathbf{P}\Big) \\ b_{n,m} &= \frac{j\omega}{2}\Big(\mu\mathbf{h}_{i(n,m)}e^{jk_{z(n,m)}z}\cdot\mathbf{M}+ \\ &\qquad -\mathbf{e}_{i(n,m)}e^{jk_{z(n,m)}z}\cdot\mathbf{P}\Big) \\ c_{n,m} &= -\frac{j\omega}{2}\Big(\mu\mathbf{h}_{e(n,m)}e^{-jk_{z(n,m)}z}\cdot\mathbf{M}+ \\ &\qquad -\mathbf{e}_{e(n,m)}e^{-jk_{z(n,m)}z}\cdot\mathbf{P}\Big) \\ d_{n,m} &= -\frac{j\omega}{2}\Big(\mu\mathbf{h}_{e(n,m)}e^{jk_{z(n,m)}z}\cdot\mathbf{M}+ \\ &\qquad -\mathbf{e}_{e(n,m)}e^{jk_{z(n,m)}z}\cdot\mathbf{P}\Big)\end{aligned} \tag{3}$$

The dipoles **P** and **M** in (3) are proportional to the true field on the hole through the polarizability tensors $\underline{\underline{\alpha}}_m$ and $\underline{\underline{\alpha}}_e$:

$$\begin{aligned} \mathbf{M} &= \underline{\underline{\alpha}}_m \cdot (\mathbf{H}_0 + \mathbf{H}_i - \mathbf{H}_e)\Big|_{\substack{r=b \\ \varphi=z=0}} \\ \mathbf{P} &= \varepsilon \underline{\underline{\alpha}}_e \cdot (\mathbf{E}_0 + \mathbf{E}_i - \mathbf{E}_e)\Big|_{\substack{r=b \\ \varphi=z=0}} \end{aligned} \tag{4}$$

Substituting the expressions of the fields in (4) we derive the following linear system for the dipole components:

$$\begin{pmatrix} 1+\alpha_m\mu S_{\varphi\varphi} & -\alpha_m\mu S_{\varphi z} & \alpha_m S_{\varphi r} \\ \alpha_m\mu S_{\varphi z} & 1-\alpha_m\mu S_{zz} & \alpha_m S_{zr} \\ \frac{\alpha_e}{c^2} S_{\varphi r} & -\frac{\alpha_e}{c^2} S_{zr} & 1+\alpha_e\varepsilon S_{rr} \end{pmatrix} \begin{pmatrix} M_\varphi \\ M_z \\ P_r \end{pmatrix} = \begin{pmatrix} \alpha_m H_{0\varphi} \\ 0 \\ \alpha_e \varepsilon E_{0r} \end{pmatrix} \tag{5}$$

where we have defined:

$$\begin{aligned} S_{\varphi\varphi} &= \frac{j\omega}{2}\sum \left(h^2_{i\varphi(n,m)} - h^2_{e\varphi(n,m)}\right)\Big|_{\substack{r=b \\ \varphi=0}} \\ S_{\varphi z} &= \frac{j\omega}{2}\sum \left(h_{i\varphi(n,m)}h_{iz(n,m)} + \right. \\ &\qquad \left. - h_{e\varphi(n,m)}h_{ez(n,m)}\right)\Big|_{\substack{r=b \\ \varphi=0}} \\ S_{\varphi r} &= \frac{j\omega}{2}\sum \left(h_{i\varphi(n,m)}e_{ir(n,m)} + \right. \\ &\qquad \left. -h_{e\varphi(n,m)}e_{er(n,m)}\right)\Big|_{\substack{r=b \\ \varphi=0}} \\ S_{zz} &= \frac{j\omega}{2}\sum \left(h^2_{iz(n,m)} - h^2_{ez(n,m)}\right)\Big|_{\substack{r=b \\ \varphi=0}} \\ S_{zr} &= \frac{j\omega}{2}\sum \left(h_{iz(n,m)}e_{ir(n,m)} + \right. \\ &\qquad \left. - h_{ez(n,m)}e_{er(n,m)}\right)\Big|_{\substack{r=b \\ \varphi=0}} \\ S_{rr} &= \frac{j\omega}{2}\sum \left(e^2_{ir(n,m)} - e^2_{er(n,m)}\right)\Big|_{\substack{r=b \\ \varphi=0}} \end{aligned} \tag{6}$$

If we consider the simple case of frequencies below the cutoff of the TE and TM modes, there is propagation in the outer pipe only through a TEM mode. The system in (5) reduces therefore to:

$$\begin{pmatrix} 1+\alpha_m\mu S_{\varphi\varphi} & \alpha_m S_{\varphi r} \\ \frac{\alpha_e}{c^2} S_{\varphi r} & 1+\alpha_e\varepsilon S_{rr} \end{pmatrix} \begin{pmatrix} M_\varphi \\ P_r \end{pmatrix} = \begin{pmatrix} \alpha_m H_{0\varphi} \\ \alpha_e \varepsilon E_{0r} \end{pmatrix} \tag{7}$$

with

$$S_{\varphi\varphi} = \frac{j\omega}{2} h^2_{e0\varphi}\Big|_{\substack{r=b \\ \varphi=0}} \quad , \quad S_{\varphi r} = \frac{j\omega}{2} h_{e0\varphi} e_{e0r}\Big|_{\substack{r=b \\ \varphi=0}}$$
$$\text{and} \quad S_{rr} = \frac{j\omega}{2} e^2_{e0r}\Big|_{\substack{r=b \\ \varphi=0}}, \tag{8}$$

where the single subscript 0 designates the TEM modal function.

Since the longitudinal impedance is [1]

$$Z_{//}(\omega) = -j\frac{\omega Z_0}{2\pi q b}\left[\frac{1}{c}M_\varphi + P_r\right] \tag{9}$$

we finally get:

$$Z_{//}(\omega) \approx \frac{Z_0}{6\pi^2} k_0 R (R/b)^2 \left[-j + \frac{k_0 R}{6\pi}\frac{(R/b)^2}{ln(d/b)}\right] \tag{10}$$

Solving (7) one can also derive the dipole longitudinal and transverse impedances [8]. They are respectively:

$$Z^{n=1}_{//}(r,\varphi) = -j\frac{2k_0 Z_0}{3\pi^2 b^4} R^3 \frac{r r_1 cos\varphi cos\varphi_1}{\Delta} \tag{11}$$

and

$$\mathbf{Z}_\perp(\omega) = -j\frac{2Z_0}{3\pi^2}\frac{R^3}{b^4}\frac{cos\varphi_1}{\Delta}\hat{\mathbf{r}} \tag{12}$$

where

$$\Delta = 1 - j\frac{k_0 R (R/b)^2}{6\pi \ln(d/b)} \tag{13}$$

2.2 Coaxial Resonator

When the outer pipe is closed by conducting plates (Fig. 2), the expansion in propagating modes (2) is substituted by a sum of resonant modes [5]:

$$\begin{aligned} \mathbf{E}_e &= \sum_n c_n \mathbf{e}_{e(n)} \\ \mathbf{H}_e &= \sum_n d_n \mathbf{h}_{e(n)} \end{aligned} \tag{14}$$

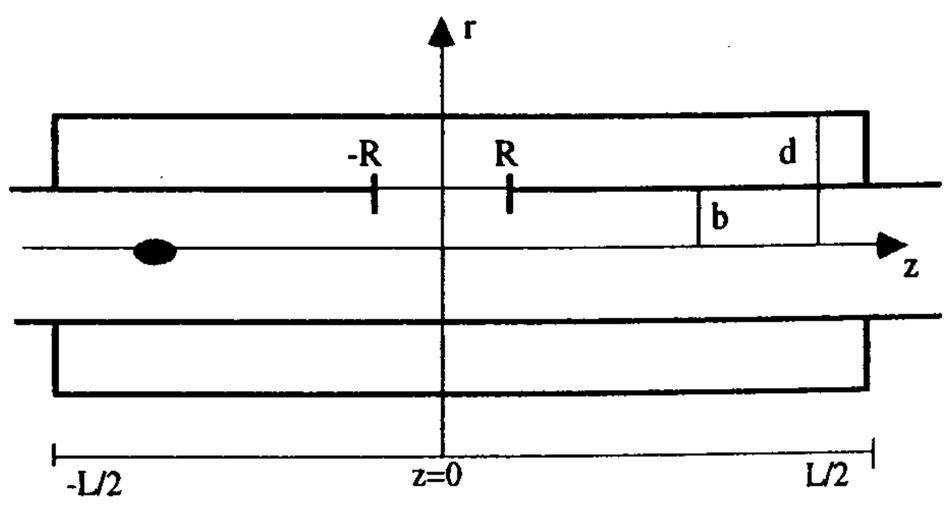

Figure 2 : Coaxial resonator.

The expressions of the coupling coefficient also change, so that we have:

$$c_n = \frac{-j\omega\mu k_n \mathbf{h}_{e(n)} \cdot \mathbf{M} + \omega^2 \mu \left(1 + \frac{1-j}{Q_n}\right) \mathbf{e}_{e(n)} \cdot \mathbf{P}}{k_n^2 - k_0^2 \left(1 + \frac{1-j}{Q_n}\right)} \qquad (15)$$

$$d_n = \frac{j\omega k_n \mathbf{e}_{e(n)} \cdot \mathbf{P} + k_0^2 \mathbf{h}_{e(n)} \cdot \mathbf{M}}{k_n^2 - k_0^2 \left(1 + \frac{1-j}{Q_n}\right)}$$

If we limit ourselves to frequencies below the beam pipe cutoff, assuming to have the TEM_1 mode only resonating in the cavity, the linear system in (7) becomes

$$\begin{pmatrix} 1 + \alpha_m \frac{k_0^2}{\tilde{k}} H_1^2 & -j\alpha_m \omega \frac{k_1}{\tilde{k}} E_1 H_1 \\ j\alpha_e \omega\mu\varepsilon \frac{k_1}{\tilde{k}} E_1 H_1 & 1 + \alpha_e \frac{k_0^2}{\tilde{k}} \tilde{q} E_1^2 \end{pmatrix} \begin{pmatrix} M_\varphi \\ P_r \end{pmatrix} = \qquad (16)$$

$$= \begin{pmatrix} \alpha_m H_{0\varphi} \\ \alpha_e \varepsilon E_{0r} \end{pmatrix}$$

where, for the sake of compactness, we have defined

$$\tilde{q} = 1 + \frac{1-j}{Q_1}, \quad \tilde{k} = k_1^2 - k_0^2 \tilde{q} \qquad (17)$$

the quality factor Q_1 for such a cavity is given in appendix.

When z_0=0, that is the hole is at the cavity mid-length, it is easy to show that the real part of the longitudinal impedance is

$$Z_{RE} = \frac{2 Z_K \eta k_1^2 k_0^2 Q_1^{-1}}{\left[k_1^2 - k_0^2 (1+2\eta)(1+Q_1^{-1})\right]^2 + \left[k_0^2 (1+2\eta) Q_1^{-1}\right]^2} \qquad (18)$$

where

$$Z_K = \frac{k_0 Z_0 R^3}{6\pi^2 b^2} \text{ and } \eta = \frac{(R/b)^2 (R/L)}{3\pi \ln(d/b)}, \qquad (19)$$

and that its maximum value

$$Z_{RE,\max} = \frac{2 Z_K \eta (Q_1 + 1)}{1 + 2\eta} \approx 2\eta Q_1 Z_K \approx \approx Z_0 \eta^2 Q_1 \ln(d/b) \qquad (20)$$

is reached when

$$k_0 = \frac{k_1}{\sqrt{(1+2\eta)(1+Q_1^{-1})}} \qquad (21)$$

The imaginary impedance is given by

$$Z_{IM} = -jZ_K \left\{1 - 2\eta k_0^2 \times \frac{k_1^2 (1+Q_1^{-1}) - k_0^2 (1+2\eta)(1+2Q_1^{-1})}{\left[k_1^2 - k_0^2 (1+2\eta)(1+Q_1^{-1})\right]^2 + \left[k_0^2 (1+2\eta) Q_1^{-1}\right]^2}\right\} \qquad (22)$$

so that it is zero when condition (21) is fulfilled. It should be noted that, in the two cases presented, the real part can change dramatically from negligible values up to several times Z_K near the cavity resonance.

3 CONCLUSIONS

The impedance of coaxial open and resonant structures, coupled by a hole to the beam pipe, has been computed. The analytical results agree reasonably well with numerical simulations with 3D codes. The method presented is being used to compute more general impedances for the resonant structure.

Appendix

The quality factor for the TEM_1 mode of a coaxial-line resonator is

$$Q_1 = \frac{2L}{\delta \left(4 + \frac{L(1+d/b)}{d \ln(d/b)}\right)} \qquad (23)$$

where δ is the skin depth, given by

$$\delta = \sqrt{2} k_0^{-1} \left[\sqrt{1 + (\sigma/\omega\varepsilon)^2} - 1\right]^{-1/2} \qquad (24)$$

REFERENCES

[1] S.S. Kurennoy, Part. Acc. **39**, 1 (1992).

[2] R.L. Gluckstern, CERN SL/92-05 (AP), 1992.

[3] R.L. Gluckstern, Phys. Rev. A **46**, 1110 (1992).

[4] S.S. Kurennoy, SSCL-Preprint No. 636, 1993.

[5] R.E. Collin, *Field Theory of Guided Waves* (IEEE, New York,1991), 2nd Ed.

[6] G.V. Stupakov, Phys. Rev. E **51**, 3515 (1995).

[7] R.L. Gluckstern, S.S. Kurennoy, and G.V. Stupakov, Phys. Rev. E **52**, 4354 (1995).

[8] S. De Santis, M. Migliorati, L. Palumbo, and M. Zobov, *Coupling Impedance of a Hole in a Coaxial Beam Pipe*, Phys. Rev. E (to be published).

[9] L. Palumbo, V.G. Vaccaro, and M. Zobov, LNF-94/041 (P) (1994).

FIRST RESULTS OF THE DAΦNE INJECTION SYSTEM COMMISSIONING

The DAΦNE Project Team*
presented by Fernando Sannibale
INFN Laboratori Nazionali di Frascati - C.P. 13 - 00044 Frascati (Roma) - Italy

Abstract

The injection system of DAΦNE, the Φ-Factory under construction at LNF in Frascati, consists of an S-band 800 MeV electron, 550 MeV positron Linac, an intermediate 510 MeV Accumulator and about 140 m long Transfer Lines. The whole system is designed to work at the operating energy of the double storage ring collider, in order to refill the rings frequently in a "topping up" mode. Construction and assembly of the Linac and Accumulator have been completed in fall 1995 and winter 1996 respectively. Results of commissioning and measurements of beam parameters are described.

1 INTRODUCTION

DAΦNE [1] is provided with a full energy injector [2]. Electron and positron beams are generated and accelerated up to the nominal energy of 510 MeV along the Linac and then stored and phase space damped in the Accumulator ring before the injection into the Main Rings. The injection rate is 50 Hz in the Accumulator and 1 Hz in the Main Rings. Phase adjustments between the rings RF's jointly with a proper timing will allow to fill each of the Main Rings 120 buckets. Positron and electron production and injection are not simultaneous and the design time to fill all of the Main Rings buckets is ~ 2 min for positrons and ~ 1 min for electrons. The overall injection time should be ≤ 10 min, including the time necessary for switching between positron and electron modes. The Main Rings beam life time is ~ 3 hours but considerations concerning integrated luminosity optimization, suggest to adopt a 'topping-up' scheme by injecting every hour approximately.

The Linac commissioning with electrons started at the beginning of the year and the up to date results are presented. The Accumulator electron injection has just started and the encouraging first results are described. Positron beam tests are scheduled for the next future.

* M. Bassetti, M.E. Biagini, C. Biscari, R. Boni, S. Chen, V. Chimenti, A. Clozza, G. Delle Monache, S. De Simone, G. Di Pirro, H. Dong, A. Drago, S. Faini, A. Gallo, N. Ganlin, A. Ghigo, S. Guiducci, Y. He, F. Marcellini, C. Marchetti, M.R. Masullo, M. Migliorati, C. Milardi, M. Modena, L. Palumbo, L. Pellegrino, M. Preger, G. Raffone, C. Sanelli, F. Sannibale, M. Serio, F. Sgamma, B. Spataro, A. Stecchi, C. Vaccarezza, M. Vescovi, S. Vescovi, G. Vignola, D. Yao, M. Zobov.

2 INJECTION SUB-SYSTEMS

2.1 Linac

The Linac, the first part of the injection chain, was assigned to the American company TITAN BETA on the base of a 'turn key' contract [3]. It is a ~ 60 m long linac able to deliver (50 pps) 800 MeV electron beam and 550 MeV positron beam with a FWHM bunch length of 10 ns. The positron conversion energy is 250 MeV.

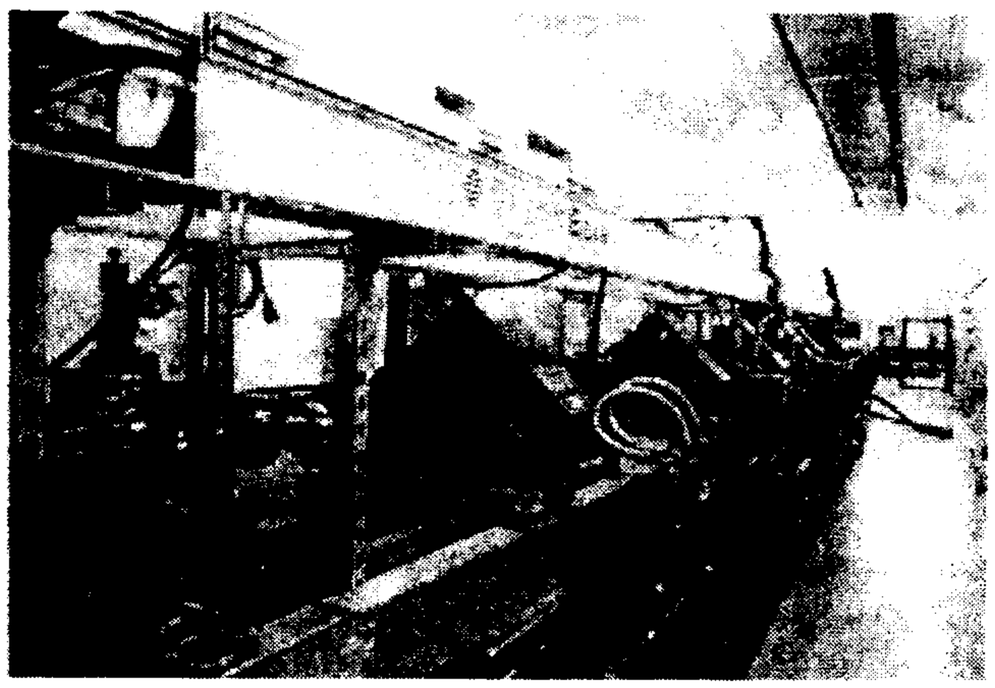

Figure 1. DAΦNE-Linac low energy part view.

The RF scheme includes 4 S-band (2856 MHz) 45 MW klystrons each one equipped with a pulse compression device (SLED). The accelerating structure is composed by 15 SLAC type sections 3 m long, while the injector has a 120 keV thermoionic gun followed by a harmonic prebuncher and a five cells buncher. A pulsed solenoidal lens (SLAC flux concentrator) and ~ 7 m of 0.5 T DC solenoids compose the positron capture system. A positron separator downstream the positron converter allows to stop the secondary electron beam.

A portion of the Linac is shown in figure 1.

2.2 Accumulator

The Accumulator ring design has been based on the Orsay ring ACO [4,5]. The high values of the energy and emittance acceptances, ± 1.5% and 10 mm mrad @ 510 MeV respectively, allowed to relax the requirements on the Linac beams. Moreover the low values of the energy spread and emittance of the extracted beams, ± 0.1 % and 0.25 mm mrad @ 510 MeV respectively, permit the injection into the 'tight' buckets of the Main Rings.

Figure 2. Accumulator view.

The Accumulator length, 32.56 m and the RF, 73.65 MHz, are respectively 1/3 and 1/5 of the Main Rings ones, the RF harmonic number is 8.

The linear lattice periodicity is 4 and each period has 2 sextupoles for chromaticity correction. In the straight sections are placed the RF cavity [6] and the injection and extraction kickers [7] and septa [8]. The diagnostics scheme [9] distributed along the ring includes also 2 synchrotron radiation monitors.

Figure 2 shows a 'fish-eye' view of the Accumulator.

2.3 Transfer Lines

Linac, Accumulator and Main Rings are connected to each other by ~ 140 m of transfer lines [10].

Due to the requirement of using the pre-existing civil structures, the transfer lines have a fairly complex geometry that includes a section where the beams passes through, either during the Accumulator injection or in the extraction.

Downstream the Linac are placed the diagnostics for measuring the physical quantities of the out coming beam [11,12]. A Beam Test Facility, that can operate in parasitic mode with the Main Rings injection, is also present [13].

3 EXPERIMENTAL RESULTS

The Linac operation with the electron beam started on January 96. Since then the shifts have been shared between electron beam commissioning and the completion of the Linac control system integration. The latter is now completed and the electron commissioning is going ahead in parallel with the Accumulator electron injection first operation.

3.1 Linac Electron Beam Commissioning

Electron gun

It is a 150 keV (max) Pierce geometry triode gun with a 3 cm^2 dispenser cathode able to 8 A (max) output. Typical operation values are 6 A 120 keV in the positron mode and 0.5 A 120 keV in the electron one. Figure 3 shows an example of the gun pulse.

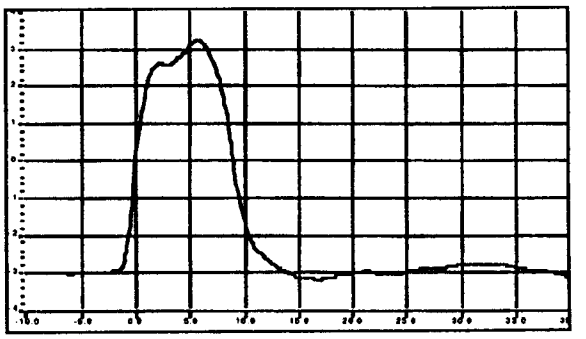

Figure 3. Typical Gun Pulse. The horizontal scale unit is 5 ns/div and the current peak value is 3.8 A. The monitor used is of the resistive wall type.

Current, energy and spot size at positron converter (PC).

With the design values for these quantities, 4 A, 250 MeV and 1 mm (sigma), the expected positron conversion efficiency is 0.9%. Concerning current, simulations showed that 7.3 A at the electron gun are required to obtain the design value. So far we did not operate in the positron mode, anyway during a preliminary test, 3 A at PC have been achieved with 7 A at gun. Finally it is worth to say that during the factory tests performed on May 1994 at TITAN BETA 4 A at PC have been reached with 6.2 A at gun.

Because of the RF structure geometry, the system spectrometer, placed downstream the Linac, cannot be used for measuring the beam energy at the PC position. Anyway an estimate has been done by using a steering coil and a flag placed just before the PC. The measured value was (200±20) MeV. This value is lower than the design one because one of the two klystrons that deliver the RF power to four of the five accelerating sections upstream the PC, saturates at a low power level (35 MW instead of 45 MW). In the factory tests, mentioned above, a value of (240±20) MeV was measured.

The spot size design value, 1 mm (σ), has been achieved either during the factory or in the actual test.

Current and energy at Linac end.

During the injection into the Accumulator, the Linac is running in the following configuration: 20 ÷ 300 mA electron bunches with energy (510±5) MeV at 1 pps.

Figure 4 shows an example of beam transverse spot size at the Linac end. The monitor used is a chrome-doped allumina flag viewed by a CCD camera connected to an image analyzer.

From the electron beam commissioning point of view we are doing a number of measurements necessary to characterize and optimize the Linac. Between these, it is worth to mention the one concerning the accelerating sections electrical field, a value of 17.8 MV/m has been measured against the design value of 18 MV/m.

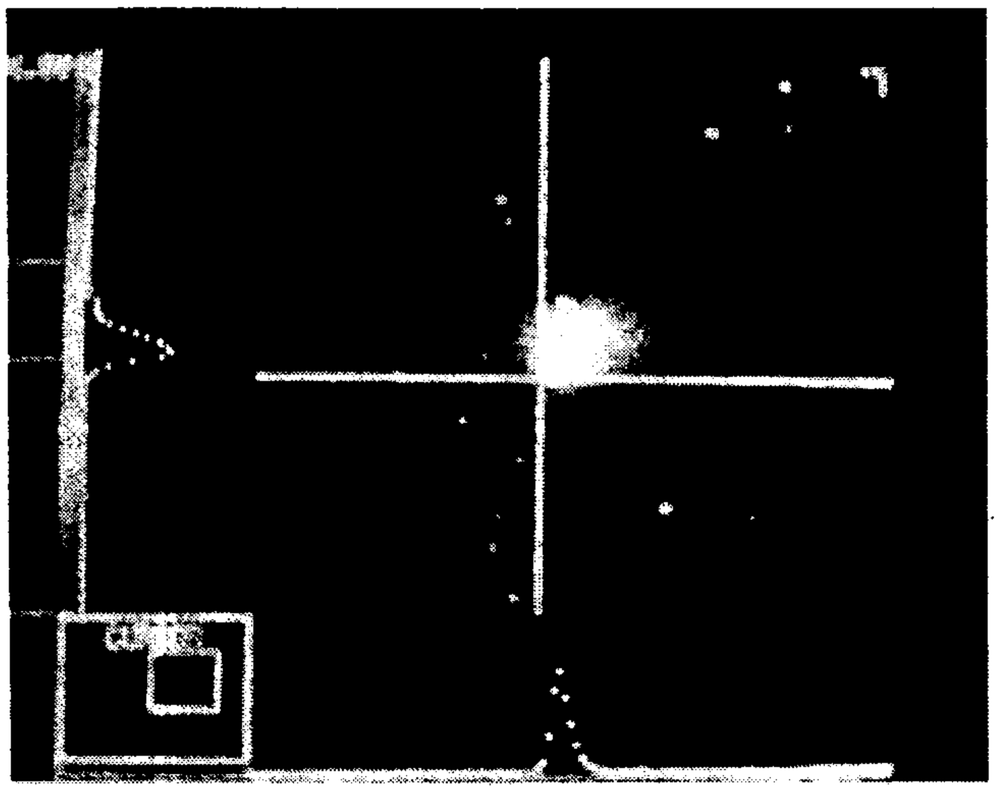

Figure 4. Electron beam spot at Linac end. The energy is 510 MeV and the sigma is ~ 1.5 mm.

3.2 Accumulator Electron Beam Injection

Transfer line set up.
The Linac is connected to the Accumulator by ~ 45 m of transfer line, which include 4 horizontal and 2 vertical bending magnets, two septa, 18 quadrupoles and 8 corrector magnets. A distributed scheme of diagnostics, including 7 strip lines, 3 beam charge monitors and 6 fluorescent screens, allowed us to transport the electron beam to the Accumulator in few hours.

Accumulator injection.
Four strip lines beam position monitors, one in each of the Accumulator periods, permit to follow the beam during the first turns. Simulations showed that with the nominal tunes and without firing the injection kickers, the beam must complete ~ 2.5 turns before hitting the vacuum chamber. The beam first turn was achieved in one shift and during the second shift the 2.5 turns were reached. In the following two shifts the kickers were tuned up and after minor adjustments to correct a small vertical orbit the beam was successfully circulated for more than 300 turns. The beam circulating in the Accumulator is presented in figure 5, where the electrode signals sum of one of the strip lines is shown. Several passages are clearly visible and the distance in frequency between two contiguous peaks is ~ 9.2 MHz which correspond to the Accumulator revolution frequency.

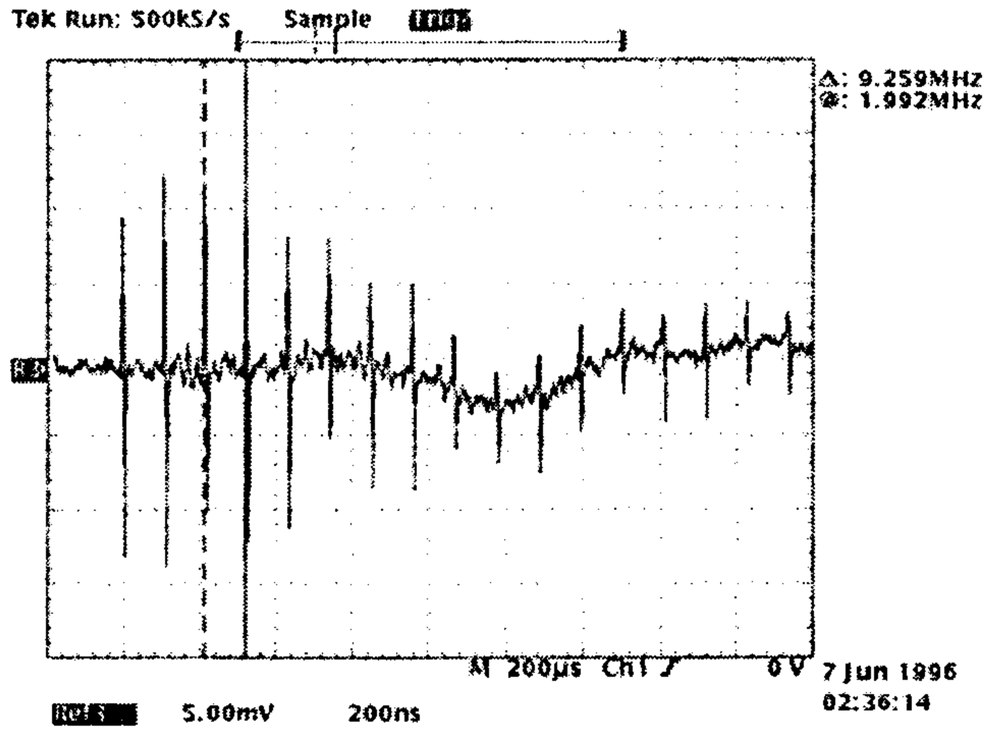

Figure 5. Circulating beam seen through one of the Accumulator strip lines.

REFERENCES

[1] G.Vignola, "DAΦNE: the First Φ−Factory", This Conference.

[2] R. Boni et al., "The Frascati Φ−Factory Injection System", PAC 91, S. Francisco, May 1991.

[3] K. Whitham et al., "Design of the e+/e- Frascati Linear Accelerator for DAΦNE", PAC 93 Washington, May 1993.

[4] M. Preger, "A Positron an Electron Accumulator for DAΦNE" DAΦNE Technical Note I-1, Nov. 90.

[5] M.R. Masullo et al., "DAΦNE Accumulator Update-3" DAΦNE Technical Note I-9, May. 92.

[6] S. Bartalucci et al., "RF Cavity Design of the DAΦNE Accumulator", DAΦNE Technical Note RF-4, September 1991.

[7] S. De Simone, A. Ghigo, "DAΦNE Accumulator Kickers", EPAC 92, Berlin, March 1992.

[8] M. Modena et al., "High Current Density Septa for DAΦNE Accumulator and Storage Rings", EPAC 92, Berlin, March 1992.

[9] M.E. Biagini et al., "Overview of DAΦNE Beam Diagnostics", EPAC 94, London, June 1994.

[10] C. Biscari, "Transfer Line for DAΦNE Injection", DAΦNE Technical Note I-8, April 1992.

[11] F. Sannibale, M. Vescovi, " LINAC to Accumulator Area Transfer Line (LAAT) & DAΦNE-LINAC Spectrometer (DLS)", DAΦNE Technical Note LC-3, February 1992.

[12] F. Sannibale, "DAΦNE-LINAC Beams Emittance Measurement Design", DAΦNE Technical Note LC-5, September 1992.

[13] A. Ghigo, F. Sannibale, "Single Electron Operation Mode in DAΦNE BTF", EPAC 94, London, June 1994.

IMPEDANCE OF DAΦNE SHIELDED BELLOWS

A. Gallo, A. Ghigo, F. Marcellini, B. Spataro, M. Zobov, INFN-LNF, Frascati, Italy
L. Palumbo, Rome University and INFN-LNF, Frascati, Italy

Abstract

In order to avoid sliding contacts in the DAΦNE bellows design, the bellows screen is made of thin strips oriented in the vertical plane and separated by small gaps. The strips are produced by a hot forming method and have a waved shape, allowing both the longitudinal expansion and the horizontal shift.

The results of numerical simulations and impedance measurements for the shielded bellows are presented. The methods to eliminate and damp the residual Higher Order Modes (HOM) in such a complicated structure are discussed. The possible power losses and the impact of the bellows impedance on the beam dynamics are estimated.

1 INTRODUCTION

The bellows placed between the DAΦNE [1] arcs and straight sections must allow 35 mm longitudinal expansion and 10 mm horizontal offset. It was decided to avoid any sliding contacts in the bellows which can be burned out due to the high current flowing on the bellows screen. Moreover, if, for any reason, there is no contact between the sliding surfaces the capacitance between the sliding contacts can create a resonant circuit with the rest of the bellows. This can affect the multibunch beam stability and is a source of possible high power loss. Another potential danger is creation of dust particles between the sliding surfaces.

The bellows design originally proposed for DAΦNE [2] is shown in Fig. 1.

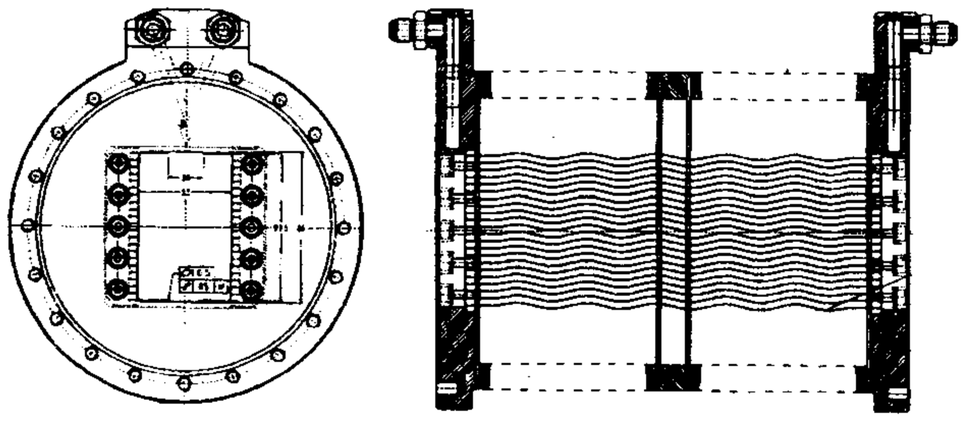

Figure 1 - Initially proposed DAΦNE bellows design.

The bellows screen is made of thin waved strips oriented in the vertical plane and separated by 4 mm gaps. The width of a strip is 5 mm, i. e. wider than the gap between the strips in order to attenuate radiation outside the screen.

In this paper we discuss the results of bellows impedance measurements and numerical simulations and describe methods to damp residual High Order Modes (HOMs) in such a complicated structure.

2 PROTOTYPE MEASUREMENTS

In order to check the effectiveness of the screen and to measure the bellows impedance a prototype has been built. The bellows itself was substituted by a pill-box cavity having approximately the same sizes as bellows.

Figure 2 shows the results of the impedance measurements with a standard wire method [2]. Dotted lines correspond to HOMs trapped in the pill-box volume without the screen, while solid ones show the shunt impedance of the HOMs remaining in the structure with the inserted screen.

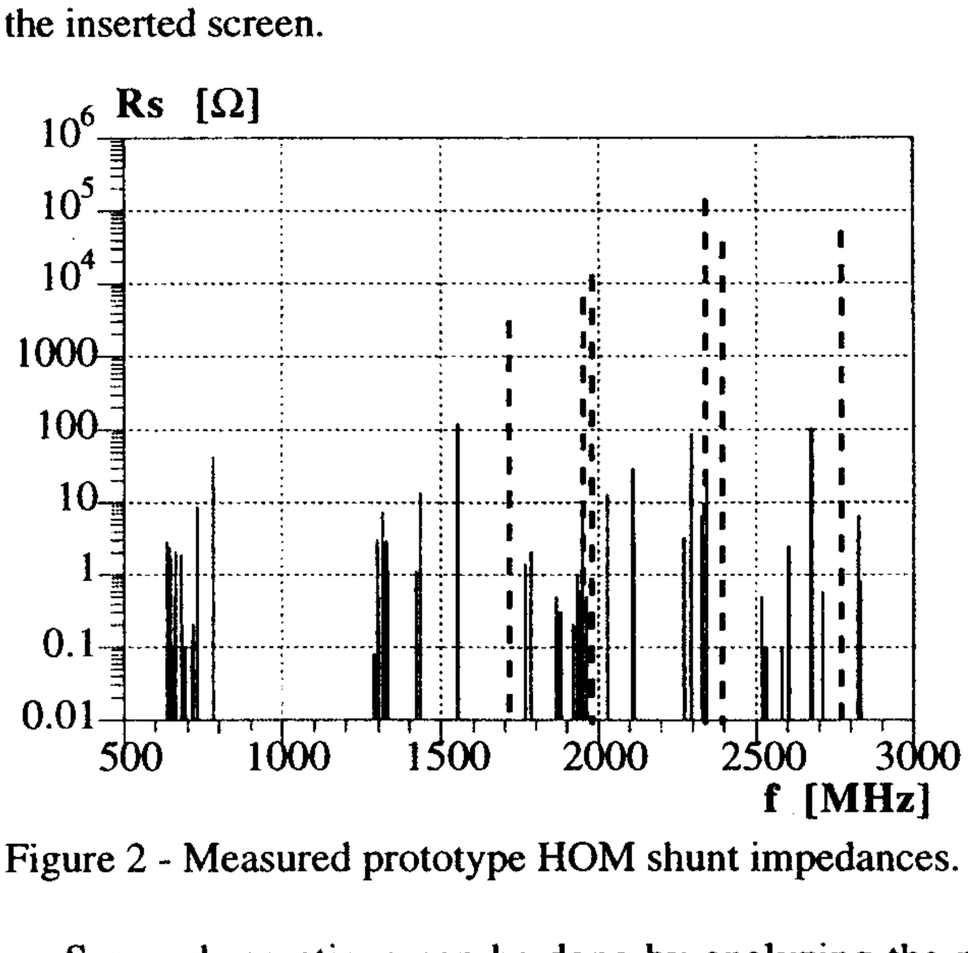

Figure 2 - Measured prototype HOM shunt impedances.

Some observations can be done by analyzing the results presented in Fig. 2. First, the HOMs of the cavity itself having the shunt impedances up to 10^5 Ω are successfully eliminated by the screen. On the other hand, the screen introduces new HOMs. Some of them are at very low frequencies.

The frequencies of the new modes appear to cluster around frequencies f = nc/2l, where n = 1,2,3,.. and l is the strip length. Even though the shunt impedances of these mode are very low the rise time of the multibunch instabilities due to the modes is at a manageable limit of the DAΦNE longitudinal feedback system. Moreover, the number of the modes is high and the frequency distribution is rather dense.

This means that probability of the coupling of the beam power spectrum lines to the HOMs is not negligible. The power loss in case of the full coupling can be of the order of some thousand watts.

This gives rise to the problem of how to dissipate such a power. If the HOM fields were mostly trapped between the strips, the problem would get unsolvable: it is practically impossible to dissipate the power under vacuum without strong heating and breaking the strips.

So numerical simulations were undertaken in order to understand why these new modes appear, what is the field configuration of the modes and how to damp them to a harmless level.

3 NUMERICAL SIMULATIONS

Numerical simulations for a 1/4 of the structure have been performed with MAFIA [4]. Due to the memory and CPU time limitations we have simulated the structure with the straight strips. Table 1 shows the first found HOMs.

Table 1. Parameters of HOMs found by MAFIA

mode	f [MHz]	Rs [Ω]	Q
1	807.631	0.109	8830
2	823.323	0.387	6651
3	828.950	0.059	5322
4	830.912	0.193	4671
5	831.744	0.018	4319
6	832.165	0.004	4131
7	832.316	0.327	4042
8	833.016	**7.062**	13880
9	1608.646	0.529	12440
10	1644.461	0.247	9400
11	1655.915	2.479	7517
12	1659.926	0.032	6572
13	1661.939	0.231	6027
14	1662.651	1.389	5746
15	1663.741	1.234	19370
16	1969.460	0.043	19820
17	2392.983	1.072	15120

Again we can observe the clusters of modes with wavelengths close to $\lambda = 2l/n$. The strongest mode in each cluster is the mode of TEM kind (see Fig. 3)) concentrated between the pill-box surface and the screen structure playing the role of the inner conductor for such a coaxial. The other modes are trapped between the strips (see Fig. 4 as an example) having relatively low shunt impedances.

The shunt impedances in the simulations are lower than in the measurements. This is because the strips were straight in the simulations while in the measurements the strips had the waved shape.

The simulations of the prototype with the waved strip screen have been performed with HFSS code [5] modeling the measurement by the wire method. It has been found that the mode pattern still has the same clustered structure but the shunt impedances are substantially increased. In particular, the TEM mode in the first cluster reaches the shunt impedance values of 56 Ω, in the second cluster the coaxial mode has the shunt impedance of 206 Ω.

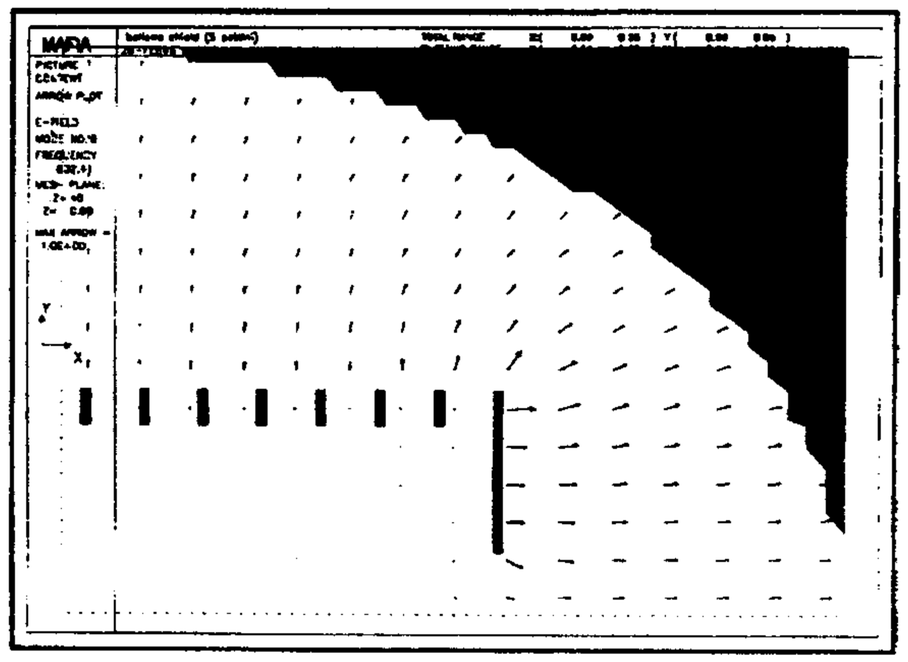

Figure 3 - Example of coaxial HOM (mode 8 in Table 1).

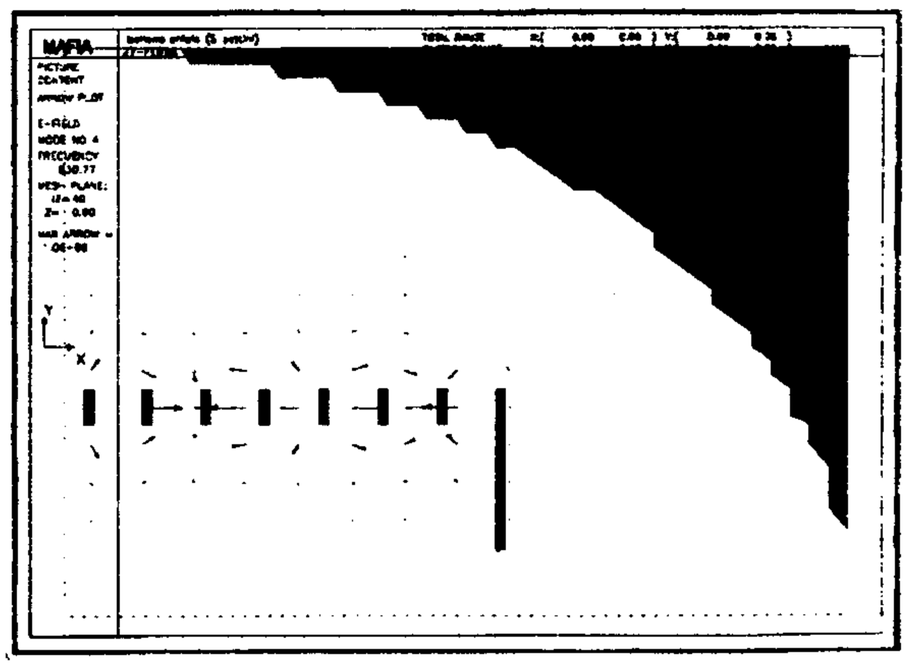

Figure 4 - Example of a HOM trapped between strips.

This agrees reasonably well with measurements on the prototype, where these mode have the shunt impedance of 43 Ω and 121 Ω, respectively. The same increase is observed also for the other modes in the waved strip screen.

4 MEASURES TO DAMP HOMS

In order to push frequencies of the HOMs beyond the bunch spectrum, i. e. to avoid dangerous power losses, it was proposed to put transverse connections between nodes of the waved strips. In this way we reduce the length of the slots created between each neighbouring strips. It means that TM wave guide modes with wavelength $\lambda > 2l$, where l is the reduced slot length, can not penetrate outside the screen and excite resonant HOMs. As far as the connections are placed between the nodes the flexibility of the screen does not change much.

However, due to the fact that the bellows are placed between arcs and straight section there are two lateral slots along the screen which are foreseen for the synchrotron radiation exit. It is clear *a priori* that some modes are left in the structure. At most we can close one lateral slot on the side where the synchrotron radiation does not go.

In order to damp further the remaining modes we propose in addition to the connections to use transverse plates as shown in Fig. 5. To fit the bellows shape the plates have been chosen to have the "half of the moon" shape.

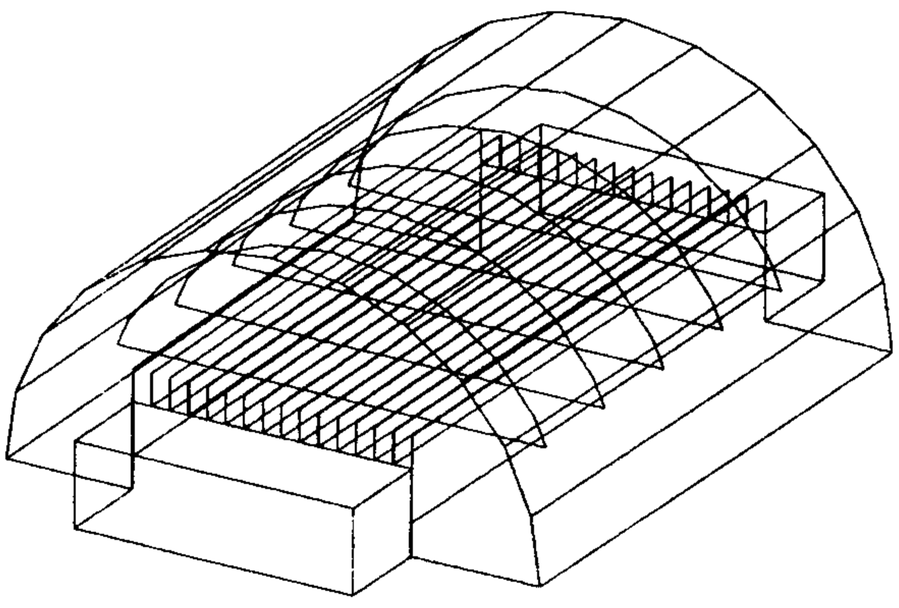

Figure 5 - Sketch of the screen with transverse plates.

In our understanding these plates push the electric fields of the coaxial type modes further away from the beam axis thus reducing the coupling of these modes to the beam. The second advantage is that the plates prevent penetration of the TE modes into the outer volume. The third, the plates can be considered as an radiator which helps to dissipated lost power.

The measurements were performed on a new prototype with thinner strips (0.2 mm) allowing to measure the shunt impedance of the modes as a function of the bellows expansion.

Table 2 shows the measured HOM parameters and the estimated longitudinal multibunch instability rise times for 217 mm bellows length (Maximum expansion is 230 mm).

Table 2. Parameters of measured HOMs.

mode	f [MHz]	Rs [Ω]	τ [ms]
1	667.0	0.8	258.9
2	954.1	1.3	132.5
3	974.8	2.2	77.8
4	1511.8	0.9	191.2
5	1528.5	----	
6	1750.2	0.8	233.5
7	2415.9	6.5	40.7
8	2482.4	----	
9	2645.8	1.9	159.0

As it can be seen, the rise time is higher than the radiation damping time which is equal to 17.8 ms for DAΦNE. Remembering that there are 8 bellows in the ring one could expect a proportional reduction of the rise time. However, we believe that all the bellows will be differently expanded, i.e. it is hardly possible that all the frequencies of the HOMs having similar field configuration in different bellows coincide exactly. Nevertheless, if this happens the multibunch instability rise time will be still longer than the damping time provided by the feedback system.

In order to estimate the losses in the worst case let us consider the full coupling (hardly possible) of the mode at 974.8 MHz with a bunch power spectrum line for 120 equally spaced bunches. It gives 85 W. This is a quite acceptable value. We should also stress here that not all the power is dissipated under the vacuum. Due to the coaxial nature of the remaining modes a part of the power is dissipated on the bellows surface on air.

One of our concerns was the transverse instability. We have no a set for the measurements of the transverse modes yet and have to rely on MAFIA simulations in this case. Fortunately, the rise times due to the transverse modes calculated by MAFIA are very much higher (order of seconds) than the damping time which is 36 ms for horizontal plane and 37 ms for the vertical one. Certainly, the transverse plates ("half of the moon") help much in damping of the modes.

CONCLUSIONS

A bellows design without sliding contacts has been proposed. Complete set of measurements on the prototype and numerical simulations confirmed that there are no HOMs dangerous for the beam dynamics both in the expanded and squeezed state of the bellows. The remaining modes can drive neither transverse nor longitudinal multibunch instability. Even in the most unfavourable situation the power loss due to these modes is acceptable.

ACKNOWLEDGMENTS

The authors wish to thank G. Sensolini and V. Andreassi for the prototype mechanical design and fabrication, and A. Cecchineli, S. Quaglia, M. Scampati and A. Sprecacenere for their continuos support to the experimental activity.

REFERENCES

[1] "DAΦNE Machine Project", LNF - 94/055 (P).
[2] Hank Hsieh, private communications.
[3] F. Caspers, Joint US-CERN School on Particle Accelerators, Lecture Notes in Physics, No. 400, Springer - Verlag, 1992.
[4] R. Klatt, et. al., SLAC report 303, 1986.
[5] Hewlett-Packard Co., "HFSS, The High Frequency Structure Simulator HP85180A^{TM}".

HIGH POWER TEST OF THE WAVEGUIDE LOADED RF CAVITY FOR THE FRASCATI Φ-FACTORY MAIN RINGS

R. Boni, A. Gallo, F. Marcellini, INFN-LNF, Frascati, Italy

Abstract

The Φ-Factory DAΦNE is a high current, multibunch electron-positron double ring collider in construction in Frascati. The high order modes (HOMs) of the accelerating cavities can drive longitudinal and transverse coupled-bunch instabilities. A single-cell cavity connected to the vacuum chamber through long tapered beam tubes and loaded with rectangular waveguides to damp the HOMs has been designed, fabricated and high power tested. This paper reports the results of the power tests and the up to date progress of the whole DAΦNE RF system.

1 INTRODUCTION

The accelerating cavity for the Frascati Φ-Factory [1] is a normal conducting single cell made of oxygen free high conductivity (OFHC) copper.

The cavity design was optimised to reduce as much as possible both the HOM content, the primary source of longitudinal and transverse coupled-bunch instabilities, and the contribution to the broadband machine impedance [2].

The cavity cell has a rounded shape without nose cones and is connected to the ring vacuum chamber through large tapered tubes 80 cm long.

This unusual choice allows to reduce significantly the cavity loss factor as well as the impedances of the HOMs (i.e. the R/Q values), even without external damping devices. On the other hand, this solution impacts negatively on the fundamental mode shunt impedance, but this is not of primary importance in DAΦNE since the required accelerating voltage is rather low (250 KV/ring). The HOM Q damping is accomplished by 5 waveguides, 3 connected to the cavity cell and aimed to couple out the low frequency HOMs, and 2 connected on the tapers, where the high frequency HOMs are essentially located. The main characteristics of the DAΦNE RF cavity are summarized in Table I, while a picture of the first DAΦNE cavity, not including the taper waveguides, is shown in Fig. 1.

Table I: DAΦNE RF Cavity parameters

f_{RF}	Resonant frequency	368.32 MHz
V_c	Cavity voltage	250 kV
Q_0	Cavity unloaded quality factor	33,000
R_s	Cavity shunt impedance	2 MΩ
β	Cavity input coupling factor	2.5
P_{MAX}	Max klystron RF power	150 kW
I_b	Max beam current	5 Amps
E_r	Energy loss / turn	15 keV
P_{HOM}	Cavity HOM power	≈ 3 kW
Δf_{bl}	Max. beam loading detuning	≈ - 500 kHz

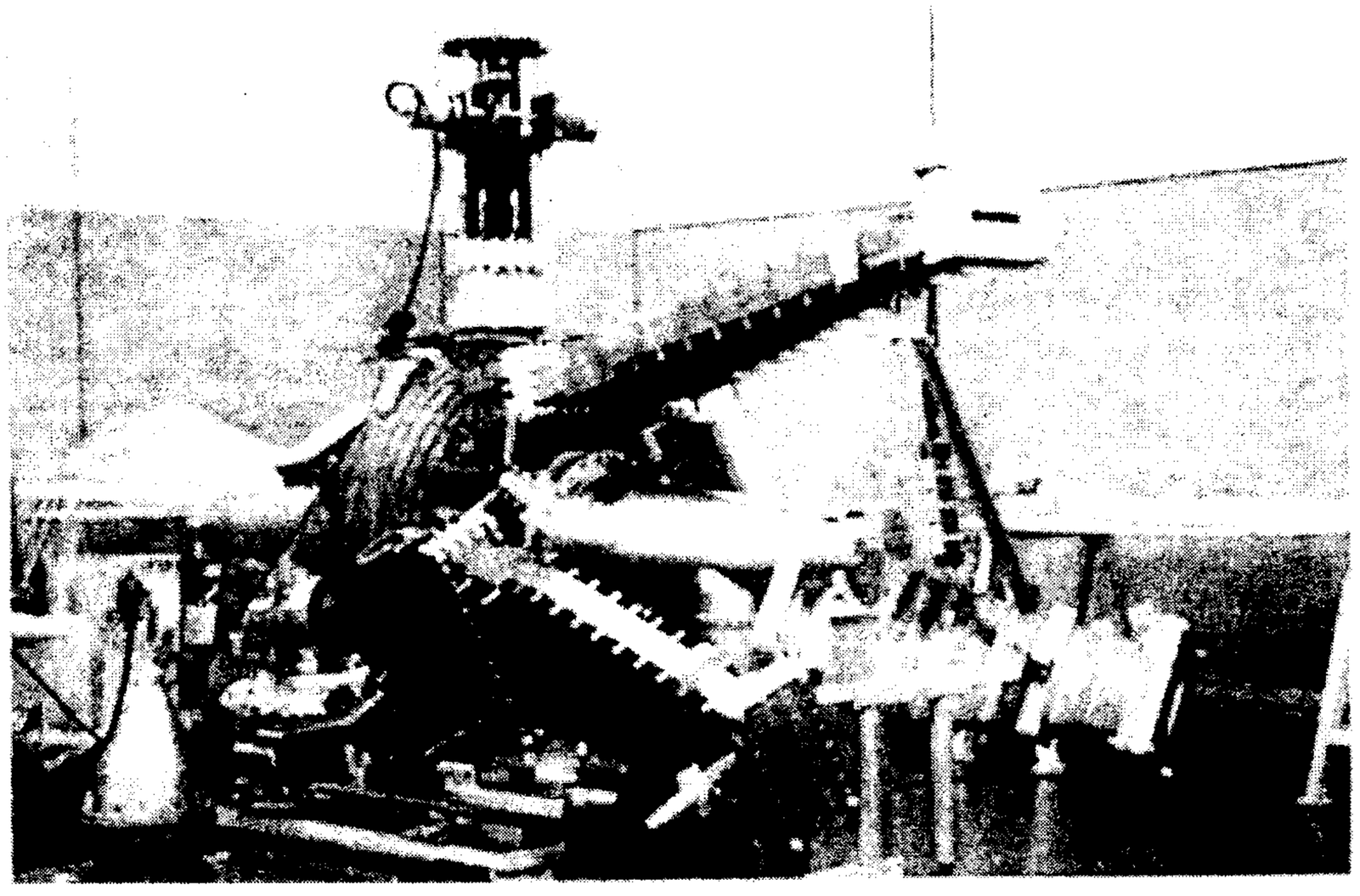

Figure 1: The first DAΦNE RF cavity

2 THE DAΦNE RF CAVITY

The cavity, manufactured by Zanon (Italy), is made from a single copper billet to avoid large vacuum tightness weldings. The internal surface was entirely worked out by automatic milling machine. The long taper tubes are joint to the cavity with 300 mm diameter flanges.

The circular ports of vacuum pumps, tuner and power coupler are TIG welded; conflat flange to copper joints are made with the electron beam welding (ebw) technique. The cavity water cooling is guaranteed by circular tubes brazed onto the surface. The cooling system has been designed with the code ANSYS [3] which takes into account the distribution of the cavity RF wasted power.

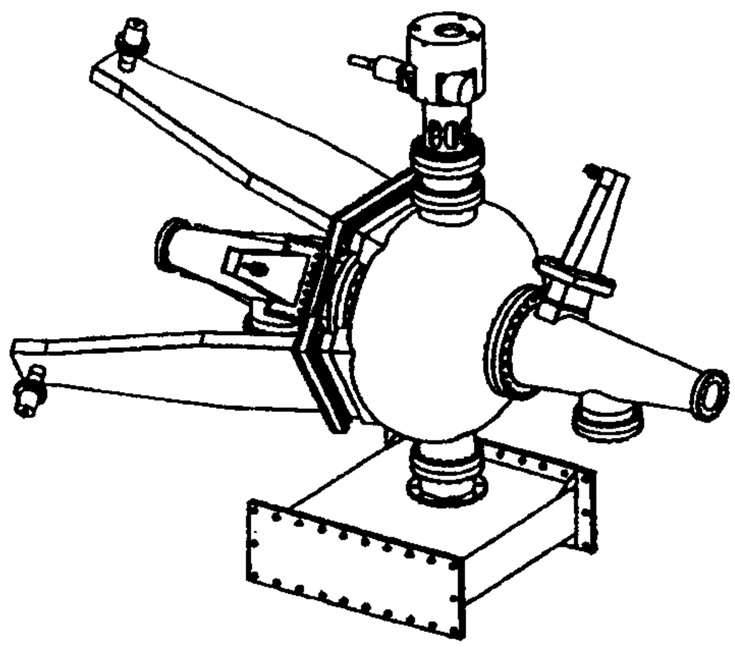

Figure 2: DAΦNE RF cavity sketch.

The HOM damping system consists of three rectangular 305 x 40 mm waveguides (WG) connected at 120° to the cavity main body. Their position is optimised in order to have the highest coupling to the most dangerous HOMs which can propagate in the TE10 dominant WG mode. The WG frequency cut-off is above the cavity FM which therefore is trapped in. Two additional 140 x 40 mm rectangular WGs are located on the tapers with a relative angular position of 90°. They extract those highest frequency HOMs which propagate through the tubes. The WGs are then converted to coaxial by means of a smooth broadband double ridge transition [4]. Figure 2 shows a sketch of a fully equipped DAΦNE cavity. The HOM power is dissipated on an external standard 50 Ω load via a 7/8" coaxial Al_2O_3 feedthrough designed at Frascati and manufactured by Meta.Ceram (France). The feedthrough frequency response is flat (VSWR < 2) from DC to 3 GHz; the device has been power tested up to 4 kW-cw at 370 MHz. The WG to Coaxial Transitions avoid the use of under vacuum RF lossy materials for HOM power dissipation. They consist of two OFHC Copper half shells longitudinally brazed together. Water cooling is provided on the transition broader side to dissipate the evanescent FM. Ribs are used to reinforce the structure against the atmospheric pressure. A picture of one WG to coaxial transition is shown in Fig. 3. Elicoflex gaskets are used for the vacuum tightness of the WG rectangular flanges and the RF contact is obtained with Cu-Be springs.

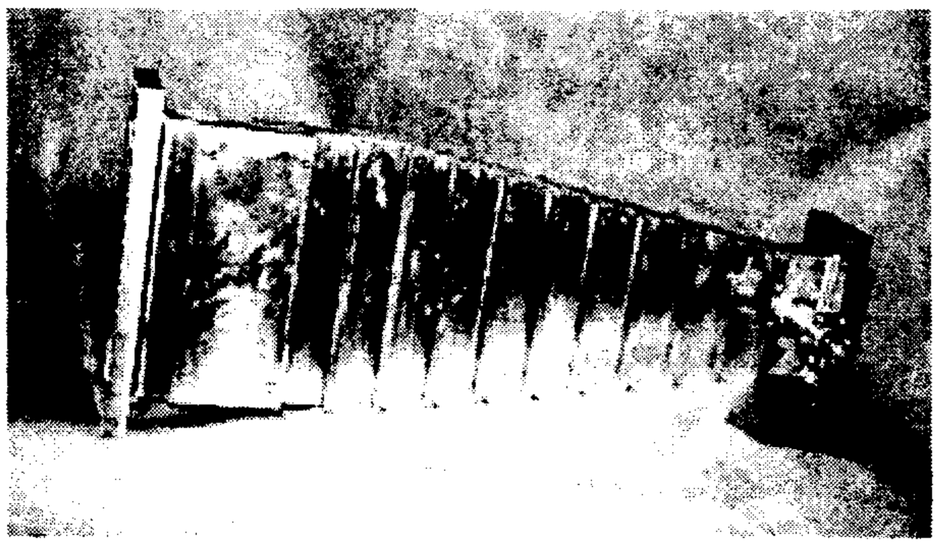

Figure 3: DAΦNE WG-to-Coaxial transition.

Cavity tuning is made with a stepping motor driven cylindrical plunger; the RF power coupler consists of a WG to coaxial transition terminated with a rotating loop to adjust the cavity-generator coupling; the vacuum separation is made with a cylindrical ceramic window. To protect the ceramic in case of arcs or overheating, the vacuum window is monitored by arc detector and infrared sensor.

3 CAVITY POWER TESTS

The cavity power station comprises one 368 MHz - 150 kW-cw klystron amplifier (Thomson, France), linked to the cavity with a 6-1/8" coaxial line via a three port ferrite circulator (AFT, Germany) for protection against high standing wave regime.

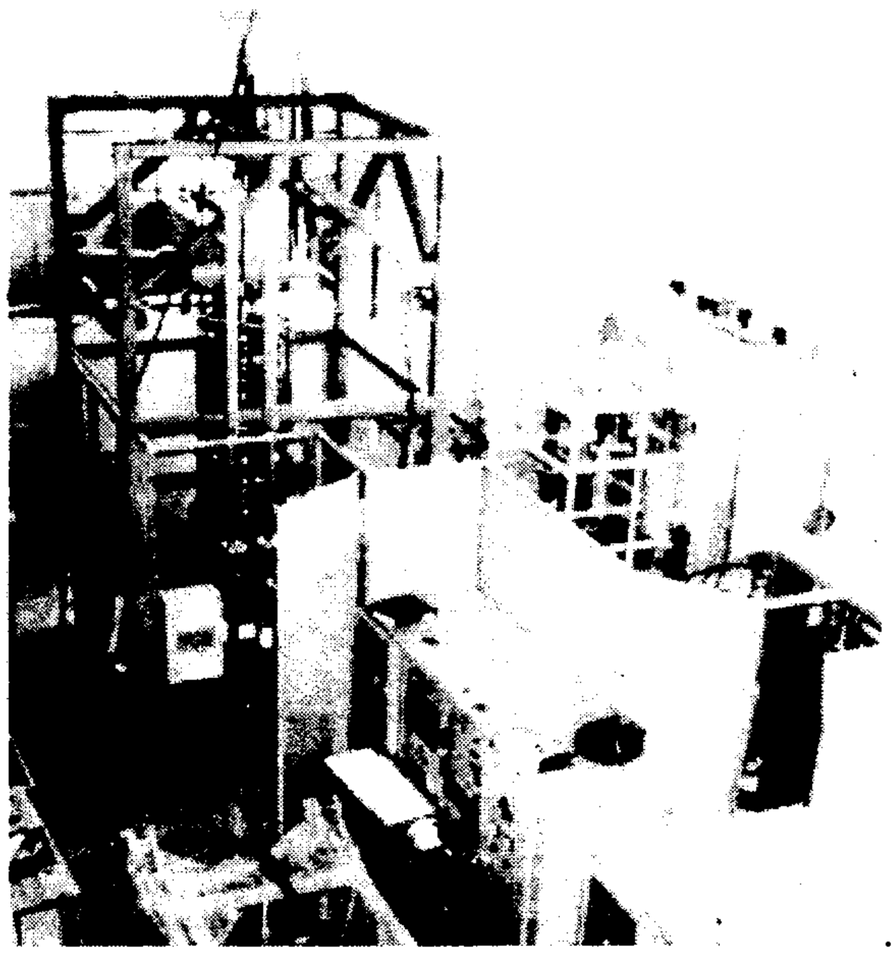

Figure 4: DAΦNE RF Test Hall

A coaxial line instead of a waveguide was chosen to improve the system compactness. To avoid any mechanical stress on the klystron ceramic window, the coaxial line, made by Spinner, is provided with flexible sections and is internally air cooled to prevent over-heating. Figure 4 shows a picture of the DAΦNE RF test hall. The low power control electronics includes the tuning system and the servo-loops to control and stabilize the amplitude and phase of the RF cavity voltage.

A RF feedback circuit around cavity and klystron has been developed to prevent the beam loading instability [5]. The first DAΦNE cavity has been power tested in April '96. The nominal accelerating field V_C = 250 kV, corresponding to a cavity power dissipation of ≈ 16 kW, has been reached in less than 24 hours of cw RF conditioning. No evidence of multipacting or discharge phenomena has been remarked, in spite of the fact that the evanescent penetration of the fundamental mode in the plane, parallel surface region of the waveguide HOM couplers is a potential source of resonant discharges.The cavity has been kept continuously powered for 2 weeks at various accelerating field levels up to 350 KV without faults, so that the RF test has been considered completely satisfactory. The cavity vacuum was limited to $2 \cdot 10^{-8}$ mbar because, to make the RF tests quickly, we made only a moderate and short baking to 150° C. Therefore the cavity shall be newly cleaned and baked before the next power test, scheduled on the late summer.

4 HOM DAMPING

As already mentioned, the HOM damping was the principal cavity design goal. In order to have an evaluation of the achieved damping rate, a measurement of the residual HOM longitudinal impedances based on the wire technique has been carried out. The plots of the cavity longitudinal spectrum up to 1.5 GHz with shorted and matched damping waveguides are shown in Fig. 5.

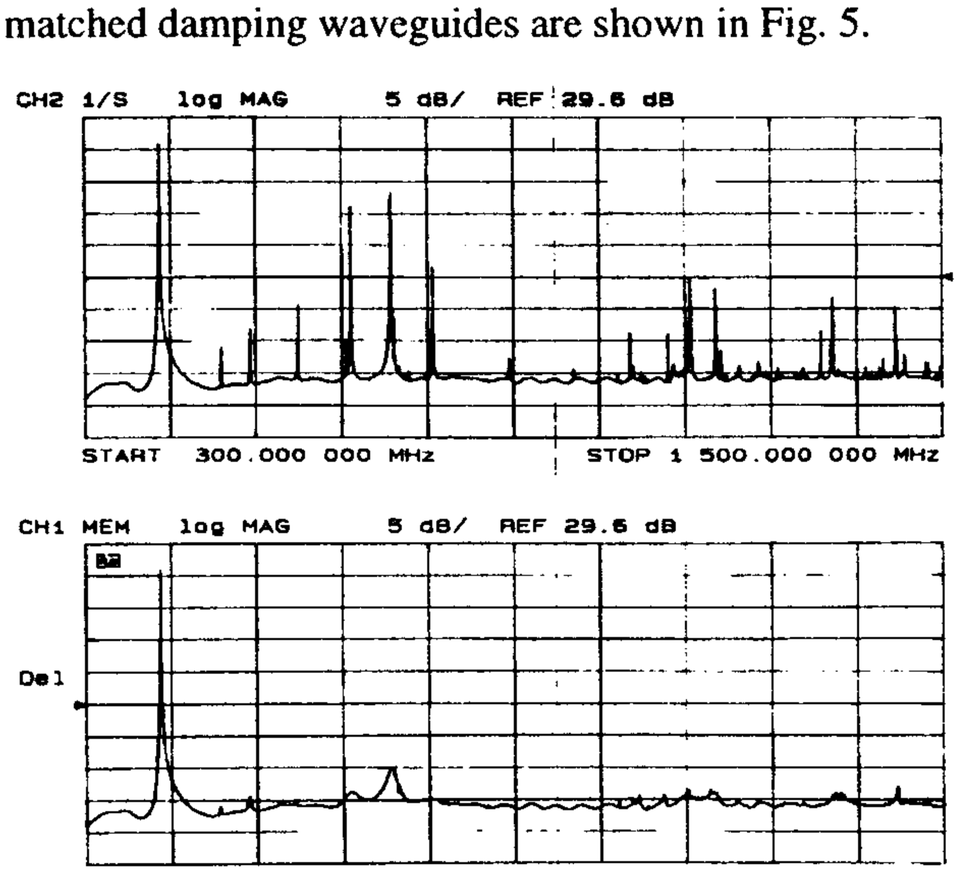

Figure 5 : DAΦNE Cavity longitudinal spectrum. Damping waveguides terminated on shorts (up); Damping waveguides terminated on matched loads (down).

The reference impedance of the wire-beam tube system is ≈ 260Ω. The wire technique has been preferred to other methods (port-to-port measurements, bead perturbations) since it allows to have an immediate picture of the behaviour of those modes having significant fields nearby the beam axis (the only modes affecting the beam dynamics) and it is especially effective in low-Q mode measurements.

On the other hand we are aware that the wire perturbs significantly the resonant frequencies, and the impedance measurements are not very much accurate.

No modes appear to remain undamped in Fig. 5, and the damping factor in some cases exceeds 30 dB. The highest impedance in the damped plot is located around 700 MHz and corresponds to the first monopole TM011. The damped peak impedance is ≈400 Ω, giving a coupled bunch instability rise time of ≈ 0.5 msec in case of full coupling at the maximum machine current. This growth rate strongly dominates the natural damping (17 msec) but it is still at well manageable level for the DAΦNE bunch-by-bunch longitudinal feedback system[6].

More accurate longitudinal and transverse impedance measurements are in program in the very near future.

5 CONCLUSIONS

The first DAΦNE cavity, fully equipped with RF main coupler, tuner, waveguide HOM dampers and special coaxial ceramic feedthroughs, has been power tested far beyond the nominal accelerating field in the DAΦNE RF test hall. A power station, reproducing the final RF system configuration, including the TH2145 DAΦNE klystron, the high power circulator, the RF transmission line complex and the low level control electronics, has been assembled to perform the test. No multipacting or discharge phenomena, as well as other kind of RF system faults, have been observed during two-weeks of continuous operation.

ACKNOWLEDGEMENTS

The authors wish to thank warmly the members of the DAΦNE RF group P. Baldini, F. Lucibello, S. Quaglia, M. Scampati, A. Sprecacenere, T. Tranquilli and A. Cecchinelli for their precious contribution to the design, assembly and operation of the whole RF system. Thanks are also due to V. Chimenti, A. Clozza and the DAΦNE vacuum group for their support to the cavity power test.

REFERENCES

[1] G. Vignola, "DAΦNE: The First Φ-Factory", invited paper, this Conference.

[2] S. Bartalucci et al., "Analysis of methods for controlling multibunch instabilities in DAΦNE", Particle Accelerators, vol. 48, p. 213, 1995.

[3] ANSYS, Swanson Analysis System Inc., Houston, Pennsylvania, 15342 (USA).

[4] R. Boni et al., "A Broadband waveguide to coaxial transition for High Order Mode damping in particle accelerators RF cavities", Particle Accelerators, vol. 45 (4), p. 195, 1994.

[5] R. Boni et al., "Experimental test of the DAΦNE RF Feedback System", this Conference.

[6] R. Boni et al., "Kickers and Power Amplifiers for the DAΦNE Bunch-by-Bunch Longitudinal Feedback System", this Conference.

EXPERIMENTAL TESTS OF THE DAΦNE RF FEEDBACK SYSTEM

R. Boni, A. Gallo, F. Marcellini, INFN-LNF, Frascati, Italy

Abstract

The Φ-Factory DAΦNE is a high current, multibunch e^+e^- double ring collider in construction at INFN Frascati Laboratories. The operating current has to reach 5 Amps to get the ultimate luminosity, while the required gap voltage per ring is quite small (250 kV). For this reasons the beam loading effect is really emphasised in the machine. A fast RF feedback system has been implemented to prevent the beam loading instability, and a prototype of the control circuit has been tested in a real environment, including the RF cavity, the high power klystron and the rest of the RF servo loops. A general description of the system and the experimental results are reported in this paper together with some considerations on the effects of the beam-cavity interaction on the whole RF control electronics.

1 INTRODUCTION

The main characteristics of the DAΦNE [1] RF system are summarized in Table I.

Table I: DAΦNE RF system parameters

f_{RF}	RF frequency (MHz)	368.32
V_c	Cavity voltage (kV)	250
Q_0	Cavity unloaded quality factor	33,000
R_s	Cavity shunt impedance (MΩ)	2
β	Cavity input coupling factor	2.5
P_{MAX}	Max klystron RF power (kW)	150
E_r	Energy loss / turn (keV)	15
f_s	Synchrotron freq. (@V_c=250kV) (kHz)	42
h	Harmonic number	120
I_b	Max beam current (Amps)	5

The interaction between the cavity accelerating mode and the beam is the primary source of the coupled-bunch, rigid-mode instability (sometimes called "center-of-mass" instability) in multibunch storage rings [2]. As the stored current increases the synchrotron equation parameters, i.e. the damping constant α and the synchrotron angular frequency Ω_S, are not lattice constants anymore, but they are affected by other variables such as the beam current itself and the cavity tuning angle.

Under certain conditions the damping constant α can get negative giving anti-damped rigid-mode oscillations (the so called "Robinson instability"), while above a certain current threshold the synchrotron angular frequency Ω_S, i.e. the longitudinal focusing force, is reduced to zero, getting the beam suddenly lost (beam loading instability).

More specifically, considering the perturbation induced by the beam-cavity interaction on the synchrotron equation, the beam loading current limit is given by:

$$I_b = - \frac{V_C \sin(\varphi_S)}{2 Z_i(j\omega_{RF})} \qquad (1)$$

where V_C is the cavity accelerating peak voltage, φ_S is the synchronous phase and $Z_i(j\omega_{RF})$ is the cavity impedance imaginary part as seen by the beam at the frequency of the RF master generator.

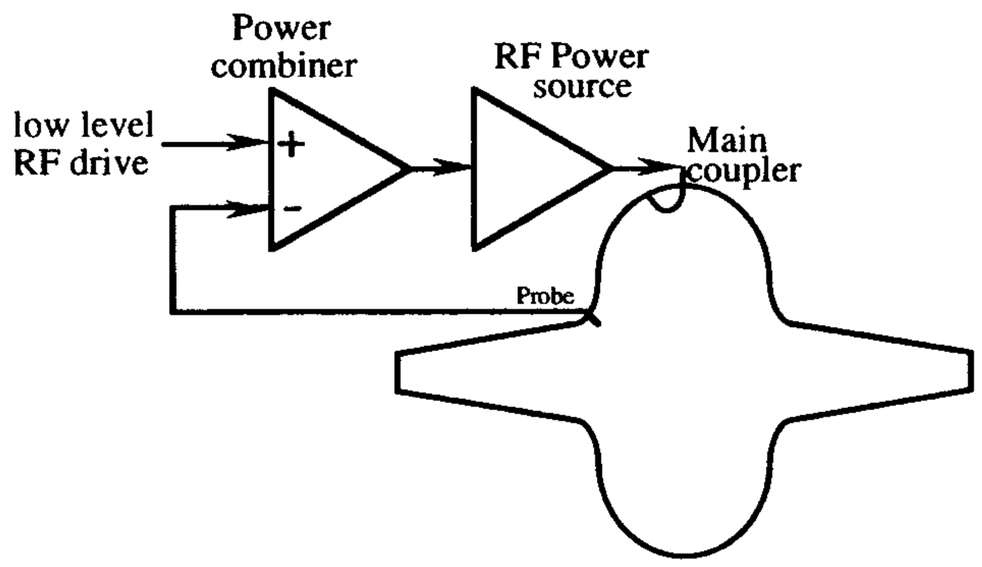

Figure 1: RF feedback general scheme.

The RF feedback scheme, reported in Fig. 1, is a cure of the beam loading instability and consists in adding out-of-phase a sample of the cavity voltage to the RF master source. In this case the impedance seen by the beam $Z(j\omega)$ is that of the cavity accelerating mode reduced by the open loop gain $H(j\omega)$, accordingly to:

$$Z(j\omega) = \frac{Z_C(j\omega)}{1+H(j\omega)} \qquad (2)$$

and the impedance dynamic reduction pushes the beam loading instability current limit toward higher values.

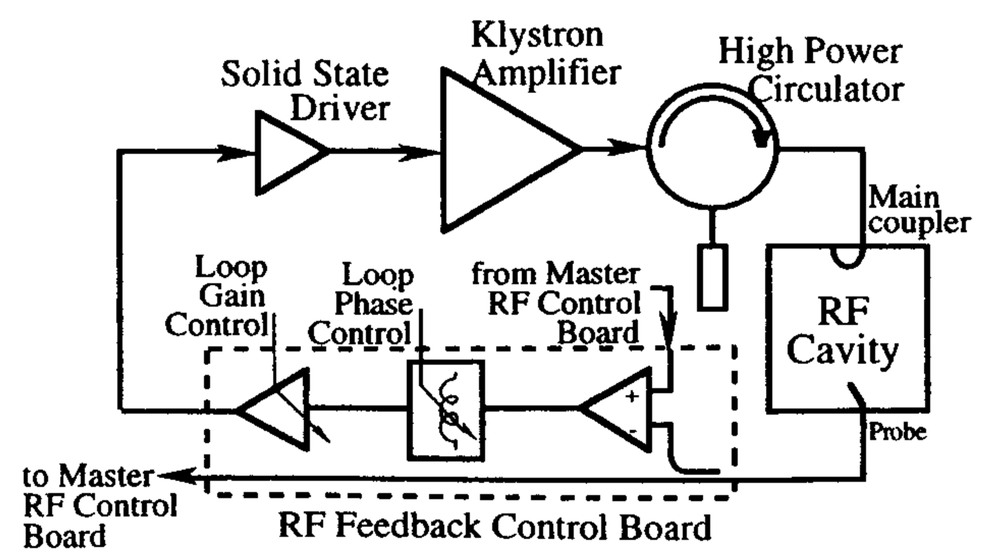

Figure 2: DAΦNE RF feedback system schematics.

The cavity accelerating mode tail may also couple to the sidebands of multibunch instability modes other than the rigid one, especially when the beam loading causes the cavity to be largely detuned toward lower frequencies. The RF feedback is a cure also for this kind of instabilities. Anyway, only long machines, having low revolution frequencies, are affected by this phenomenon [3]. This is not the DAΦNE case.

2 DAΦNE RF SYSTEM AND RF FEEDBACK CONTROL ELECTRONICS

The DAΦNE RF system schematics, including the RF feedback control board, is shown in Fig. 2.

The loop group delay value τ in a span of $\approx$ 2 MHz around the cavity resonant frequency f_C is the parameter determining the maximum achievable loop gain G for a given phase margin φ_m accordingly to:

$$G = \frac{(\pi/2 - \varphi_m)\, Q_0}{\pi\, \tau\, f_C\, (1+\beta)} \qquad (3)$$

where Q_0 is the cavity unloaded quality factor and β is the generator-to-cavity coupling factor. As a safety measure, the loop operational phase margin should always exceed $\pi/4$.

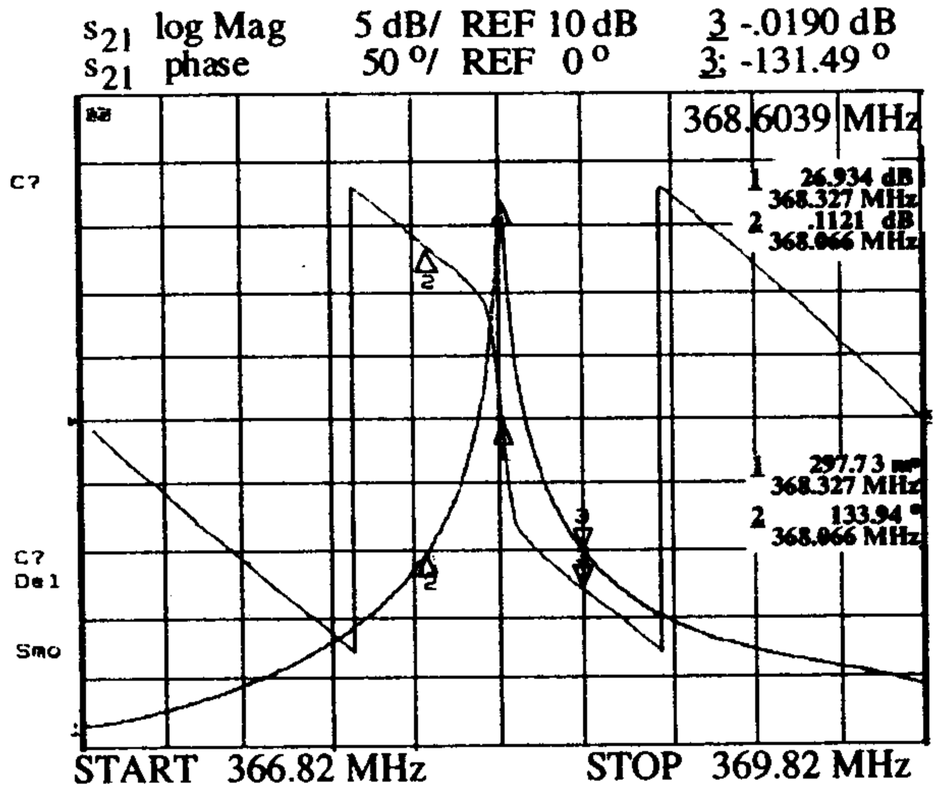

Figure 3 : Measured open loop gain.

The loop group delay is mainly made of two contributions: the "physical" delay due to the cable lengths, the control electronics and the solid state amplifiers (τ_l) and the group delay of the DAΦNE klystron TH2145 related to the tube frequency response (τ_k). The compactness of the RF power plant, obtained locating the klystron amplifiers in the machine hall and connecting them to the cavities through only a ≈15 m long transmission line, is beneficial for the minimization of the "physical" delay τ_l ; on the other hand a great care has been taken in the klystron tuning operation in order to enlarge the tube bandwidth and minimize its contribution to the loop group delay.

3 EXPERIMENTAL TESTS

Recently the first DAΦNE cavity has been high power tested [4] in the LNF RF test hall in a layout configuration very similar to that of the DAΦNE machine hall where the RF system will be finally located. A special session of the power tests has been dedicated to set up and operate the RF feedback system with a control electronics prototype board.

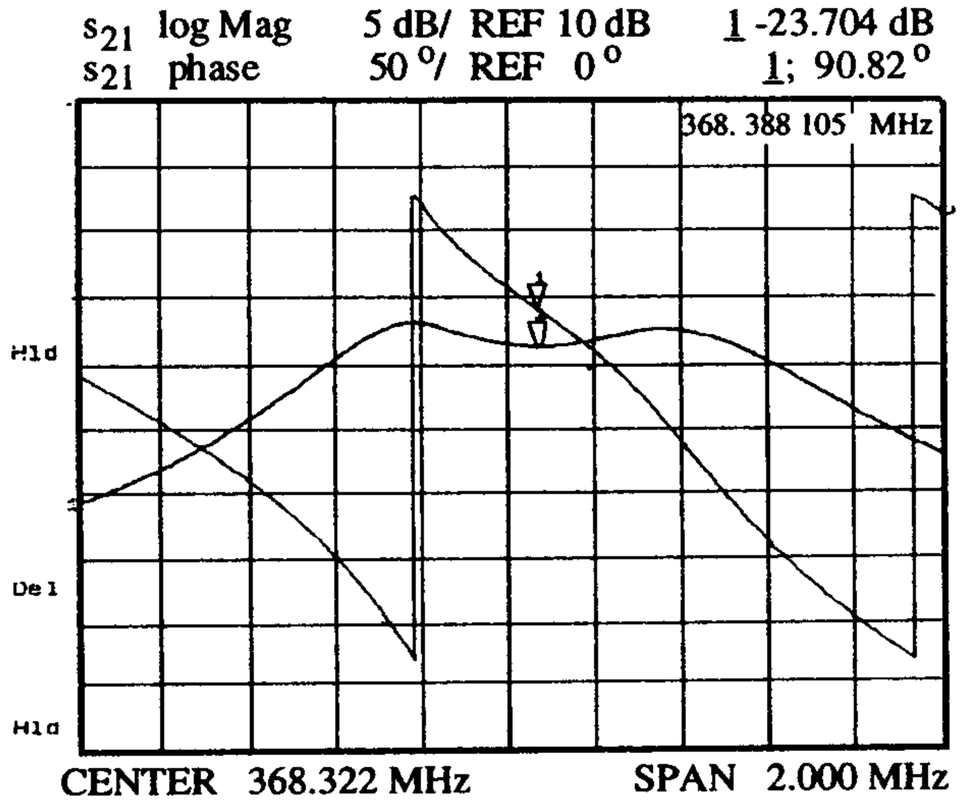

Figure 4: Measured closed loop gain.

No special criticality has been found in setting-up and operating the feedback system, and the presence of a klystron tube in the loop does not distort too much the overall frequency response.

The open and closed loop frequency responses of the system measured with a vector network analyzer are shown in Figs. 3 and 4 respectively. By adjusting the loop gain amplitude and phase a $\pi/4$ phase margin stable configuration with a ≈27 dB maximum gain G has been obtained, while the loop group delay, given by the slope of the phase plot of Fig. 3 in the region external to the cavity bandwidth, is $\tau \approx 500$ nsec.

These values are consistent with eq. 3 considering that the generator-to-cavity coupling factor β has been temporarily set to 1.4 to decrease the input line VSWR during these very first high power tests. Therefore restoring the operational β value of 2.5 should decrease the maximum achievable gain by ≈ 3.3 dB.

By excluding the klystron from the loop layout, a physical delay $\tau_l \approx 320$ nsec has been measured, so that a $\tau_k \approx 180$ nsec klystron contribution has been estimated. It is possible to further reduce the τ_l value; we estimated that using faster, air-dielectric cables and shortening them to the minimum in the DAΦNE hall, a physical delay as low as 170 nsec can be achieved, corresponding to a total delay $\tau \approx 350$ nsec.

The delay reduction will allow to recover ≈ 3 dB in the loop gain.

A phase margin φ_m value lower than $\pi/3$ produces an impedance frequency dependence similar to that of Fig. 4 plot, showing a local minimum corresponding to the cavity resonant frequency. This cause the beam to be Robinson unstable, with an estimated minimum rise time as low as 2.5 msec in the DAΦNE case, that has to be cured by the DAΦNE bunch-by-bunch feedback system [5] or by a dedicated feedback system based on fast cavity phase modulation.

4 BEAM LOADING INSTABILITY CURRENT LIMIT

With the reported experimental data it is possible to realistically estimate the RF feedback performances in terms of instability threshold current.

An useful representation of the RF system status is the Y/φ_L plot [6], where Y is a beam loading parameter related to the beam current I_b accordingly to:

$$Y = \frac{2\, I_b\, R_s}{(1+\beta)V_c} \qquad (4)$$

while φ_L is the phase of the load seen from the RF input coupler, including the cavity and the beam.

The Y/φ_L plot for the DAΦNE RF system is shown in Fig. 5.

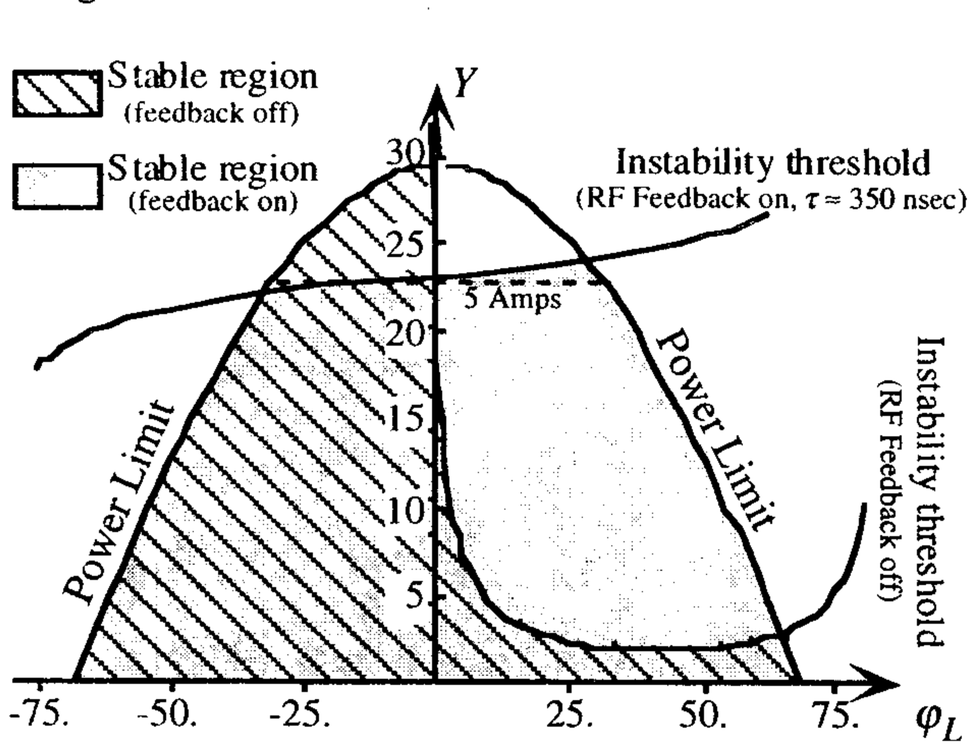

Figure 5: DAΦNE RF system Y/φ_L plot.

The curves on the plane represent the power limits and the instability thresholds with and without the RF feedback system. It is clear from the plot that in principle the system can operate up to 5 Amps even without the RF feedback by setting a working point with a small negative φ_L value. Anyway, this would not be a safe choice being the operation close to the instability limit too critical and sensitive to any phase oscillation. On the other hand the RF feedback system operation allows to approach the maximum current being the working point φ_L value limited only by the available RF power and not by instability thresholds.

The situation is a little more worrying if, in order to lengthen the bunches or for any other reason, the system should be operated at a lower cavity voltage level. Let us consider, for instance, a 150 kV cavity voltage. In this case the expected cavity detuning is much wider, and the beam loading effects are really emphasised. By recomputing the Y/φ_L plot with V_C =150 kV, an instability current threshold of ≈3 Amps has been obtained, well below the DAΦNE maximum beam current. In order to operate the system up to the maximum current even in this case, a sophisticated equalization of the loop frequency response, to decrease the group delay and increase the loop gain, is required.

5 CONCLUSIONS

The DAΦNE RF feedback system has been tested during a high power conditioning session of the first DAΦNE RF cavity. The cavity has been powered well beyond the nominal voltage (250 kV) in the feedback configuration and no special difficulties have been encountered while operating the system.

A total group delay of ≈500 nsec has been measured, an acceptable value that can be further reduced to 350 nsec by optimizing the cable layout in the DAΦNE hall. The DAΦNE RF feedback performances are sufficient to allow a safe and stable operation of the RF system up to the maximum beam current (5 Amps) at the nominal cavity voltage (250 kV), while not trivial system improvements are required to approach the maximum beam current at voltages significantly lower than nominal value.

ACKNOWLEDGEMENTS

The authors wish to thank warmly P. Baldini and M. Scampati for their invaluable, continuos support to the experimental activity. Thanks are due also to F. Lucibello, S. Quaglia, T. Tranquilli, A. Sprecacenere and A. Cecchinelli that contributed to design, assembly and operate the whole RF system.

REFERENCES

[1] G. Vignola, "DAΦNE: The First Φ-Factory", invited paper, this Conference.

[2] D. Boussard, "Control of Cavities with Heavy Beam Loading", IEEE Trans. Nucl. Sci. Vol. NS-32, n 5, 1985.

[3] P. Corredoura et al., "RF Feedback Development for the PEP-II B-Factory", Proc. 4th European Particle Accelerator Conference, Vol. 3, 1994.

[4] R. Boni et al., "High Power Test of the Waveguide Loaded cavity for the Frascati Φ-Factory", this Conference.

[5] R. Boni et al., "Kickers and Power Amplifiers for the DAΦNE Bunch-by-Bunch Longitudinal Feedback System", this Conference.

[6] A Gallo, "An RF Feedback for DAΦNE", DAΦNE Technical Note RF-6, D.A. INFN - LNF, 1992.

KICKERS AND POWER AMPLIFIERS FOR THE DAΦNE BUNCH-BY-BUNCH LONGITUDINAL FEEDBACK SYSTEM

R. Boni, A. Drago, A. Gallo, A. Ghigo, F. Marcellini, M. Migliorati, M. Serio, M. Zobov
INFN-LNF, Frascati, Italy

Abstract

The multibunch operation of the Frascati Φ-Factory DAΦNE calls for a very efficient longitudinal feedback system to damp the coupled bunch instabilities. A bunch-by-bunch feedback scheme, capable of kicking any bunch proportionally to the time derivative of its position error has been adopted. A special longitudinal kicker based on a waveguide overloaded pill box cavity has been designed and fabricated for this task. A broadband linear power amplifier to drive the kicker has been selected and fully characterised. A description of the power section of the longitudinal feedback system, including kicker, power amplifier, broadband circulator, fast amplitude modulator, together with time and frequency domain measurements, is reported in this paper.

1 INTRODUCTION

In DAΦNE, the Frascati Φ-Factory, up to 120 bunches, 2.7 nsec spaced one each other, can be injected. Coupled-bunch instabilities with rise time faster than the natural damping time could be driven by narrowband machine impedances.

A longitudinal feedback capable to damp all the coupled-bunch modes and the injection transient has been developed in collaboration with the B-Factory group at SLAC.

A bunch-by-bunch feedback scheme, capable of kicking any bunch proportionally to the time derivative of its position error has been adopted [1].

In reference [2,3,4] the description of the feedback chain employing DSP techniques is reported.

2 BUNCH BY BUNCH FEEDBACK BACK-END SECTION

Once the bunch phase errors from the front-end section are processed by the DSP board, the outcoming signals have to be converted in longitudinal kicks to give to the bunches the proper energy correction. The "back-end" section is the analog hardware dedicated to this task, and its schematic representation is shown in Fig. 1.

A bunch synchronous and coherent carrier signal is fast amplitude modulated by a double balanced mixer accordingly to the kick level elaborated by the DSP board. The amplitude modulated signal is then amplified by a linear, broadband power amplifier and sent to the kicker input ports through ferrite circulators.

The choice of the power amplifier is crucial for the system efficiency since an actual rise time much shorter than the bunch time spacing (2.7 nsec) is required, corresponding to a real bandwidth much larger than the RF frequency (368.32 MHz). A 250 W pure class-A linear device (mod. AS0814-250R, MILMEGA Ltd, UK) has been adopted; the amplifier frequency response nearby saturation is shown in Fig. 2.

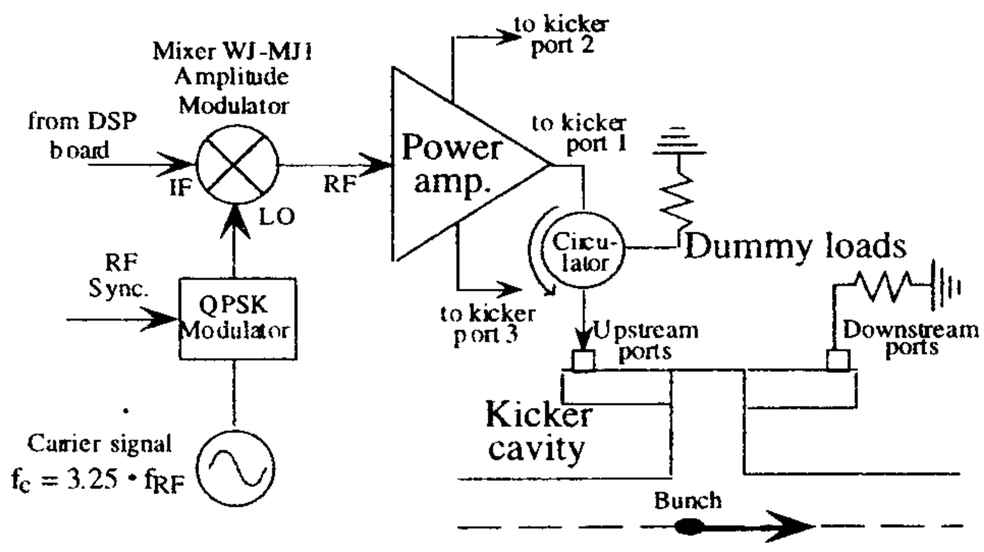

Figure 1: Back-end sketch.

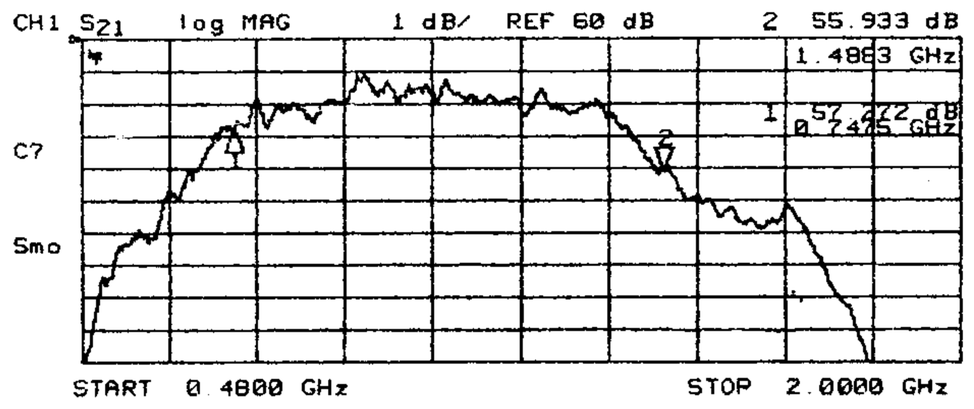

Fig. 2: Power amplifier frequency response

3 LONGITUDINAL KICKER

The longitudinal kicker, the last element of the feedback chain, is the electromagnetic structure capable of transferring the proper energy correction to each bunch.

A possible choice is to use a stripline multi-electrode device for this task [5]. In order to increase the kicker shunt impedance and decrease the parasitic High Order Mode (HOM) content, a longitudinal kicker based on a waveguide overloaded pill-box cavity has been designed and fabricated for the DAΦNE feedback system [6].

A sketch of the DAΦNE longitudinal kicker is shown in Fig. 3. The extremely large band required to fill the cavity to any kick value in a time interval corresponding to the bunch time spacing is obtained by loading the accelerating mode with three single-ridged waveguides placed 120° apart on each pill-box side.

The coupled out field is transformed in a TEM wave by a broadband waveguide-to-coaxial transition and ceramic coaxial feedthroughs allow on-air connection to inputs and output cables. Being a very broadband cavity, the kicker does not require tuning and cooling, and the input coupling is obtained by powering in-phase the three coaxial upstream ports, while the downstream ports are connected on dummy loads.

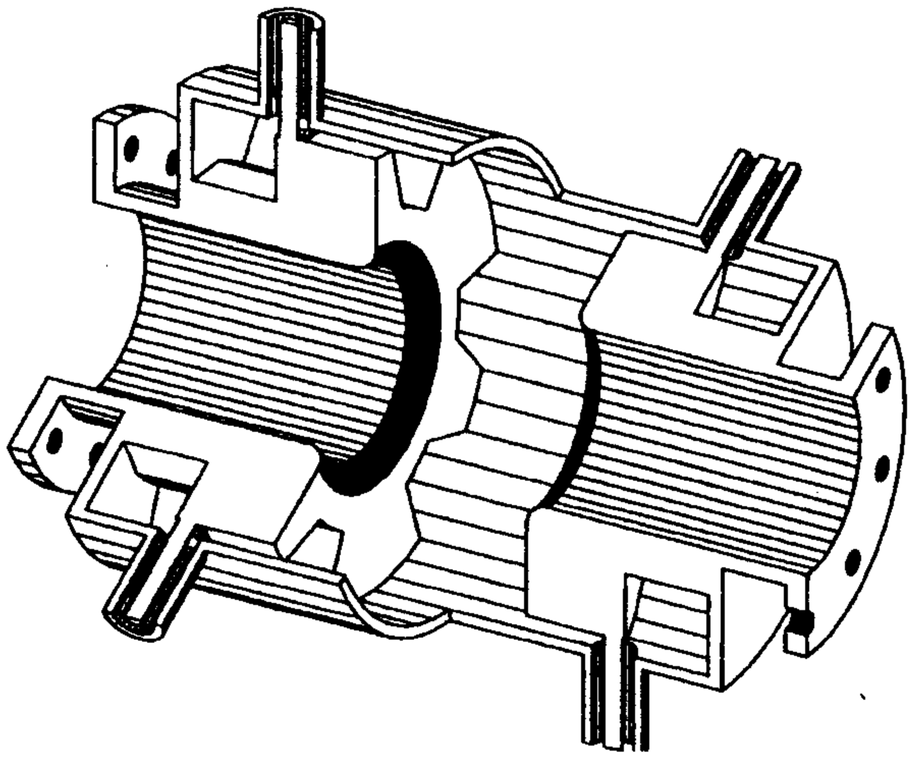

Figure 3: Kicker cavity cutview sketch.

The kicker resonant frequency f_k has been tuned to ≈1200 MHz, corresponding to 3.25 times the RF frequency (f_{RF} = 368.3 MHz). The minimum required bandwidth f_{BW} to preserve an acceptable damping efficiency on any coupled bunch mode is $f_{BW} \approx f_{RF}/2 \approx 180$ MHz. The carrier signal in the back-end section is therefore the 13/4th fractional harmonic of the master radiofrequency which needs to be fast QPSK modulated with a 90^{o} phase jump back every RF period to remain synchronised with the bunch passage when the machine is operated with all buckets filled The kicker beam coupling impedance has been measured with the wire technique and the result is shown in Fig. 4.

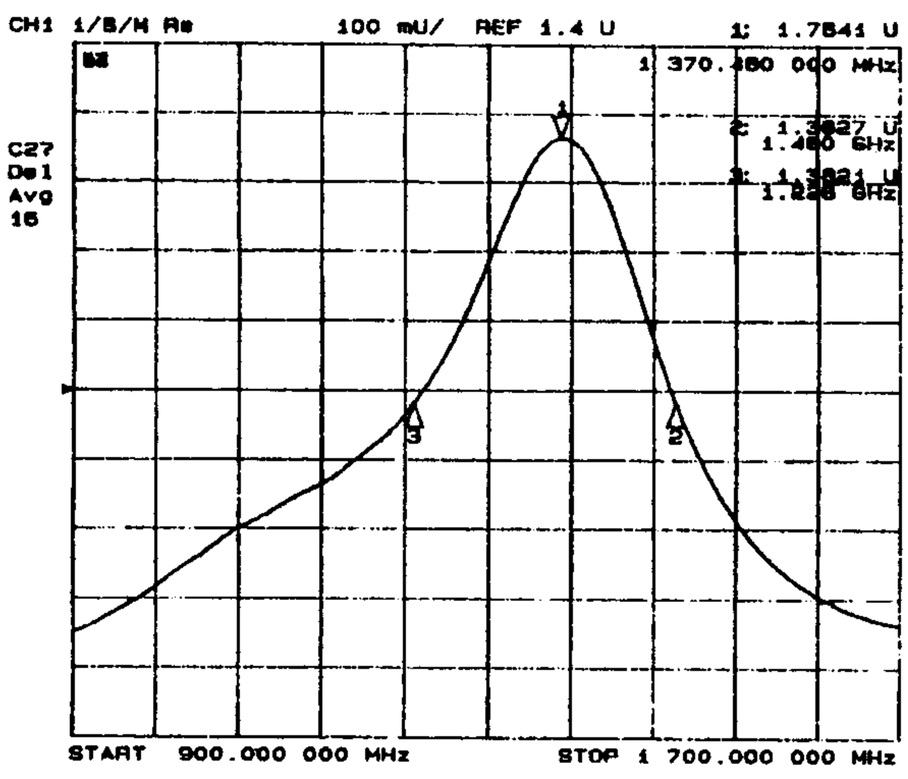

Figure 4: Kicker beam-coupling impedance wire measurement: $\Re e[1/s_{21}]$ vs. frequency.

The beam-coupling Z_{bc} impedance is related to the transmission coefficient between the wire ports s_{21} accordingly to:

$$Z_{bc} = 2\,Z_0 \left(\frac{1}{s_{21}} - 1 \right)$$

where $Z_0 \approx 202\ \Omega$ is the wire-beam tube coaxial characteristic impedance.

From Fig. 4, while taking into account that the kicker shunt impedance is twice the coupling impedance real part, a shunt impedance $R_S \approx 600\ \Omega$ and a bandwidth $f_{BW} \approx 250$ MHz have been obtained. The kicker beam-coupling impedance appears to be largely detuned by the presence of the wire in Fig. 4. The loading waveguides heavily damp the kicker HOMs; no high-order monopoles are measurable, while the first two dipole pairs are damped to values that are considered of no concern for the beam transverse dynamics.

4 POWER BUDGET

The DAΦNE maximum luminosity will be reached progressively by operating the machine with an increasing number of equispaced bunches.

Accordingly to a prudent estimate, a kick voltage of ≈ 1600 V is required to cope with an injection error of 100 psec at the maximum beam current. The required kick scales linearly with the current value.

The power and layout strategy for the different regimes is summarized in Table I.

Table I: Feedback power budget for a DAΦNE main ring

Number of bunches	30	60	120
Beam current [Amps]	1.35	2.7	5.4
Number of kickers	1	1	2
Total shunt impedance [Ω]	600	600	1000
Number of amplifiers	1	3	6
Total feedback power [W]	210	750	1500
Kick voltage [V]	500	950	1730
Beam coupled power per kicker waveguide [W]	400	800	1500

Thanks to a built-in option, the AS0814-250R power amplifier can be used as a 3x70 W triple output amplifier so that just one piece is needed in the 30 bunch operation. The 120 bunches operation foresees the installation of a second kicker cavity per ring. A 20% reduction of the shunt impedance has to be considered in 120 bunch operation because the cavity can not be completely filled in the time between two adjacent bunches.

Being mostly a standing-wave structure, the kicker cavity is not a directional device and the beam coupled power flows indifferently through both input and output ports. Since the beam coupled power may exceeds by several factors the kicker input power, dedicated broadband ferrite circulators have been developed by AFT (Germany) to protect the feedback amplifiers against backward power.

The circulator transmission and isolation frequency responses, as measured at low-level, are presented in Fig. 5; since the estimated beam coupled power is ≈ 1.5 KW per guide at the maximum current and the circulator isolation is ≈ 20 dB in the operating band (1÷1.4 GHz), the backward power to the amplifier input is limited to the tolerable amount of about 15 W.

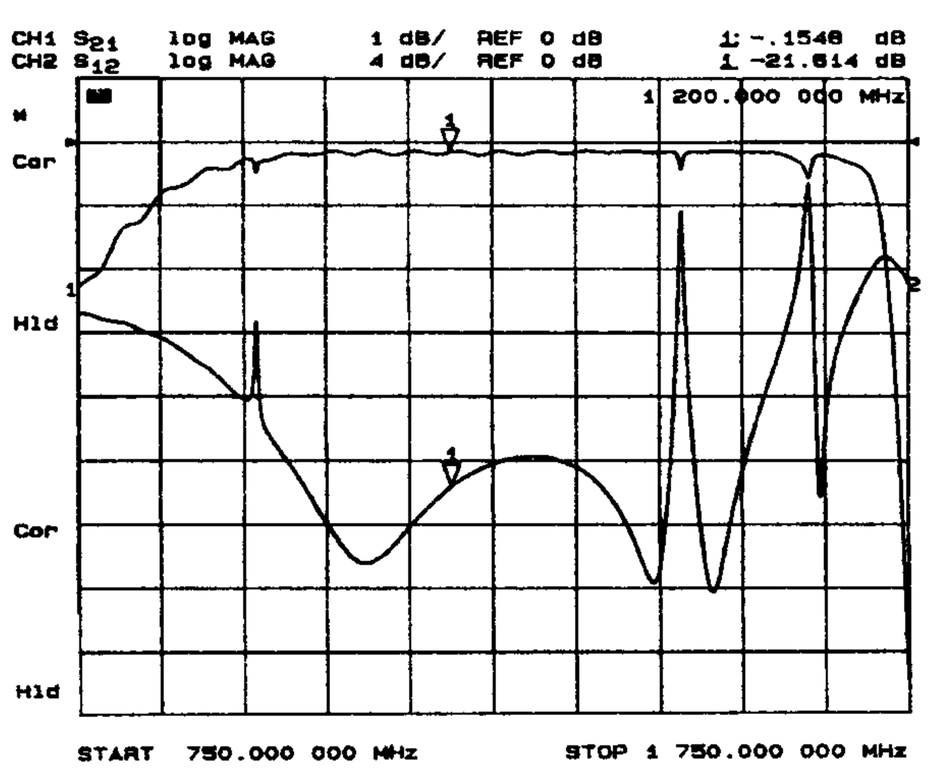

Figure 5: Custom circulator frequency response.

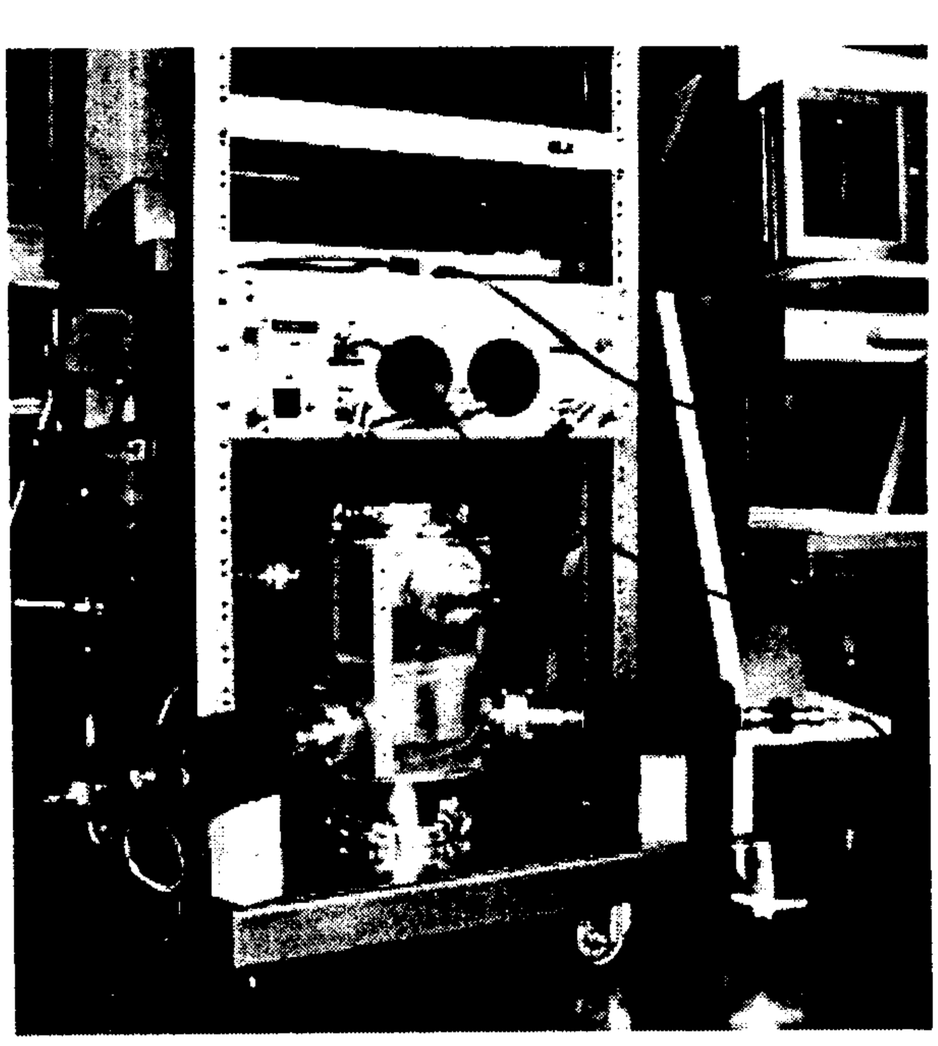

Figure 6: Kicker and power amplifier on bench.

5 TIME DOMAIN MEASUREMENTS

A bench measurement on the DAΦNE bunch-by-bunch feedback system back-end, including all the hardware but the circulators, has been recently carried out. A bench picture is shown in Fig. 6, and a typical result is reported in Fig. 7.

Referring to the Fig. 1 sketch, a modulating square wave switching from zero to a positive selected value has been sent to the mixer IF port to simulate the severe case where only one bunch over two has to be kicked, at a power rate close to the amplifier saturation. The kicker input and output signals have been captured by a fast digitalizing oscilloscope, and the result is shown in Fig. 7.

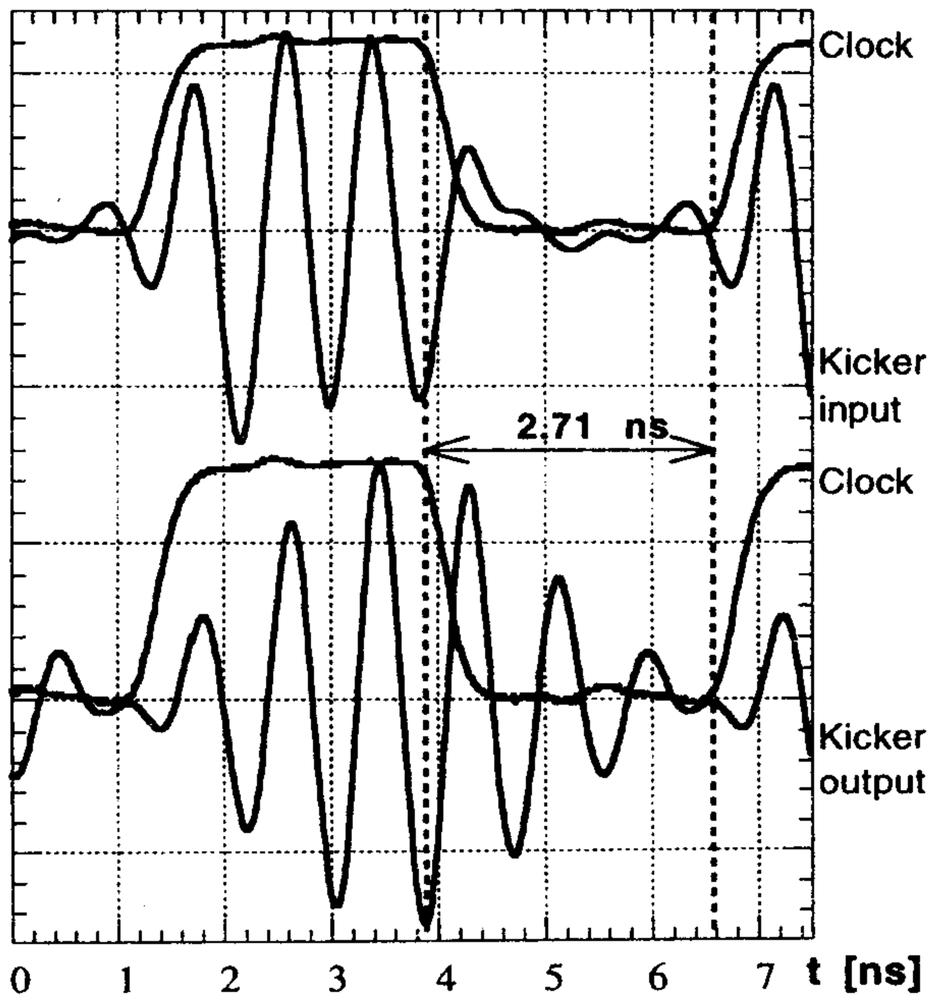

Fig. 7: Kicker input and output time-domain signals

The dynamics of the kicker input signal is comparable to that of the ECL square wave, that confirms in the time domain the excellent bandwidth features of the power amplifier. The kicker filling time is evident in the outcoming signal; even though the signal dynamics is limited in this case by the cavity bandwidth, the Fig. 7 vertical markers show that the residual kick transferred to the stable virtual bunch is a negligible fraction of the kick given to the unstable one.

CONCLUSIONS

The time domain measurements have confirmed that the overall back-end bandwidth is large enough to efficiently operate the feedback system up to the maximum DAΦNE beam current.

REFERENCES

[1] M.Bassetti et al., "DAΦNE longitudinal feedback", EPAC 92, Berlin.

[2] G.Oxoby et al., "Bunch-by-bunch longitudinal feedback system for PEP-II", EPAC 94, London, .

[3] H.Hindi et al., "Downsampled signal processing for B Factory bunch-by-bunch feedback system", SLAC-PUB 5772, 1992.

[4] L.Sapozhnikov et al., "A longitudinal multi-bunch feedback system using parallel digital signal processors", SLAC-PUB 6365, 1993.

[5] J.N.Corlett et al., "Longitudinal and transverse feedback kickers for the ALS", EPAC 94, London.

[6] R.Boni et al., "A waveguide overloaded cavity as longitudinal kicker for the DAΦNE bunch-by-bunch feedback system", Particle Accelerators, in pub.